NASA Technical Paper 1065

Improvement of Maneuver Aerodynamics by Spanwise Blowing

Gary E. Erickson and James F. Campbell

DECEMBER 1977

NASA

NASA Technical Paper 1065

Improvement of Maneuver Aerodynamics by Spanwise Blowing

Gary E. Erickson
The George Washington University
Hampton, Virginia
and
James F. Campbell
Langley Research Center
Hampton, Virginia

National Aeronautics
and Space Administration

**Scientific and Technical
Information Office**

1977

SUMMARY

Spanwise blowing was used to test a generalized wind-tunnel model to investigate new component concepts in order to provide improved maneuver characteristics for advanced fighter aircraft. Primary emphasis was placed on performance, stability, and control at high angles of attack and subsonic speeds. The investigation was focused on various methods of controlling and delaying the leading-edge vortex breakdown and of optimizing component interactions. In particular, spanwise blowing was used on a 44° swept trapezoidal wing to determine the effect of leading-edge vortex enhancement on leading- and trailing-edge flap effectiveness and on horizontal- and vertical-tail effectiveness, and to assess the concept as a roll control device. In addition, the effect of spanwise blowing on the canard or wing on close-coupled canard-wing effectiveness was investigated. The aerodynamic performance of spanwise blowing was compared with other maneuver concepts such as canards and strakes.

Test data were obtained in the Langley high-speed 7- by 10-foot tunnel at free-stream Mach numbers up to 0.50 for a range of model angles of attack, jet momentum coefficients, and leading- and trailing-edge flap deflection angles. Spanwise blowing resulted in significant vortex-induced lift increments at the higher angles of attack with consequent improvement in the drag polar. The data suggested that blowing was more effective at the higher free-stream Mach numbers. In addition, the longitudinal aerodynamic performance of spanwise blowing compared favorably with the performance of a highly swept wing-strake configuration. Small deflections of a leading-edge flap delayed the more beneficial effects on lift due to blowing to higher angles of attack, but the data suggested that a forward rotation of the vortex-lift vector resulted in leading-edge thrust recovery and, hence, polar improvement. Spanwise blowing in conjunction with a deflected trailing-edge flap resulted in lift and drag benefits that exceeded the summation of the effects of each high lift device acting alone. Spanwise blowing on the canard was more effective than spanwise blowing on the wing of a close-coupled canard-wing configuration. The performance of canard blowing compared very well with the performance of canard-wing configurations featuring a straked canard. Adding a horizontal tail reduced the lift effectiveness of blowing at high angles of attack.

In addition, blowing resulted in stabilizing increments in the effective dihedral and directional stability parameters of the wing and vertical-tail configuration and the combination wing, horizontal-tail, and vertical-tail configuration. Also, blowing delayed the unfavorable break in the directional stability parameter to much higher angles of attack. Furthermore, the significant benefits in longitudinal characteristics obtained with spanwise blowing or a wing strake may be obtained without adverse effects on lateral-directional stability. Asymmetric blowing was an effective lateral control device at the higher angles of attack. This device achieved results which compared favorably with those obtained for a differential-strake configuration. The leading-edge suction analogy was used for selected configurations and provided reasonable

estimates for the longitudinal aerodynamic characteristics resulting from spanwise blowing.

INTRODUCTION

The flow on thin, highly sweptback wings at moderate to high angles of attack is characterized by a leading-edge separation which forms a stable vortex over the wing and provides significant vortex-induced lift increments. This characteristic of slender wings, of the supersonic cruise type, has been understood for many years (refs. 1 to 15). For moderately swept higher aspect-ratio wings suitable for fighter aircraft, however, these vortex-induced lift increments are not achieved because of vortex bursting, or breakdown, at moderate angles of attack. If vortex breakdown could be delayed to higher angles of attack, the resulting vortex lift would significantly improve fighter maneuver performance.

A promising technique for enhancing the leading-edge vortex on moderately swept wings and effectively delaying vortex breakdown to higher angles of attack consists of blowing a concentrated jet over the wing's upper surface in a direction essentially parallel to the wing leading edge; this technique is illustrated in the flow-visualization photographs in figure 1. References 16 to 31 describe studies which (1) demonstrate the control of separated flow regions by transverse blowing, (2) apply the spanwise blowing concepts to different types of lifting surfaces, and (3) determine the amount of vortex lift achievable on wings typical of current fighter aircraft. These studies should be extended to evaluate the effects of spanwise blowing on fighter performance, stability, and control for a variety of aircraft component arrangements.

Accordingly, the investigation described in this paper was conducted using a 44° swept trapezoidal wing configuration to determine the effects of spanwise blowing on leading- and trailing-edge flap effectiveness, on horizontal- and vertical-tail effectiveness, on close-coupled canard-wing interactions, and on rolling-moment generation, and to compare the aerodynamic performance of spanwise blowing with other maneuver concepts such as canards and strakes.

The wind-tunnel tests were performed in the Langley high-speed 7- by 10-foot tunnel at free-stream Mach numbers up to 0.50. Six-component force and moment data were acquired for a range of angles of attack, jet-momentum coefficients, and leading- and trailing-edge flap deflection angles. Details of this wind-tunnel investigation have been reported in reference 32. The present paper presents highlights of that study, including some additional data analyses, theoretical computations, and comparisons of spanwise blowing with other maneuver concepts.

SYMBOLS

Physical quantities in this paper are presented in the International System of Units (SI). Measurements and calculations were made in U.S. Customary Units. All data presented in this report are referred to the stability-axis system as indicated in figure 2. The location of the moment reference center is shown

in figure 3(a) at a point 25 percent of the theoretical wing root chord. The nozzle thrust components have been taken out of the data to obtain the aerodynamic coefficients defined below:

A aspect ratio, b^2/S

b wing span, 54.36 cm

C_D aerodynamic drag coefficient, $\frac{\text{Drag}}{q_\infty S}$

ΔC_D aerodynamic drag increment due to blowing ($C_D - C_{D,jo}$) or to adding a strake ($C_{D,\text{strake on}} - C_{D,\text{strake off}}$)

$C_{D,jo}$ aerodynamic drag coefficient with jet off

$C_{D,o}$ minimum aerodynamic drag coefficient

C_L aerodynamic lift ccefficient, $\frac{\text{Lift}}{q_\infty S}$

ΔC_L aerodynamic lift increment due to blowing ($C_L - C_{L,jo}$) or to adding a strake ($C_{L,\text{strake on}} - C_{L,\text{strake off}}$)

$C_{L,ind}$ lift coefficient at zero angle of attack due to jet-induced camber effect

$C_{L,jo}$ aerodynamic lift coefficient with jet off

$C_{L,p}$ potential lift coefficient

$C_{L,tot}$ potential lift plus vortex lift coefficient

$C_{L,vle}$ leading-edge vortex lift coefficient

$C_{L,vse}$ side-edge vortex lift coefficient

C_l aerodynamic rolling-moment coefficient, $\frac{\text{Rolling moment}}{q_\infty Sb}$

C_{l_β} rolling moment due to sideslip, $\frac{\partial C_l}{\partial \beta}$, per deg

C_m aerodynamic pitching-moment coefficient, $\frac{\text{Pitching moment}}{q_\infty Sc}$

C_n aerodynamic yawing-moment coefficient, $\frac{\text{Yawing moment}}{q_\infty Sb}$

C_{n_β} yawing moment due to sideslip, $\frac{\partial C_n}{\partial \beta}$, per deg

C_Y aerodynamic side-force coefficient, $\frac{\text{Side force}}{q_\infty S}$

C_{Y_β} side force due to sideslip, $\frac{\partial C_Y}{\partial \beta}$, per deg

C_μ jet momentum coefficient, $\dot{w}V_j/gq_\infty S$

c local wing chord, cm

c_f local flap chord, cm

c_{th} theoretical wing root chord with leading and trailing edges extended to plane of symmetry, cm

$\bar{c}$ wing mean geometric chord, cm

d nozzle diameter, cm

g gravitational acceleration, 9.8 m/sec^2

h height of nozzle center line above upper surface, cm

i_C canard incidence angle with respect to body horizontal line (positive with leading edge up), deg

M_∞ free-stream Mach number

p_∞ free-stream static pressure, Pa

$p_{t,p}$ stagnation pressure in settling chamber, Pa

q_∞ free-stream dynamic pressure, Pa

r radius, cm

S wing reference area with leading and trailing edges extended to plane of symmetry, cm^2

S_C exposed canard area, cm^2

S_H exposed horizontal-tail area, cm^2

S_T exposed vertical-tail area, cm^2

s	leading-edge suction parameter
$T_{t,p}$	average stagnation temperature in settling chamber, ^{o}R
V_j	jet velocity reached by isentropic expansion from stagnation pressure at nozzle exit to free-stream pressure, m/sec
V_∞	free-stream velocity
$\dot{w}$	nozzle air weight flow rate, N/sec
α	angle of attack, deg
β	angle of sideslip, deg
δ_l	left aileron deflection angle (positive with trailing edge down), deg
δ_r	right aileron deflection angle (positive with trailing edge down), deg
δ_{le}	leading-edge flap deflection angle, deg
δ_{te}	trailing-edge flap deflection angle, deg
η_i	trailing-edge aileron inboard span station
η_o	trailing-edge aileron outboard span station
Λ_{le}	sweep angle of lifting surface leading edge, deg
Λ_n	sweep angle of nozzle, deg

DESCRIPTION OF MODEL

Geometric details of the general research model are presented in figure 3; the canard, wing, horizontal-tail, and vertical-tail arrangements are shown. Photographs of the various model configurations installed in the wind tunnel are shown in figure 4. Table I contains the pertinent geometric parameters associated with the model.

The untwisted wing on the model in figure 3(a) is shown in detail in figure 3(b). The wing had a leading-edge sweep angle of 44° and varied linearly from an NACA 64A006 airfoil section at the wing root (the root of the wing is taken at the intersection of the fuselage and wing) to an NACA 64A004 airfoil section at the tip. The full-span leading-edge flaps, which added twist and camber to the wing when deflected, had a constant chord of 15 percent of the wing root chord and consisted of five spanwise segments, which are numbered for convenience. The trailing-edge flaps, which extended from the wing-fuselage intersection to 70 percent of the wing semispan, had local chords which were 20 percent of the local wing chords.

The canard, horizontal tails, and vertical tail used in this study (see fig. 3(a)) had neither twist nor camber and consisted of circular-arc airfoil sections whose thickness varied linearly from 6 percent of the chord at the root to 4 percent of the chord at the tip. The canard and horizontal tail were vertically positioned to be in the wing chordal plane; the vertical tail was located in the plane of symmetry of the model. The canard incidence angle could be set at 0° or 10°.

The general location and orientation of the spanwise blowing nozzles are illustrated in figure 3(a) for the various blowing arrangements evaluated in this investigation. More detailed geometric information is presented in figures 5 and 6. Two pair of convergent nozzles were used during the tests: one pair for the 44° swept trapezoidal wing, and a second pair for the canards. Each nozzle was made of stainless steel tubing. The inner diameter of the tubing converged from 0.775 cm for the wing and 0.508 cm for the canard to the respective exit diameter d shown in figure 5. The nozzles for the 44° swept trapezoidal wing extended through the fuselage and rested on the upper surface of the wing at a point approximately 23 percent of the wing root chord aft of the leading edge. The exit diameters of the right and left nozzles differed slightly for both pair. (See insert in fig. 5.) The canard nozzles were smaller than the wing nozzles. This difference reflected the lower blowing rates needed on the smaller canard surface. The canard nozzle was located at 50-percent canard root chord to enable variation of canard incidence angle without changing the nozzle location relative to the canard surface. Each canard nozzle was positioned approximately 2.33 nozzle exit diameters above the canard surface. As reference 32 explains, the differences in the sweep angles between the left and right nozzles for the wing and canard have little effect on the aerodynamic characteristics.

A continuous-flow air system was used to provide the desired dry high pressure air to each set of convergent nozzles (fig. 6). High pressure air was delivered through brass tubing which was fed through the sting. The tubing was coupled to the aft end of a six-component strain-gage balance in the model by means of a flare fitting. Airflow was routed around the balance and piped into a single, cylindrical plenum chamber located in the forward section of the model. Allen head pipe plugs were used to secure the pair of tapped holes that were not used during a given series of test runs.

APPARATUS, TESTS, AND CORRECTIONS

The present investigation was conducted in the Langley high-speed 7- by 10-foot tunnel. Six-component force and moment data were recorded by means of an internally mounted strain-gage balance. High pressure air was routed around this balance by means of two stainless steel S-shaped tubes 0.635 cm in diameter. This air-balance system is unique because the high pressure air delivery system is combined with the balance assembly so that the balance sensitivities are essentially independent of air pressure. The stagnation pressure in the plenum chamber was monitored and recorded by means of a 3.45-MPa pressure

transducer located within the model. A pressure probe and an iron-constantan thermocouple were used to monitor the plenum chamber total pressure and total temperature, respectively.

Nozzle air weight flow rate was determined by means of a venturi flowmeter located outside of the tunnel. The temperature and absolute pressure at the flowmeter inlet were monitored. Also monitored was the differential pressure across the throat, from which an air weight flow rate was determined.

The jet momentum coefficient C_μ is defined as $\dot{w}V_j/gq_\infty S$ where $\dot{w}$ is the measured air weight flow rate. The parameter V_j is the jet velocity reached by isentropic expansion from the stagnation pressure at the nozzle exit to free-stream static pressure. Taking the ratio of specific heats for air to be 1.4 yields

$$V_j = 109.6 \sqrt{T_{t,p}\left[1 - (p_\infty/p_{t,p})^{2/7}\right]} \tag{1}$$

This expression is identical to the one used for V_j in reference 23. Since the jet momentum coefficient varied slightly during a given test run, an average jet momentum coefficient was computed. For convenience, this term is designated C_μ and is used to identify the data. The C_μ values for each data point are presented in reference 32.

Each nozzle arrangement was statically calibrated in the tunnel with all lifting surfaces removed to obtain six-component force and moment data as a function of plenum total pressure. Details of all the calibrations are presented in reference 32 with additional measurements that show the total pressure at the nozzle exit to be essentially equal to the plenum total pressure for a wide range of plenum total pressure.

Tests were made at free-stream Mach numbers up to 0.50 for a free-stream Reynolds number of 2.48×10^6 based on wing mean aerodynamic chord at angles of attack from approximately -2° to 20° at sideslip angles of 0°, 4°, and -4°. The model angle of attack and sideslip angle were corrected for deflections of the balance and sting support system due to aerodynamic load. Fuselage base-cavity pressures were measured during the test, and the drag coefficients were corrected to a zero base-drag condition. Jet boundary and blockage corrections were evaluated by the method of reference 33 and were found to be negligible. Therefore, they were not applied to the data.

RESULTS AND DISCUSSION

The experimental data obtained during the wind-tunnel tests are presented in tabulated form in reference 32. The nozzle thrust components have been taken out of these data to obtain the aerodynamic coefficients that are presented in the following discussion.

44° Swept Trapezoidal Wing

Flaps undeflected.- The effect of spanwise blowing on the longitudinal aerodynamic characteristics of the 44° swept trapezoidal wing configuration is presented in figures 7 and 8 for $M_\infty = 0.30$ and 0.50, respectively. The differences between the C_μ values for these two free-stream Mach numbers are due to the differences in free-stream dynamic pressure. The data indicate that blowing results in vortex lift, increases the maximum C_L as well as the angle of attack where this maximum C_L occurs, improves the drag polars at high C_L, and provides a linear pitching moment throughout the C_L range. Since the stability level is unchanged with blowing, the wing center-of-pressure location remains approximately the same with and without blowing. These experimental trends can be better understood if they are compared with theoretical predictions which assume a stable, fully developed leading-edge vortex flow. The theoretical calculations presented here were obtained for zero leading-edge suction by using the leading-edge suction analogy method outlined in reference 34. The solid line represents attached, potential flow calculations, whereas the curve with long and short dashes represents the calculations for the full naturally generated vortex flow condition. It should be kept in mind that this theory does not account for the level of blowing but represents the full vortex-lift increments that would be expected if the fully developed vortex flow were generated and no vortex breakdown occurred. Comparing the lift data for $C_\mu = 0$ with the lift estimates indicates that the wing develops some vortex lift, although the leading-edge vortex appears to break down at relatively low angles of attack. Spanwise blowing provides favorable spanwise flow gradients that delay the vortex breakdown to higher angles of attack; as a result, there are significant increases in vortex-induced lift increments. The lift data obtained at the highest C_μ value agree reasonably well throughout the angle-of-attack range with the full vortex-lift estimate. The data suggest that with increased levels of blowing, the lift data would exceed the full vortex-lift estimate. This result has also been pointed out in reference 23.

At $\alpha = 0°$, where there is no leading-edge vortex, a small increase in C_L, defined as $C_{L,ind}$, occurs when spanwise blowing is applied. This trend has been attributed in references 22 and 26 to a jet-induced camber effect. The theoretical estimate for full vortex lift was modified to account for this jet-induced effect by adding the $C_{L,ind}$ value achieved at the highest C_μ to the full vortex-lift estimates. The resulting calculation (short-dash curve) is in better agreement with experiment at the low-to-moderate angles of attack.

Comparison between the theoretical and experimental drag-due-to-lift information shows that, for the potential flow case with the leading-edge suction omitted, $C_{L,p} \tan \alpha$ overestimates the experimental drag due to lift obtained for the blowing-off condition ($C_\mu = 0$) up to the higher C_L values. Because the wing has a leading-edge radius, it develops some leading-edge suction force. Comparison with the full suction lower bound $C_L^2/\pi A$ indicates, however, that the suction diminishes rapidly with increasing C_L. Since partial leading-edge suction is being developed, the drag is dependent on both C_L and α. Therefore, there is improvement in the drag polar due to spanwise blowing. Reducing α for a given C_L also results in a drag reduction. The difference in the theoretical values for $C_{L,p} \tan \alpha$ and $C_{L,tot} \tan \alpha$ illustrates this trend.

The effect of C_μ and M_∞ on the lift augmentation ratio $\Delta C_L/C_\mu$ and on the lift effectiveness of blowing $C_L/C_{L,jo}$ at an angle of attack of approximately 21° is presented in figure 9. The value ΔC_L is defined as the difference between jet-on C_L values and jet-off C_L values ($C_{L,jo}$). Spanwise blowing exceeds the effect of vectoring the thrust downward and perpendicular to the free stream. This vectoring would result in a lift augmentation ratio of 1 (long-dashed line). In fact, the highest augmentation ratios occur at the lowest C_μ values. In addition, the lift effectiveness of blowing increases as C_μ increases and approaches the theoretical values given by $C_{L,tot}/C_{L,p}$ (solid lines and those with long and short dashes) at the higher values of C_μ.

For the limited range of jet-momentum coefficient available for comparison, spanwise blowing is more effective in generating lift at the higher free-stream Mach number ($M_\infty = 0.50$). Similar results were reported in reference 25 for a semispan, cambered wing configuration with body and horizontal tail, where blowing at $M_\infty = 0.75$ was found to be more effective than at $M_\infty = 0.30$.

Figure 10 illustrates the effect of C_L and C_μ on the aerodynamic drag reduction ratio $\Delta C_D/C_\mu$ for $M_\infty = 0.30$ and 0.50, where ΔC_D is the difference between jet-on C_D values and jet-off C_D values ($C_{D,jo}$). At low values of lift, spanwise blowing results in a drag increase, while at the higher values of lift, blowing results in a significant reduction in drag. In fact, at the highest values of C_L, spanwise blowing becomes more effective than vectoring the thrust aft and parallel to the free stream, which would result in a drag reduction ratio of 1 (short-dashed curve). As mentioned earlier, the drag reduction is associated with the reduced angle of attack required for a given C_L which, for cases where the leading-edge suction is not developed, results in a drag reduction.

Figure 11 illustrates a comparison of the longitudinal aerodynamic performance of spanwise blowing at $M_\infty = 0.30$ (see fig. 7) with another maneuver concept, a sharp, highly swept wing strake. Data for the wing-strake configuration are taken from reference 35 and were obtained at $M_\infty = 0.40$. The authors used the same wing planform, but the fuselage had a different cross-sectional shape and a smaller cross-sectional area than the fuselage used in the present study. The aerodynamic coefficients are based on the respective reference characteristics from each investigation. Pitching moments are taken about the moment reference center used in the present study. The strake-off data from reference 35 are shown for reference.

Spanwise blowing and a wing strake result in comparable lift and drag benefits at the moderate to high angles of attack. The benefits are due to leading-edge vortex enhancement on the main wing panel. At the higher blowing rate ($C_\mu = 0.128$), the benefits exceed those of the strake, except at the higher angles of attack where the performances of spanwise blowing and a strake are nearly coincident. These comparisons, however, must be viewed in light of the dependence of spanwise blowing on available bleed air on existing airplanes. One benefit of the spanwise blowing and wing-strake concepts is, of course, that higher lifts (or load factors) can be provided without the wing weight penalty which would be associated with the larger wing area

required to accomplish the same improvement. In the case of spanwise blowing, however, the reduced wing weight must be weighed against other considerations such as ducting or air source.

Pitching-moment characteristics with spanwise blowing or a wing strake are reasonably linear throughout the test lift coefficient range. Adding a strake results in a lower stability level because of the additional lifting area ahead of the moment reference center. Note that the configuration with $C_\mu = 0$ (from ref. 35) has a different stability level than that obtained for the current configuration. (See fig. 7.)

Leading-edge flap deflection.- The effects of spanwise blowing on the longitudinal aerodynamic characteristics of the 44° swept trapezoidal wing configuration are presented in figures 12 to 19 for a range of leading-edge flap deflection angles for $M_\infty = 0.30$ and $\delta_{te} = 0°$. The $\delta_{le} = 4°$ and 8° data are presented in figures 12 and 13, respectively, together with theoretical calculations which account for the effect of leading-edge vortex flows on cambered and twisted wing aerodynamics as outlined in reference 34. The experimental results obtained with spanwise blowing in conjunction with a deflected leading-edge flap are similar to results obtained for the $\delta_{le} = 0°$ case.

One of the assumptions in the theoretical method from reference 34 is that the vortex-lift vector is rotated so that it is normal to the leading-edge flap chord; thus, unlike the case for the uncambered wing, the theoretical drag polar cannot be defined by the simple relation $C_D = C_{L,tot} \tan \alpha$. Therefore, no theoretical drag curve is presented to account for $C_{L,ind}$ effects.

This assumption appears to be justified by the agreement with experiment. The vortex-induced lift and drag benefits due to spanwise blowing at the highest C_μ are predicted very well by the theory which assumes full vortex lift and zero leading-edge suction (curves with long and short dashes in figs. 12 and 13).

References 22 and 26 indicate that jet spreading and leading-edge vortex instability occur as span distance increases, and that the jet has the largest effect on stabilizing the leading-edge vortex at inboard stations. These studies provided the basis for testing a configuration with a modified leading edge featuring differential deflections of a segmented leading-edge flap, and data for this configuration are presented in figure 14. At the inboard stations where the jet is most effective, the leading-edge flap segments I and II were undeflected. As span distances increased, leading-edge flap segments III, IV, and V were deflected to 4°, 8°, and 12°, respectively. In this manner, stabilizing the leading-edge vortex inboard was attempted as was maintaining attached flow near the leading edge farther outboard. The data for this configuration are similar to the $\delta_{le} = 8°$ case; this similarity is also seen in figure 15 which summarizes the effects of C_μ and δ_{le} on $\Delta C_L/C_\mu$ and $C_L/C_{L,jo}$ for an α of approximately 20°. Deflecting the leading-edge flap downward reduces $\Delta C_L/C_\mu$ and $C_L/C_{L,jo}$ throughout the C_μ range. This deflection is consistent with the leading-edge suction analogy, where the leading-edge flap deflection moves the stagnation point closer to the leading edge and reduces the available edge suction. It should be noted that the lift effectiveness of blowing for each of three δ_{le} values approaches or exceeds

theoretical estimates given by $C_{L,tot}/C_{L,p}$ (solid lines, lines with short dashes, and lines with long and short dashes) at the higher C_μ values.

Figure 16 presents the effect of C_L and C_μ on the percent leading-edge suction developed by the wing for a range of leading-edge flap deflection angles. The leading-edge suction parameter s, as presented here, simply represents the location of the experimental drag data in relation to the zero and full leading-edge suction boundaries shown in figures 7, 12, and 13. Although the full leading-edge suction boundaries defined by $C_L^2/\pi A$ remain the same for all cases, the zero leading-edge suction boundary is raised as leading-edge flap deflection angle increases because of the improved lift-curve slope exhibited by the twisted and cambered wing.

Deflecting the leading-edge flap downward (blowing off) results in a higher percentage of suction at the higher lift coefficients than was obtained for the basic wing ($\delta_{le} = 0^o$). The percent suction decreases to 0 at the higher values of C_L with the onset of flow separation at the leading edge. Spanwise blowing results in leading-edge suction percentages that exceed those obtained for the blowing-off case at the moderate to high lift coefficients. In addition, the percent suction developed by the wing (blowing on) is essentially unaffected by small deflections of the leading-edge flap.

Figures 17 and 18 are summary plots for the blowing-off and blowing-on cases, respectively. These figures show the effect of leading-edge flap deflection angle on the longitudinal aerodynamic characteristics for $M_\infty = 0.30$. In both figures the data indicate a slight decrease in lift at the low to moderate angles of attack because of deflection of the leading-edge flap. At the higher angles of attack, with blowing off, the deflected leading-edge flap tends to maintain attached flow near the leading edge, as evidenced by a delay in wing stall. With blowing on, the reduction in lift coefficients due to the deflected flap becomes negligible at the highest angle of attack.

Drag-due-to-lift characteristics obtained for the $\delta_{le} = 0^o$ case are improved by deflecting the leading-edge flap downward. The lowest drag-due-to-lift values for blowing off or blowing on correspond to the $\delta_{le} = 8^o$ configuration. The data suggest that the jet-induced vortex system on the cambered leading edge results in a polar with reduced drag at a given lift coefficient; this trend is most important from a sustained maneuver standpoint.

The effects of leading-edge flap deflection on the lift and drag increments caused by spanwise blowing are shown in figure 19 for $M_\infty = 0.30$. Additional data are presented for lift and drag increments resulting from the addition of a strake to the same wing planform (ref. 36). As previously discussed, these strake results were obtained at $M_\infty = 0.4$ by using the smaller fuselage. The lift and drag coefficients are based on the respective wing reference areas from each investigation.

The favorable lift increments due to blowing which occur for the $\delta_{le} = 0^o$ case are reduced at the moderate to high angles of attack when the leading-edge flap is deflected. This reduction in lift is directly reflected in a reduction in the favorable drag benefits due to blowing. The trends discussed here for lift and drag increments due to blowing are similar to the trends obtained by

adding a maneuver strake to a plain wing and a flapped wing. It should be noted that the ΔC_D values for the strake were plotted against the wrong parameter (α) in figure 9 of reference 36, but were correctly plotted as a function of C_L in figure 19.

The results shown in figures 12 to 19 suggest that blowing in combination with the cambered and twisted leading edge enables recovery of some of the thrust lost due to separation at the leading edge. Improving the drag polar by contouring the wing leading edge in combination with spanwise blowing to improve drag characteristics has been investigated in reference 25. The favorable trends thus far observed with spanwise blowing on the moderately swept trapezoidal wing with deflected leading-edge flap are analogous to those observed in reference 37 for a highly swept delta wing with cambered leading edge.

Trailing-edge flap deflection.- Figures 20 and 21 illustrate the effect of spanwise blowing in combination with a partial-span trailing-edge flap deflected to 10° and 20°, respectively, on the longitudinal aerodynamic characteristics for $M_\infty = 0.30$ and $\delta_{le} = 0^\circ$. The blowing-off data for the basic wing ($\delta_{le} = \delta_{te} = 0^\circ$) are shown for reference. The effect of blowing in conjunction with a deflected trailing-edge flap is similar to effects observed for the case with no flap deflection.

The lift and drag benefits due to spanwise blowing at the higher C_μ in combination with a deflected trailing-edge flap are more favorable than the benefits that would be attained by adding the effects of spanwise blowing or by a deflected flap acting alone (short-dashed curve). This example of aerodynamic synergism, discussed in reference 38 for a canard-wing configuration, may result from an increase in blowing effectiveness owing to the increased camber near the wing trailing edge in addition to improvement in trailing-edge flap effectiveness at the higher angles of attack.

Figure 22 shows the effect of C_μ and δ_{te} on $\Delta C_L/C_\mu$ and $C_L/C_{L,jo}$ for α approximately 21°. The data reveal that for a given C_μ, increased δ_{te} increases the lift augmentation ratio and the lift effectiveness of blowing.

Leading- and trailing-edge flap deflection.- The longitudinal characteristics obtained for the case with spanwise blowing in combination with leading- and trailing-edge flaps deflected to 8° and 10°, respectively, are compared in figure 23 with the data from figure 20. These data were obtained by blowing on the wing with a trailing-edge flap deflected to 10° ($\delta_{le} = 0^\circ$). The blowing-off data for the basic wing ($\delta_{le} = \delta_{te} = 0^\circ$) are shown for reference. The deflected leading-edge flap delays the more beneficial lift effects due to blowing to higher angles of attack. The best drag-polar shape, however, was obtained when both flaps were deflected; this observation suggests that spanwise blowing on an advanced fighter configuration employing the variable-camber concept may offer substantial improvement in maneuver performance.

Asymmetric spanwise blowing.- In order to evaluate asymmetric blowing as a roll control device, blowing was initiated on the right wing of the 44° swept

trapezoidal wing configuration for $M_\infty = 0.30$ and $\delta_{le} = \delta_{te} = 0^\circ$. The corresponding longitudinal aerodynamic characteristics are presented in reference 32.

The effect of α and C_μ on the lateral-directional characteristics is shown in figure 24. This figure also shows unpublished data obtained at the Langley Research Center for a differential-strake configuration (right strake off) for $M_\infty = 0.30$. Nozzle thrust effects are included in the coefficients, and in addition, the signs of the data for the asymmetric strake have been reversed in order to make a comparison between the two configurations. The coefficients for the strake data are based on the reference values of $S = 10.3$ cm^2 and $b = 50.8$ cm. With blowing off, C_l is essentially zero throughout the test angle-of-attack range. Asymmetric blowing or a differential wing strake results in small positive values of C_l at the low angles of attack that indicate a right-wing-down moment. At moderate to high angles of attack, asymmetric blowing or a differential strake results in large negative values of C_l. These negative values indicate right-wing-up rolling moment and adverse yawing moments. The C_l value becomes increasingly negative with increased angle of attack and increased C_μ. At the lower blowing rate ($C_\mu = 0.034$) and the higher angles of attack, asymmetric blowing results in C_l values that compare quite favorably with those obtained with a differential strake. Similar levels of yawing moment and side force are generated with each lateral control device.

The dashed line in figure 24 was obtained by using the theoretical method of reference 39 to estimate the rolling-moment coefficient due to plain trailing-edge ailerons. The aileron geometry was assumed to have the following characteristics: $c_f/c = 0.30$; $\eta_i = 0.75$; $\eta_o = 0.95$; $\delta_l = -15^\circ$; and $\delta_r = 15^\circ$. At the higher angles of attack, the effect of asymmetric blowing exceeds the theoretical rolling-moment coefficient of -0.0105 caused by the 15° aileron deflection. At $\alpha = 20^\circ$ the aileron deflection required to achieve the level of rolling moment provided by asymmetric spanwise blowing would exceed 60°.

Horizontal tail.- The effect of spanwise blowing on the longitudinal characteristics of the configuration with 44° swept trapezoidal wing and horizontal tail is presented in figure 25 for $M_\infty = 0.30$ as are theoretical calculations from reference 34 which account for the effect of leading-edge vortex flows on wing-tail aerodynamics. The discussion of the effects of blowing on the wing with the horizontal tail off (see fig. 7) applies to the data presented in figure 25 and the reader is referred to the section entitled "Flaps undeflected" for a detailed analysis. Comparison of the data with horizontal tail on (fig. 25) and off (fig. 7) shows that blowing slightly reduces the lift and nose-down pitching-moment contribution of the horizontal tail, particularly at the higher values of C_L.

The effect of adding a horizontal tail on $\Delta C_L/C_\mu$ and $C_L/C_{L,jo}$ is shown in figure 26 for $C_\mu \approx 0.060$. Blowing on the configuration with wing and horizontal tail is less effective at the moderate to high angles of attack than is blowing on the wing with tail off.

Vertical tail.- Figures 27 and 28 illustrate the effect of spanwise blowing on the lateral-directional stability characteristics of a configuration with wing and vertical tail for $M_\infty = 0.30$. With blowing off, unfavorable breaks occur in the effective dihedral and directional stability parameters, C_{l_β} and C_{n_β}, at moderate angles of attack. Spanwise blowing results in stabilizing increments in C_{l_β} and C_{n_β} at the higher angles of attack, with little or no effect on the lateral-directional stability at low angles of attack. Figure 28 presents the increments in C_{n_β} and C_{l_β} caused by application of spanwise blowing or the addition of a wing strake to the same wing planform (ref. 40). The favorable increments in C_{n_β} and C_{l_β} at the moderate to high angles of attack due to spanwise blowing or a wing strake suggest that each maneuver device may favorably affect the static lateral-directional stability. Data from this figure are inconclusive but suggest that the large benefits in longitudinal characteristics resulting from the application of blowing or the addition of a strake may be achieved without adversely affecting the lateral-directional stability characteristics.

The data in figure 29 indicate that for blowing off, addition of a horizontal tail to the configuration with wing and vertical tail prevents the unfavorable stability break in the effective dihedral parameter C_{l_β} that was observed in figure 27 for the case with the horizontal tail off. With blowing on, a favorable increment in C_{l_β} occurs throughout the angle-of-attack range; typically this increment increases with increased C_μ. As was observed in figure 27 for the case with horizontal tail off, blowing delays the unfavorable break in directional stability to higher angles of attack.

Close-Coupled Canard-Wing Configuration

Blowing on the wing.- The longitudinal characteristics that result from spanwise blowing on the 44° swept trapezoidal wing in the presence of a close-coupled canard are shown in figures 30 and 31 for $M_\infty = 0.30$ and 0.50, respectively, and for $i_c = 0°$. Also shown in the figures are theoretical calculations using the method outlined in reference 34 which account for the effect of leading-edge vortex flows on canard-wing aerodynamics. The trends with spanwise blowing shown in figures 30 and 31 are similar to those observed for the wing-alone case (see figs. 7 and 8, for example); therefore, no additional discussion of these trends is presented in this paper.

As shown in figure 32 for $M_\infty = 0.30$, the effect of spanwise blowing is more pronounced when the canard incidence angle i_c is increased to 10°. The favorable lift benefits due to blowing are larger at the higher angles of attack where the configuration has reached maximum C_L. The drag polar improvement due to blowing is similar to the improvement shown in figure 30 for $i_c = 0°$. The pitching-moment results show a favorable effect on the

stability level compared with the blowing-off case at the higher lift values but show pitch up at the highest values of C_L.

Blowing on the canard.- The longitudinal characteristics that result because of spanwise blowing on the canard are shown in figures 33 and 34 for $i_c = 0^o$ and 10^o, respectively, for $M_\infty = 0.30$. The jet momentum coefficients for the canard-blowing case are less than the values for C_μ for the wing-blowing case because the canard has a smaller converging nozzle size. The trends with canard blowing shown in figures 33 and 34 are similar to those observed in figures 30 and 32 for the wing-blowing case for $i_c = 0^o$ and 10^o, respectively. Canard spanwise blowing has a slight destabilizing effect at high lift levels, which reflects the increased canard lift. At the higher values of lift, pitching moment is relatively constant with C_L, and thus indicates neutral stability.

The longitudinal aerodynamic characteristics obtained for the wing- and canard-blowing cases are compared in figures 35 and 36 for $i_c = 0^o$ and 10^o, respectively. The data indicate that blowing on the canard with $C_\mu = 0.030$ results in lift and drag characteristics that compare favorably with those obtained by blowing on the wing with $C_\mu = 0.058$. These results imply that if air is supplied by engine bleed, spanwise blowing on the canard requires less bleed air than that required by spanwise blowing on the wing in order to produce comparable lift and drag benefits. Furthermore, for $i_c = 10^o$, the wing-blowing case exhibits unfavorable longitudinal stability trends at the moderate to high values of lift, whereas the canard-blowing case exhibits essentially neutral stability for the same range of lift coefficient.

One of the problems associated with the design of a close-coupled canard-wing configuration as a highly maneuverable aircraft is the provision of an optimum method of longitudinal trim control. Reference 41 has indicated that if trim is obtained by changing the canard incidence, a more highly swept canard seems warranted in order to alleviate canard stall at high angles of attack. Such configurations, however, tend to exhibit high induced-drag characteristics and tend to have high trim drag. Spanwise blowing on the canard may offer one means of alleviating this problem. Leading-edge vortex augmentation by spanwise blowing on a moderately swept canard would alleviate canard stall at high angles of attack and would also avoid the high induced drag and trim drag that a highly swept canard would be expected to exhibit. Reference 29 has also indicated that a modest amount of spanwise blowing on a canard at low speed would reduce canard size and permit a more optimum canard to be used in cruise.

Figure 37 presents the effect of C_μ, jet location, and M_∞ on $\Delta C_L/C_\mu$ and $C_L/C_{L,jo}$ for the canard-wing configuration at $\alpha \approx 21^o$ and with $i_c = 0^o$. For the wing-blowing case, spanwise blowing is more effective at the higher Mach number ($M_\infty = 0.50$), as evidenced by higher values of $\Delta C_L/C_\mu$ and $C_L/C_{L,jo}$. These results suggest that the spanwise blowing concept may be an effective means of augmenting maneuvering lift of fighter aircraft at higher subsonic free-stream Mach numbers. Reference 25 has noted, however, that a deterrent to utilization of spanwise blowing at transonic Mach numbers may be the lack of engine bleed air to supply the momentum required for effective vortex augmentation.

The canard-blowing case exhibits higher values of $\Delta C_L/C_\mu$ and $C_L/C_{L,j_o}$ than those obtained for the wing-blowing case for the narrow band of comparable C_μ values shown in figure 37 for $M_\infty = 0.30$. Similar trends are shown in figure 38 for $i_C = 10^o$. There are several reasons for these trends. First, for the same amount of blowing, it is more efficient to blow on the canard than on the wing because of the canard's smaller surface. Second, the benefits of blowing on the wing are delayed somewhat because of canard downwash.

Figure 39 presents the longitudinal aerodynamic performance of canard spanwise blowing and of a straked canard of larger planform (data from ref. 42). The data from reference 42 were obtained by using the smaller fuselage previously discussed. The coefficients are based on the respective reference characteristics from each study, and moments are taken about the moment reference center from the present investigation. The wing-alone data without blowing are shown in the figure for reference.

The intermediate-size canard featuring a moderate amount of blowing ($C_\mu = 0.030$) produces lift and drag benefits that are quite similar to those obtained for the large, straked-canard configuration in reference 42. In addition, the canard with spanwise blowing results in a higher stability level than that obtained for the large, straked canard.

CONCLUSIONS

A generalized wind-tunnel model has been tested in the Langley high-speed 7- by 10-foot tunnel to investigate new component concepts using spanwise blowing to provide improved maneuver characteristics for advanced fighter aircraft. Primary emphasis was placed on performance, stability, and control at high angles of attack and subsonic speeds. Since separation-induced vortex flows have been shown under certain conditions to increase maneuver performance significantly, the investigation was focused on various methods of controlling and delaying the leading-edge vortex breakdown and of optimizing component interactions. In particular, spanwise blowing was used on a 44^o swept trapezoidal wing to determine the effect of leading-edge vortex enhancement on leading- and trailing-edge flap effectiveness, horizontal- and vertical-tail effectiveness, and close-coupled canard wing interactions, and to assess spanwise blowing as a roll control device. These results were compared with data for other maneuver concepts such as strakes and canards. As a result of this study, the following conclusions can be made:

1. Spanwise blowing results in substantial improvement in the performance of the 44^o swept trapezoidal wing configuration at high angles of attack. In particular, significant vortex-induced lift increments occur at the higher angles of attack with subsequent improvement in the drag polar.

2. The longitudinal aerodynamic performance benefits due to spanwise blowing compare favorably with the performance benefits due to a wing strake.

3. Spanwise blowing is more effective at higher subsonic Mach numbers and represents a means of enhancing the higher subsonic maneuver performance of

fighter aircraft. The viability of spanwise blowing at high subsonic free-stream Mach numbers is, however, dependent on engine bleed air availability.

4. Deflecting a leading-edge flap delays the more beneficial blowing-induced effects to higher angles of attack; Ray, McKinney, and Carmichael (NASA TN D-7131) obtained similar results for a flapped wing with strake. A forward rotation of the vortex-lift vector occurs, however, and the subsequent thrust recovery results in drag-polar improvement.

5. Spanwise blowing effectiveness is enhanced by combining blowing with a deflected trailing-edge flap. In addition, blowing may improve trailing-edge flap effectiveness.

6. Asymmetric blowing is an effective lateral control device at high angles of attack.

7. Adding the horizontal tail reduces the lift effectiveness of blowing at the higher angles of attack.

8. The lateral-directional stability characteristics of the configurations with (a) wing and vertical tail and (b) wing, horizontal tail, and vertical tail are improved at the higher angles of attack by spanwise blowing on the wing. In particular, blowing results in stabilizing increments in the effective dihedral and directional stability parameters and delays the unfavorable break in the directional stability parameter to much higher angles of attack.

9. Spanwise blowing on configurations with wing and vertical tail exhibited lateral-directional stability similar to that achieved with a wing-strake configuration. The results suggest that the significant benefits in longitudinal aerodynamic characteristics due to applying blowing or adding a strake may be obtained without adverse effects on lateral-directional stability.

10. For a close-coupled canard-wing configuration, spanwise blowing on the canard is more effective than spanwise blowing on the wing.

11. The longitudinal aerodynamic performance of canard spanwise blowing compares favorably with results obtained for a straked canard-wing configuration without blowing.

12. The leading-edge suction analogy was used for selected configurations and provided reasonable estimates for the longitudinal aerodynamic characteristics due to spanwise blowing.

Langley Research Center
National Aeronautics and Space Administration
Hampton, VA 23665
November 7, 1977

REFERENCES

1. Werlé, H.: Partage et Recontre d'Écoulements Fluides. Étude Effectuée à la Cuve à Huile et au Tunnel Hydrodynamic à Visualisation de l'O.N.E.R.A. La Rech. Aeron., no. 79, Nov.-Dec. 1960, pp. 9-26.

2. Brown, Clinton E.; and Michael, William H., Jr.: On Slender Delta Wings With Leading-Edge Separation. NACA TN 3430, 1955.

3. Mangler, K. W.; and Smith, J. H. B.: A Theory of the Flow Past a Slender Delta Wing With Leading Edge Separation. Proc. Roy. Soc. (London), ser. A, vol. 251, no. 1265, May 26, 1959, pp. 200-217.

4. Hummel, D.: Experimental Investigation of the Flow on the Suction Side of a Thin Delta Wing. Z. Flugwiss., Jahrg. 13, Heft 7, July 1965, pp. 247-252.

5. Legendre, Robert: Flow in the Neighborhood of the Apex of a Highly Swept Wing at Moderate Incidences. Presented at 8th Internat. Congress of Theoretical and Applied Mechanics (Istanbul, Turkey), Aug. 1952.

6. Marsden, D. J.; Simpson, R. W.; and Rainbird, W. J.: An Investigation Into the Flow Over Delta Wings at Low Speeds With Leading Edge Separation. Rep. No. 114, Coll. of Aeronaut., Cranfield (England), Feb. 1958.

7. Örnberg, Torsten: A Note on the Flow Around Delta Wings. KTH-Aero TN 38, Div. Aeron., Roy. Inst. Technol. (Stockholm), 1954.

8. Bartlett, G. E.; and Vidal, R. J.: Experimental Investigation of Influence of Edge Shape on the Aerodynamic Characteristics of Low Aspect Ratio Wings at Low Speeds. J. Aeronaut. Sci., vol. 22, no. 8, Aug. 1955, pp. 517-533, 588.

9. Küchemann, D.: A Non-Linear Lifting-Surface Theory for Wings of Small Aspect Ratio With Edge Separations. Rep. No. Aero 2540, British R.A.E., Apr. 1955.

10. Gersten, K.: Nichtlineare Tragflächentheorie insbesondere für Tragflügel mit kleinem Seitenverhältnis Ing.-Arch., Bd. XXX, 1961, pp. 431-452.

11. Polhamus, Edward C.: A Concept of the Vortex Lift of Sharp-Edge Delta Wings Based on a Leading-Edge Suction Analogy. NASA TN D-3767, 1966.

12. Polhamus, Edward C.: Application of the Leading-Edge-Suction Analogy of Vortex Lift to the Drag Due to Lift of Sharp-Edge Delta Wings. NASA TN D-4739, 1968.

13. Wentz, William H., Jr.; and Kohlman, David L.: Wind Tunnel Investigations of Vortex Breakdown on Slender Sharp-Edged Wings. NASA CR-98737, 1968.

14. Polhamus, Edward C.: Predictions of Vortex-Lift Characteristics by a Leading-Edge Suction Analogy. J. Aircr., vol. 8, no. 4, Apr. 1971, pp. 193-199.

15. Hummel, D.: Study of the Flow Around Sharp-Edged Slender Delta Wings With Large Angles of Attack. NASA TT F-15,107, 1973.

16. Cornish, J. J., III: High Lift Applications of Spanwise Blowing. ICAS Paper No. 70-09, Sept. 1970.

17. Werlé, H.; and Gallon, M.: Flow Control by Cross Jet. NASA TT F-14,548, 1972.

18. Werlé, Henri: Sur l'Écoulement au Bord d'Attaque d'un Profil Portant. La Rech. Aerospatiale, no. 4, July-Aug. 1973, pp. 197-218.

19. Dixon, C. J.: Lift Augmentation by Lateral Blowing Over a Lifting Surface. AIAA Paper No. 69-193, Feb. 1969.

20. Dixon, C. J.: Lift and Control Augmentation by Spanwise Blowing Over Trailing Edge Flaps and Control Surfaces. AIAA Paper No. 72-781, Aug. 1972.

21. Bradley, R. G.; and Wray, W. O.: A Conceptual Study of Leading-Edge-Vortex Enhancement by Blowing. AIAA Paper No. 73-656, July 1973.

22. Dixon, C. J.; Theisen, J. G.; and Scruggs, R. M.: Theoretical and Experimental Investigations of Vortex Lift Control by Spanwise Blowing. Volume I - Experimental Research. LG73ER-0169, Lockheed Aircraft Corp., Sept. 15, 1973.

23. Bradley, R. G.; Wray, W. O.; and Smith, C. W.: An Experimental Investigation of Leading-Edge Vortex Augmentation by Blowing. NASA CR-132415, 1974.

24. Theisen, Jerome G.; Scruggs, Roy M.; and Dixon, Charles J.: Theoretical and Experimental Investigations of Vortex Lift Control by Spanwise Blowing: Volume II, Three-Dimensional Theory for Vortex-Lift Augmentation. LG73ER-0169, U.S. Navy, Sept. 1973. (Available from DDC as AD 771 304.)

25. Bradley, R. G.; Whitten, P. D.; and Wray, W. O.: Leading-Edge-Vortex Augmentation in Compressible Flow. AIAA Paper No. 75-124, Jan. 1975.

26. Campbell, James F.: Effects of Spanwise Blowing on the Pressure Field and Vortex-Lift Characteristics of a 44° Swept Trapezoidal Wing. NASA TN D-7907, 1975.

27. Campbell, James F.: Augmentation of Vortex Lift by Spanwise Blowing. AIAA Paper No. 75-993, Aug. 1975.

28. Bradley, R. G.; Jeffries, R. R.; and Capone, F. J.: A Vectored-Engine-Over-Wing Propulsive-Lift Concept. AIAA Paper No. 76-917, Sept. 1976.

29. Jenkins, M. W. M.; and Meyer, R. T.: A Large-Scale Low-Speed Tunnel Test of a Canard Configuration With Spanwise Blowing. AIAA Paper No. 75-994, Aug. 1975.

30. Erickson, Gary E.; and Campbell, James F.: Flow Visualization of Vortices Locked by Spanwise Blowing Over Wings Featuring a Unique Leading- and Trailing-Edge Flap System. NASA TM X-72788, 1975.

31. Erickson, Gary E.; and Campbell, James F.: Flow Visualization of Leading-Edge Vortex Enhancement by Spanwise Blowing. NASA TM X-72702, 1975.

32. Erickson, Gary E.; and Campbell, James F.: Augmentation of Maneuver Performance by Spanwise Blowing. NASA TM X-73998, 1977.

33. Gillis, Clarence L.; Polhamus, Edward C.; and Gray, Joseph L., Jr.: Charts for Determining Jet-Boundary Corrections for Complete Models in 7- by 10-Foot Closed Rectangular Wind Tunnels. NACA WR L-123, 1945. (Formerly NACA ARR L5G31.)

34. Lamar, John E.; and Gloss, Blair B.: Subsonic Aerodynamic Characteristics of Interacting Lifting Surfaces With Separated Flow Around Sharp Edges Predicted by a Vortex-Lattice Method. NASA TN D-7921, 1975.

35. Henderson, William P.; and Huffman, Jarrett K.: Effect of Wing Design on the Longitudinal Aerodynamic Characteristics of a Wing-Body Model at Subsonic Speeds. NASA TN D-7099, 1972.

36. Ray, Edward J.; McKinney, Linwood W.; and Carmichael, Julian G.: Maneuver and Buffet Characteristics of Fighter Aircraft. NASA TN D-7131, 1973.

37. Wentz, W. H., Jr.: Effects of Leading-Edge Camber on Low-Speed Characteristics of Slender Delta Wings. NASA CR-2002, 1972.

38. Campbell, J. F.; Gloss, B. B.; and Lamar, J. E.: Vortex Maneuver Lift for Super-Cruise Configurations. NASA TM X-72836, 1976.

39. USAF Stability and Control Datcom. Contracts AF 33(616)-6460 and F33615-74-C-3021, McDonnell Douglas Corp., Oct. 1960. (Revised Jan. 1975.)

40. Henderson, William P.; and Huffman, Jarrett K.: Lateral-Directional Stability Characteristics of a Wing-Fuselage Configuration at Angles of Attack up to 44°. NASA TM X-3087, 1974.

41. McKinney, Linwood W.; and Dollyhigh, Samuel M.: Some Trim Drag Considerations for Maneuvering Aircraft. J. Aircraft, vol. 8, no. 8, Aug. 1971, pp. 623-629.

42. Gloss, Blair B.: Effect of Wing Planform and Canard Location and Geometry on the Longitudinal Aerodynamic Characteristics of a Close-Coupled Canard Wing Model at Subsonic Speeds. NASA TN D-7910, 1975.

TABLE I.- GEOMETRIC CHARACTERISTICS OF MODEL

Body:	
Length, cm	101.05
44° swept trapezoidal wing:	
A	2.56
b/2, cm	27.18
Λ_{le}, deg	44
$\bar{c}$, cm	24.56
c_{th}, cm	35.75
Longitudinal model station at 25 percent c_{th}, cm	51.81
Airfoil section:	
Root	NACA 64A006
Tip	NACA 64A004
S, cm^2	1155.74
Root chord (at wing-fuselage juncture), cm	29.80
Tip chord, cm	6.77
Canard:	
Λ_{le}, deg	51.7
Airfoil section	Circular arc
S_C, cm^2	226.90
b/2, cm	17.5
Root chord (at canard-fuselage juncture), cm	15.88
Tip chord, cm	3.18
Maximum thickness, percent chord at:	
Root	6.0
Tip	4.0
Horizontal and vertical tails:	
Λ_{le}, deg	51.7
Airfoil section	Circular arc
S_T, cm^2	144.39
S_H, cm^2	288.80
b/2, cm	19.03
Root chord (at tail-fuselage juncture), cm	17.92
Tip chord, cm	3.59
Maximum thickness, percent chord at:	
Root	6.0
Tip	4.0

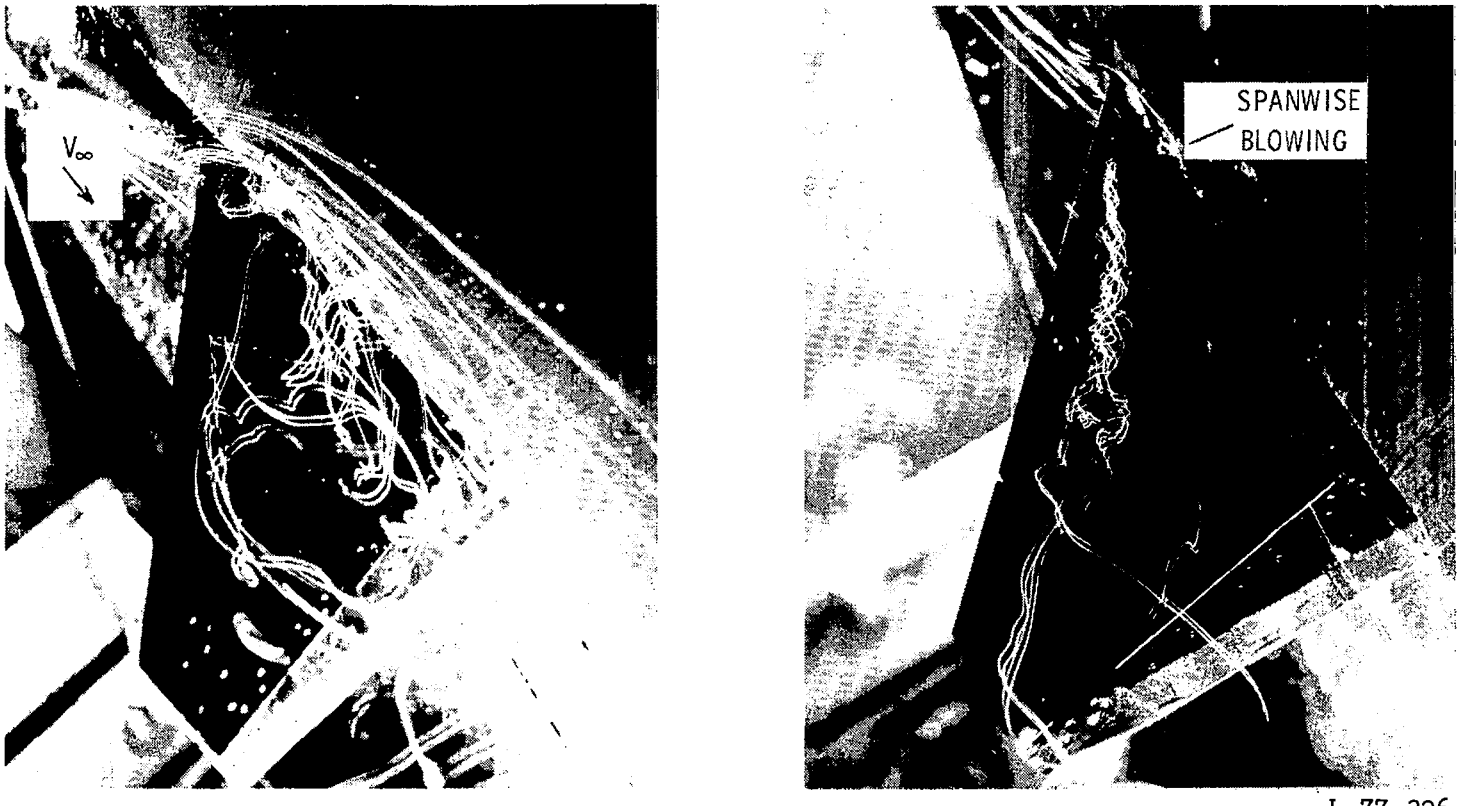

(a) Blowing off; vortex breakdown.

(b) Blowing on; vortex breakdown delayed.

Figure 1.- Flow-visualization photographs of spanwise blowing on 44° swept trapezoidal wing at $\alpha = 30^\circ$ (from ref. 31).

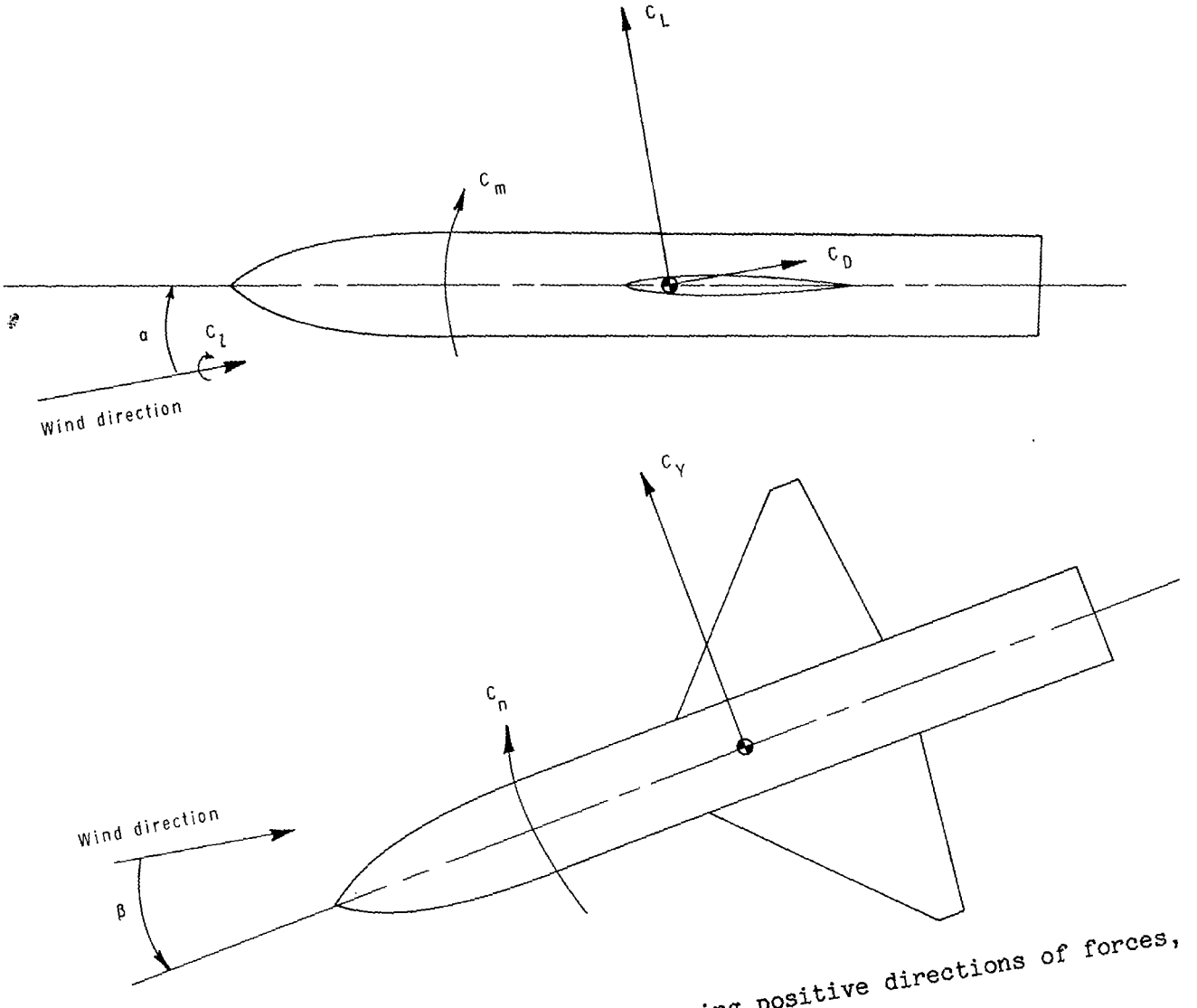

Figure 2.- Stability-axis system showing positive directions of forces, moments, and angles.

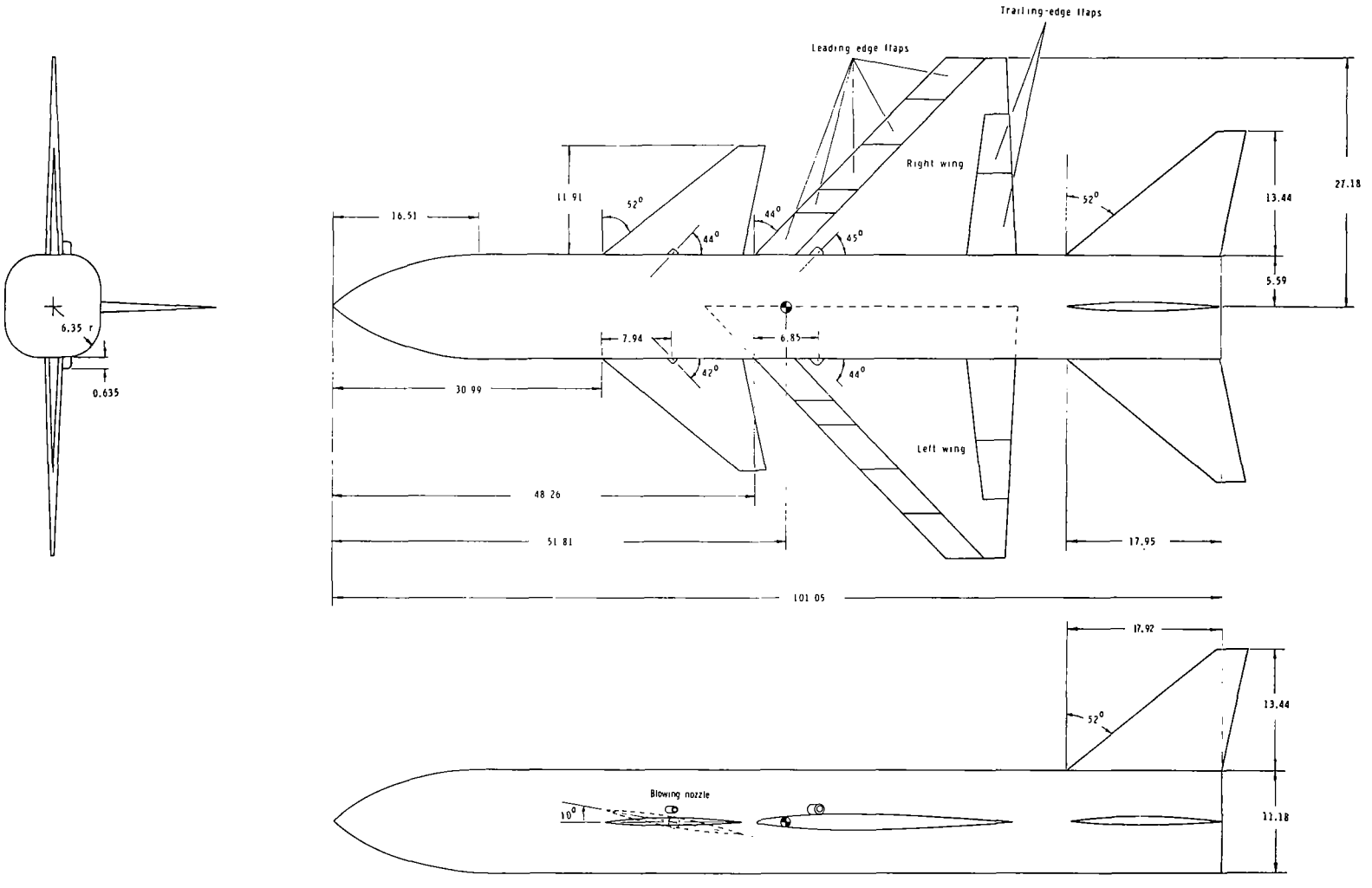

(a) Three-view drawing.

Figure 3.- Details of wind-tunnel model. (All dimensions except those marked otherwise are in cm.)

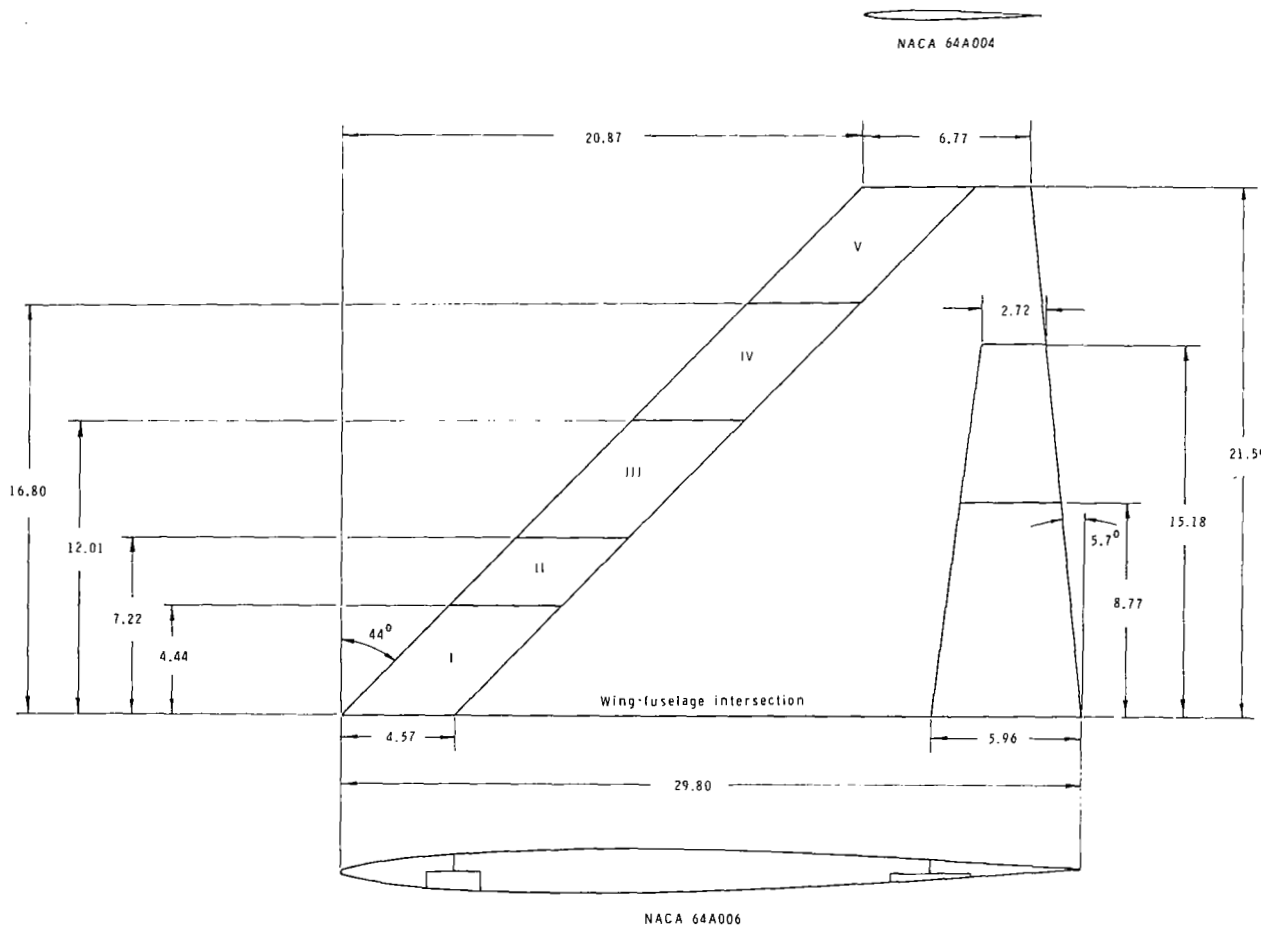

(b) 44° swept trapezoidal wing.

Figure 3.- Concluded.

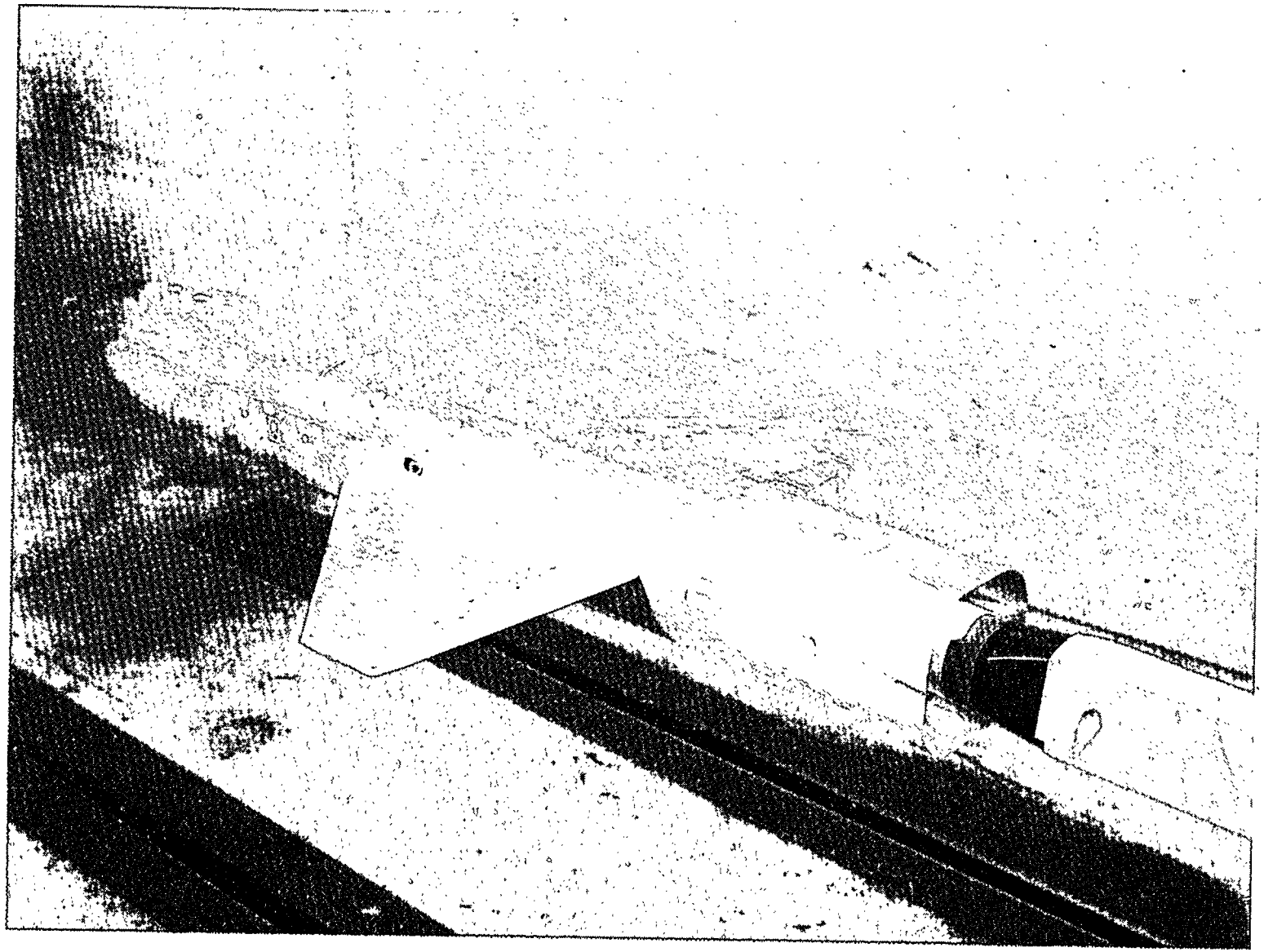

L-77-327

(a) Spanwise blowing on 44° swept trapezoidal wing.

Figure 4.- Model configurations installed in wind tunnel.

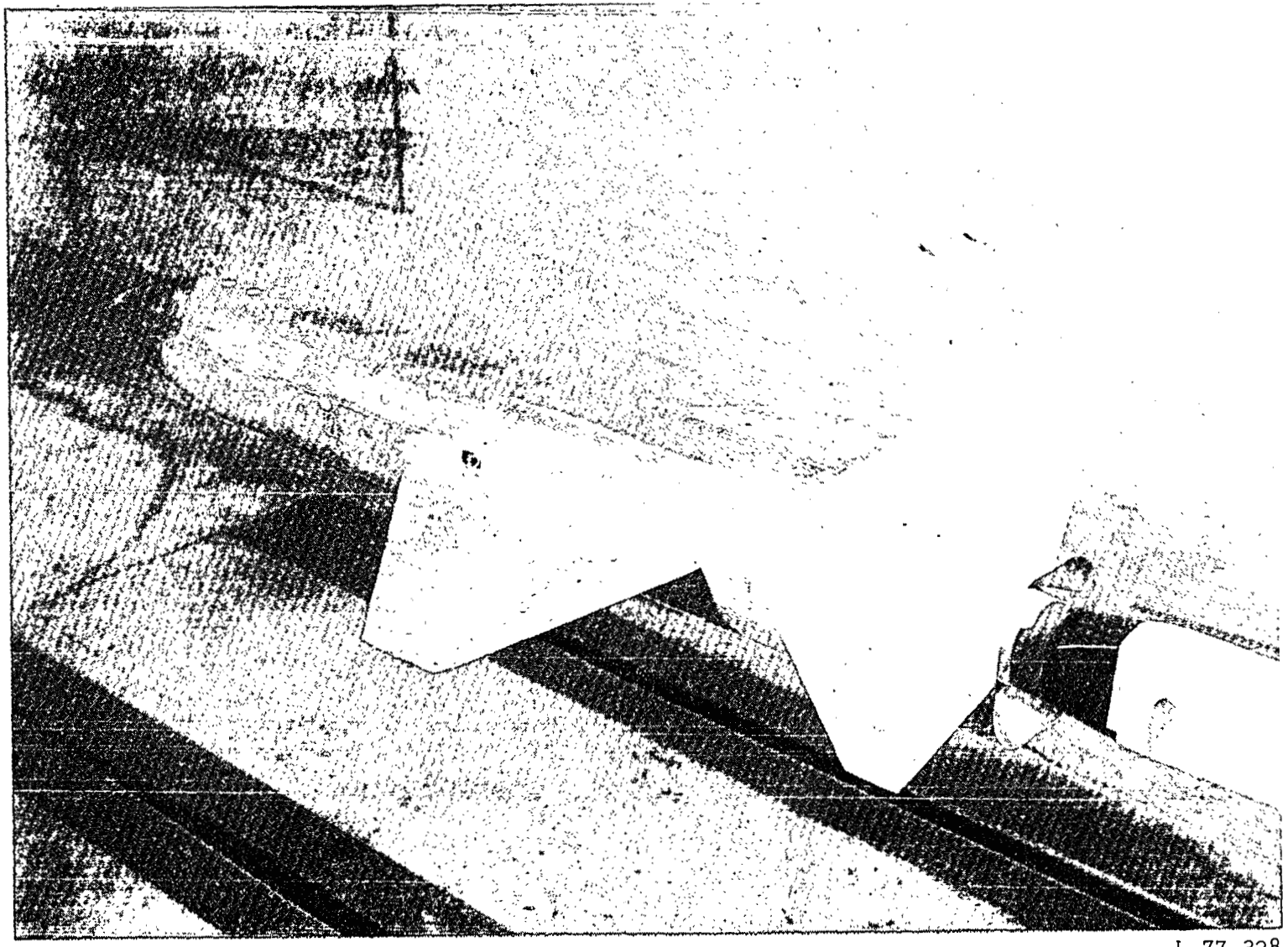

L-77-328

(b) Spanwise blowing on 44° swept trapezoidal wing with horizontal and vertical tails on.

Figure 4.- Continued.

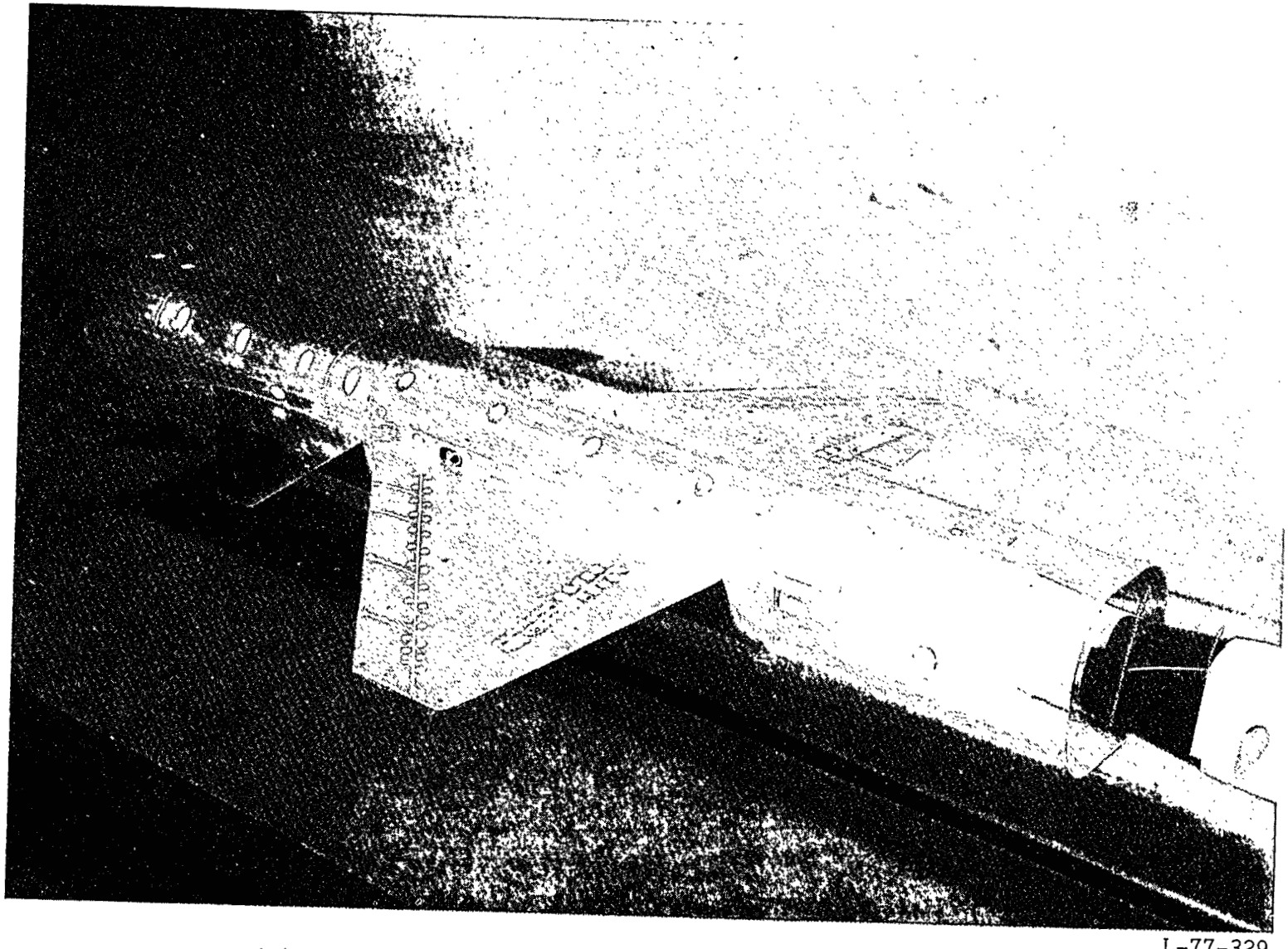

L-77-329

(c) Spanwise blowing on wing of canard-wing configuration.

Figure 4.- Continued.

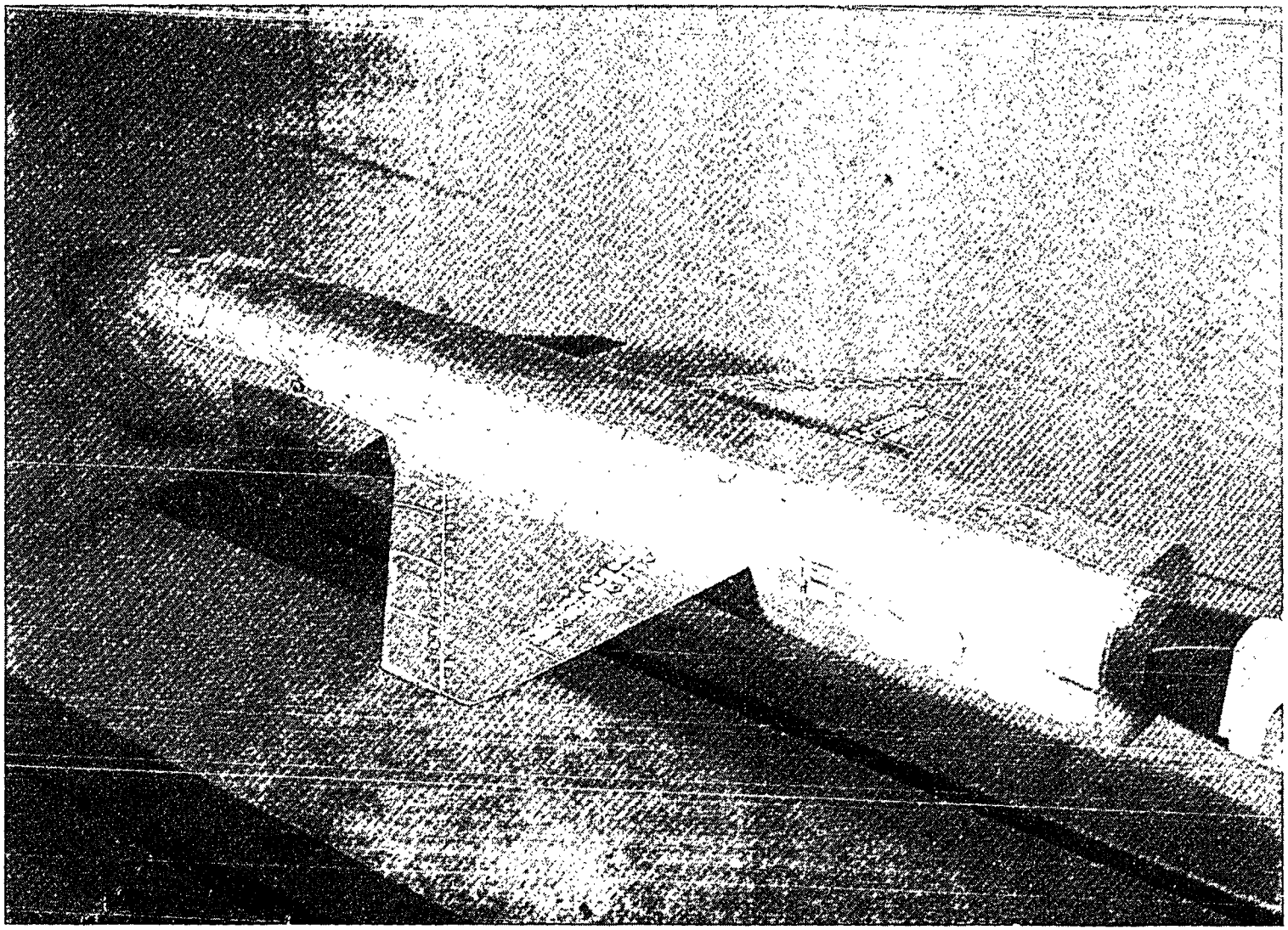

L-77-330

(d) Spanwise blowing on canard of canard-wing configuration.

Figure 4.- Concluded.

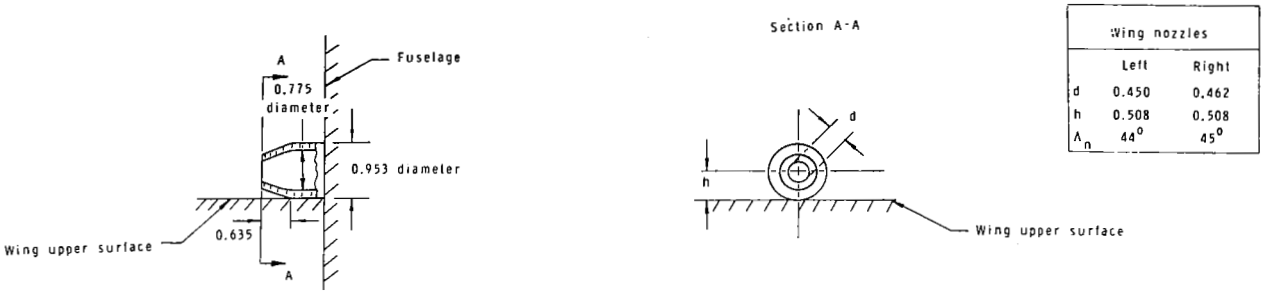

(a) Wing nozzle.

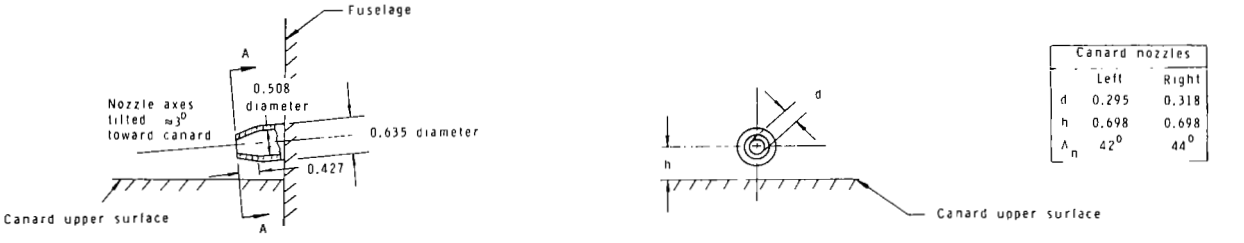

(b) Canard nozzle.

Figure 5.- Wing and canard nozzle geometry, vertical location, and sweep angle. All dimensions are in centimeters.

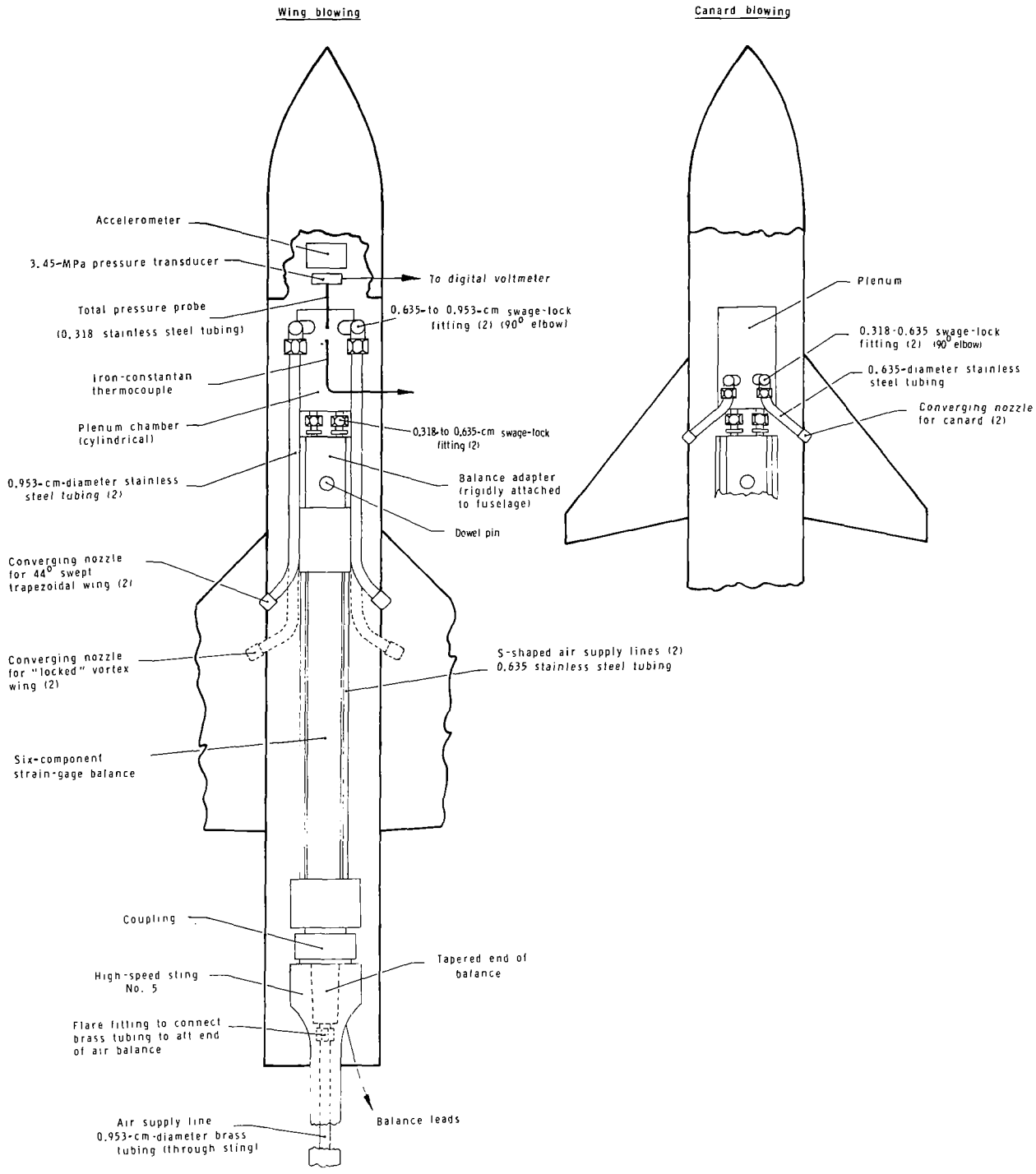

Figure 6.- Planview of air supply system and internal model assembly for spanwise blowing model. (All dimensions are in cm unless otherwise noted.)

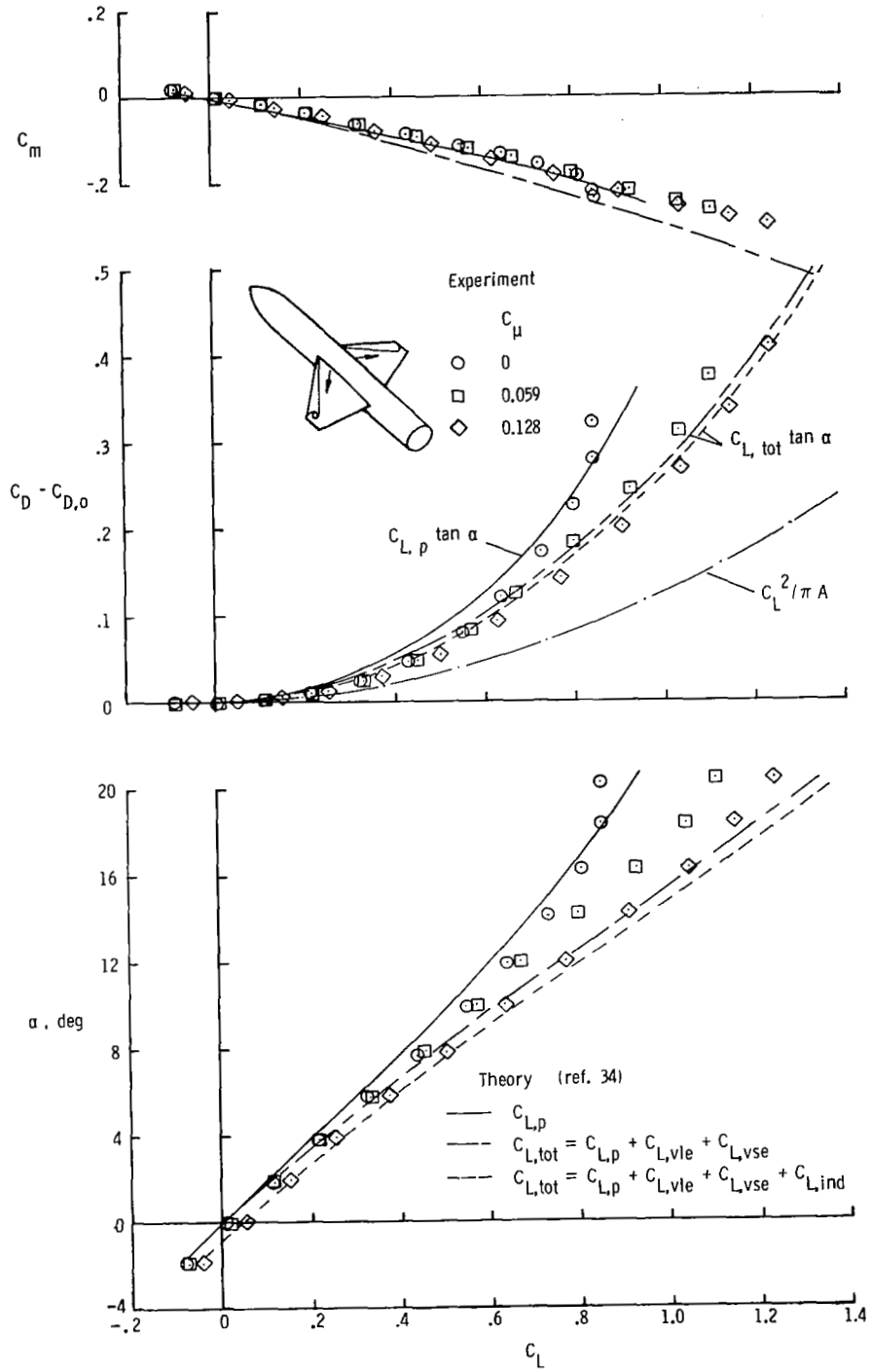

Figure 7.- Comparison of theoretical and experimental longitudinal aerodynamic characteristics of 44° swept trapezoidal wing configuration with $\delta_{le} = \delta_{te} = 0°$; $M_\infty \approx 0.30$.

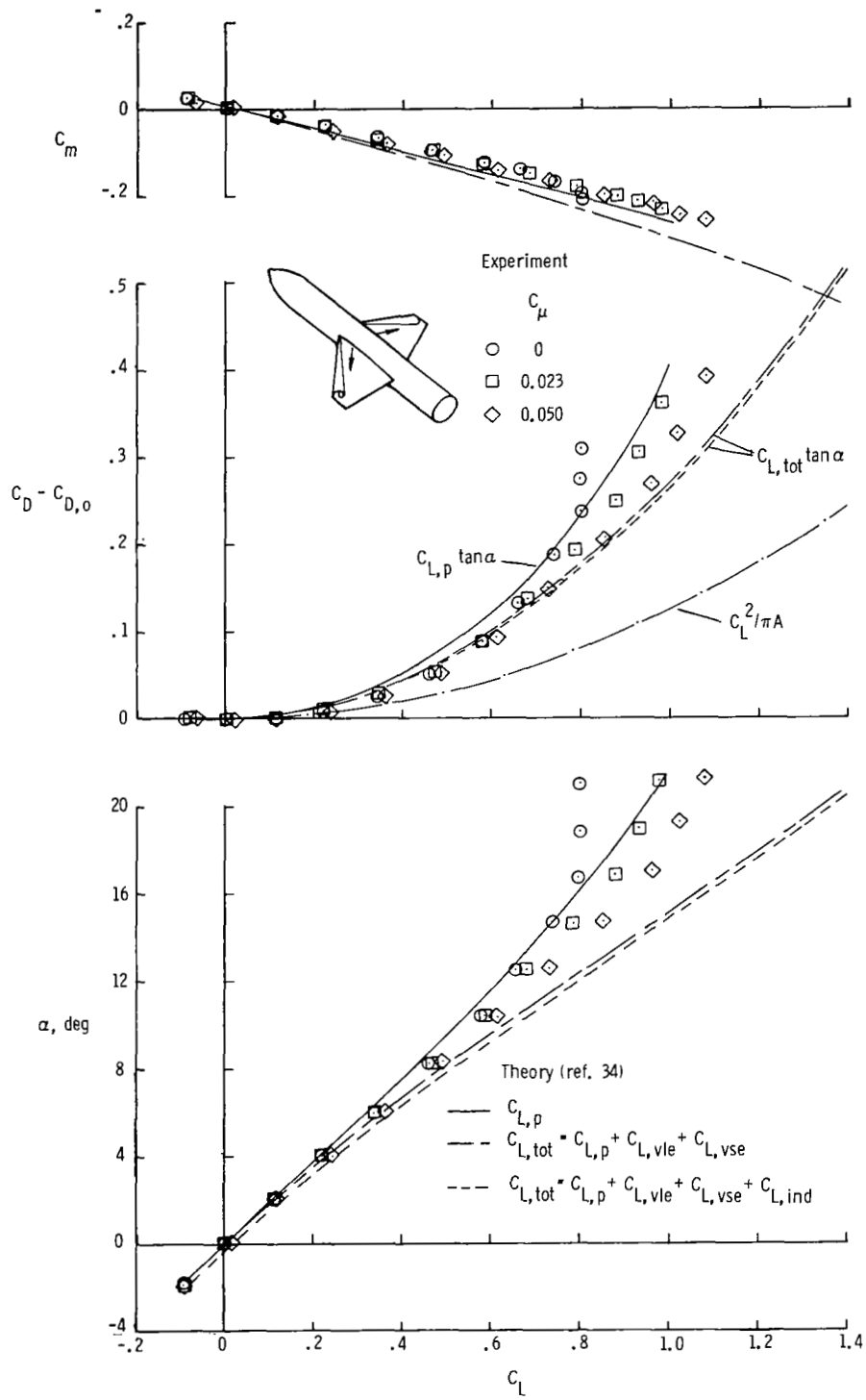

Figure 8.- Comparison of theoretical and experimental longitudinal aerodynamic characteristics of 44° swept trapezoidal wing configuration with $\delta_{le} = \delta_{te} = 0°$; $M_\infty = 0.50$.

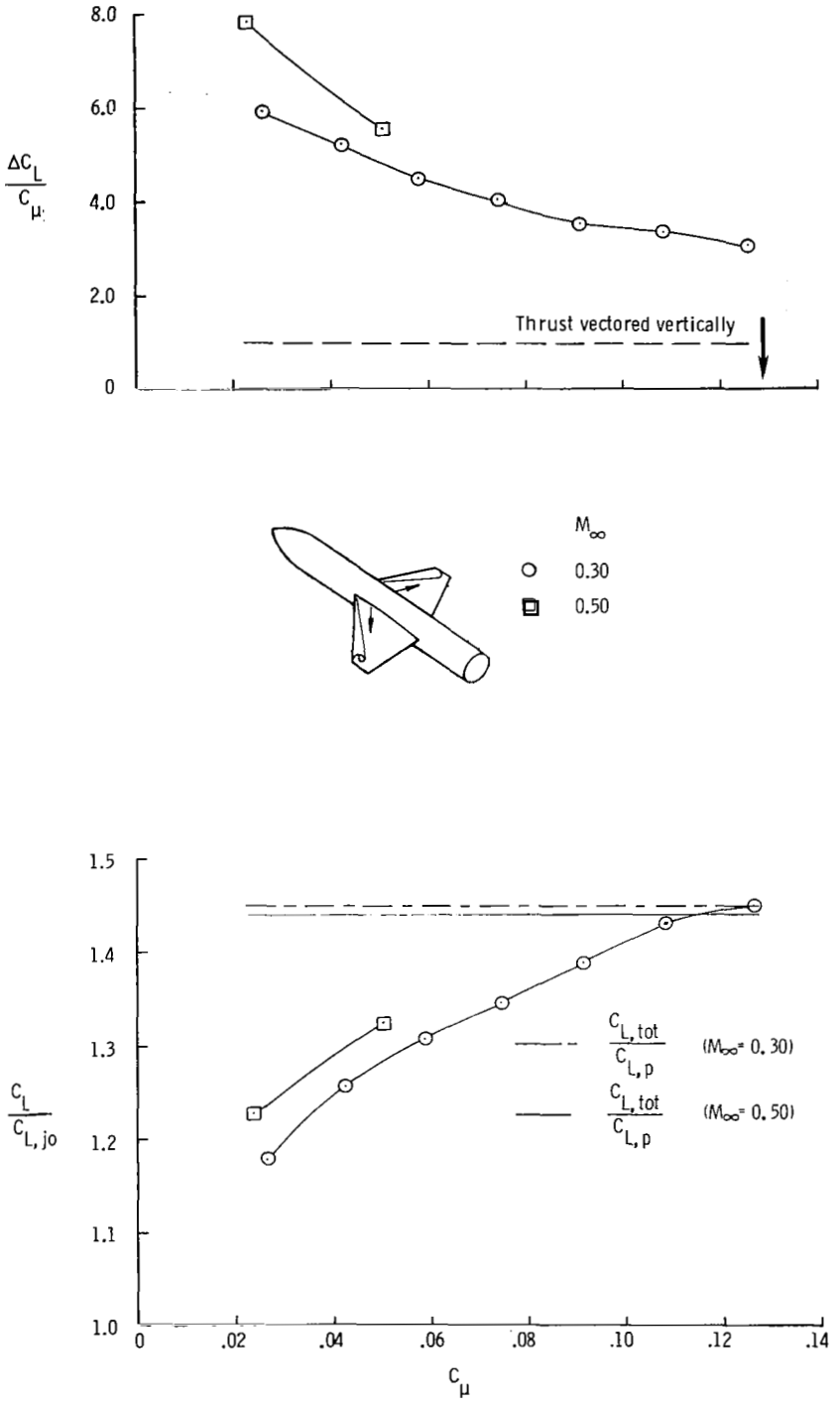

Figure 9.- Effect of C_μ and M_∞ on lift augmentation ratio and lift effectiveness of blowing for 44° swept trapezoidal wing configuration for $\alpha \approx 21°$.

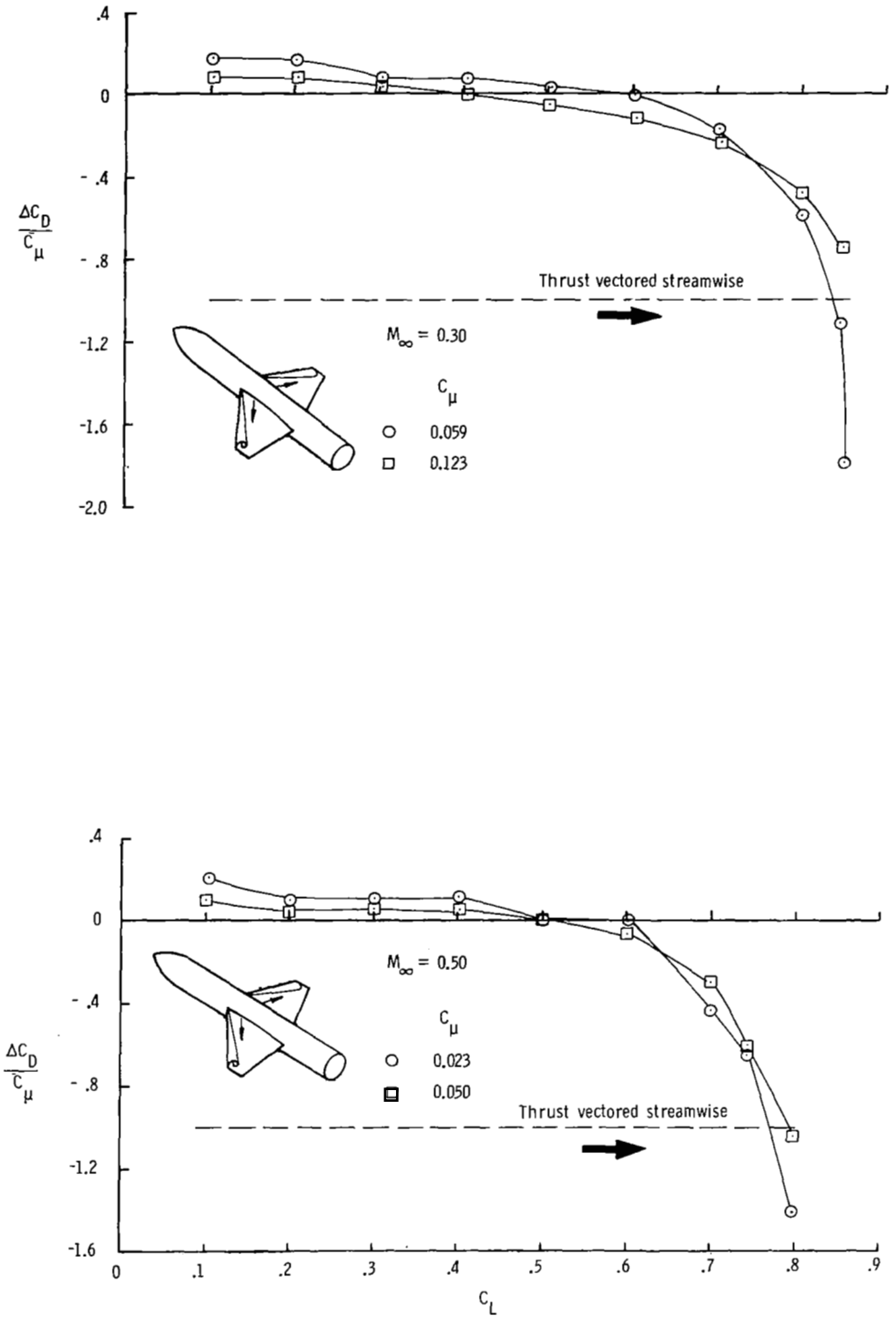

Figure 10.- Effect of C_L and C_μ on drag reduction ratio for 44° swept trapezoidal wing configuration for two free-stream Mach numbers.

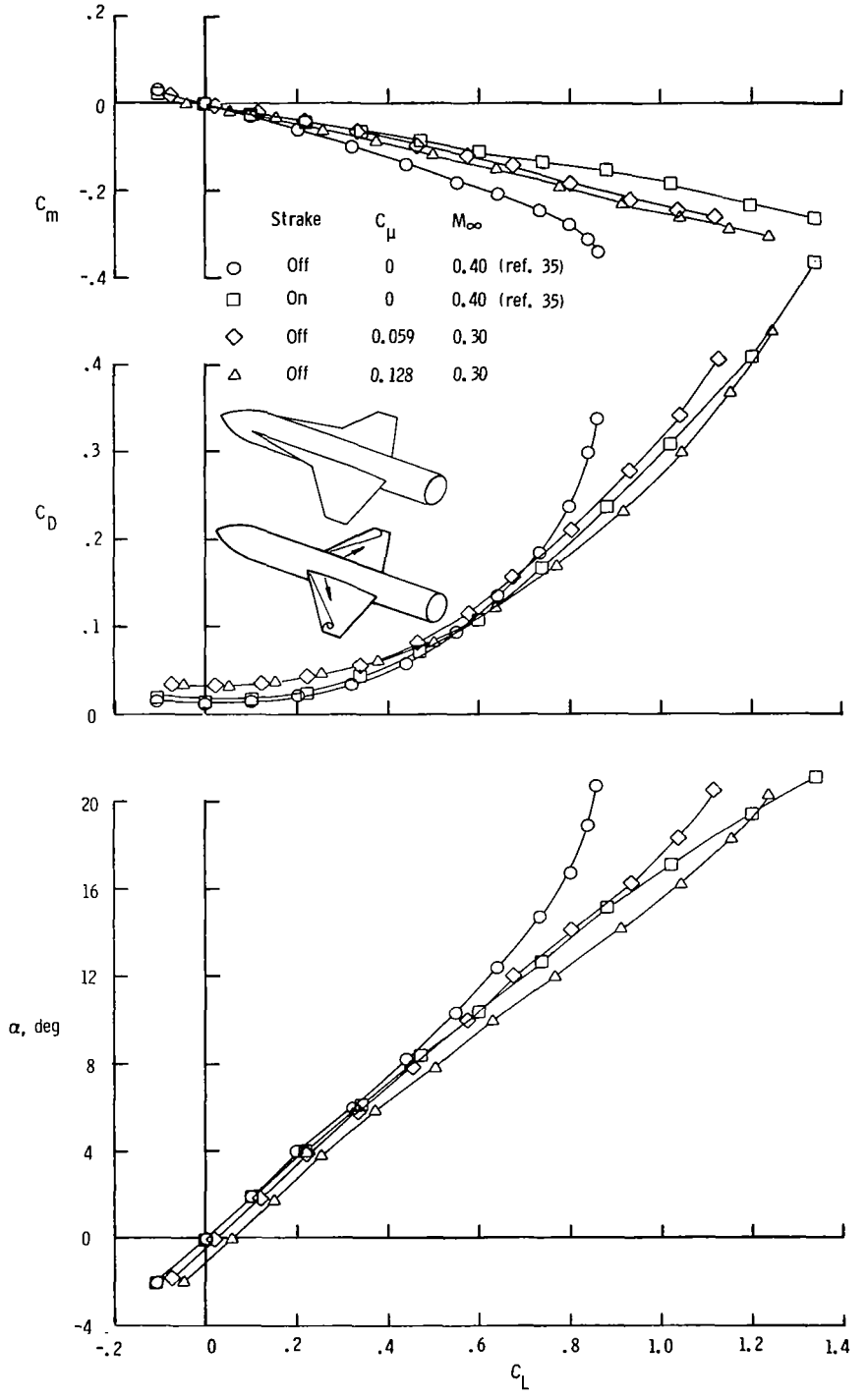

Figure 11.- Effect of wing strake and spanwise blowing on longitudinal aerodynamic characteristics of 44° swept trapezoidal wing configuration. $\delta_{le} = 0°$.

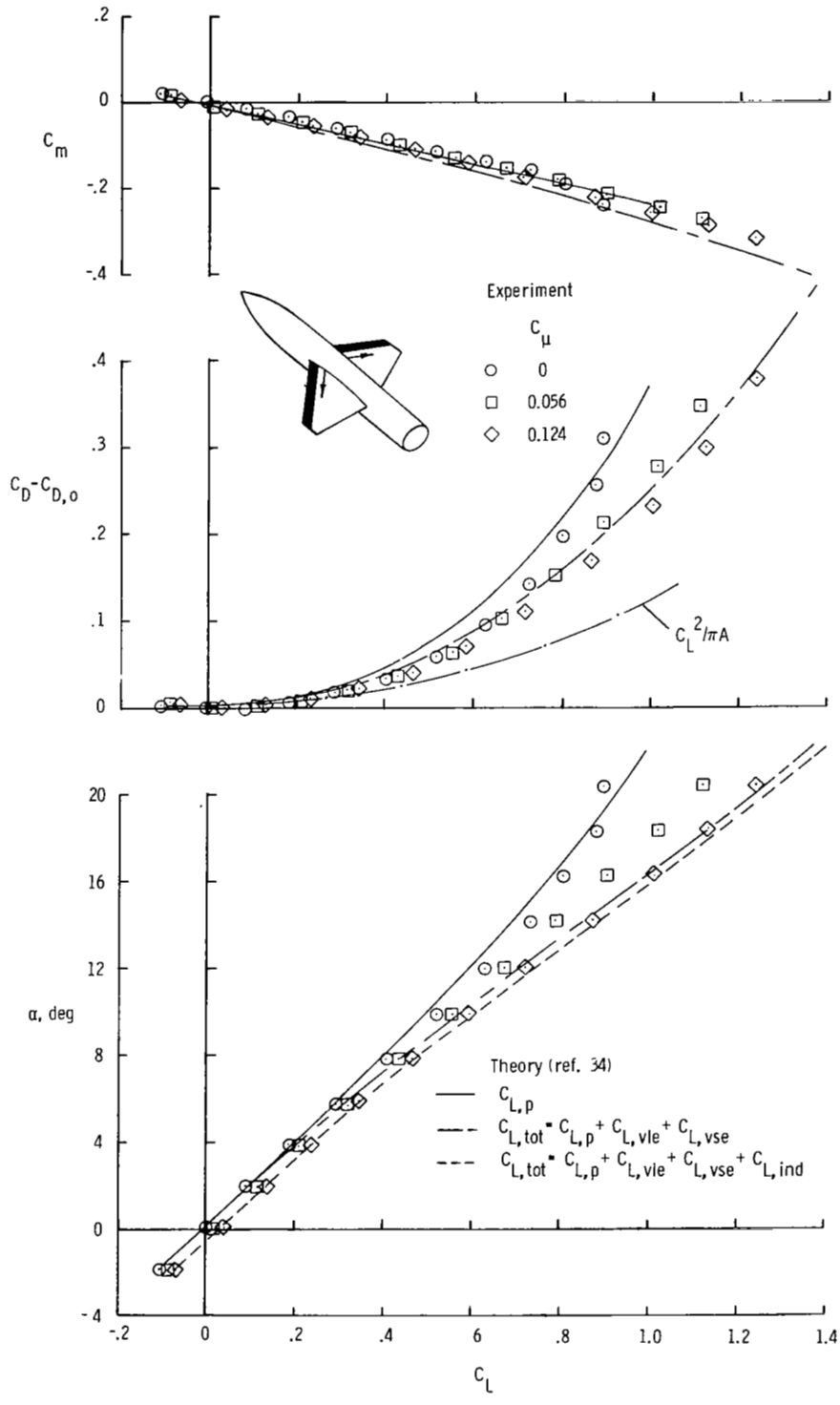

Figure 12.- Comparison of effect of spanwise blowing on theoretical and experimental longitudinal aerodynamic characteristics of 44° swept trapezoidal wing configuration with $\delta_{le} = 4°$; $\delta_{te} = 0°$; $M_\infty = 0.30$.

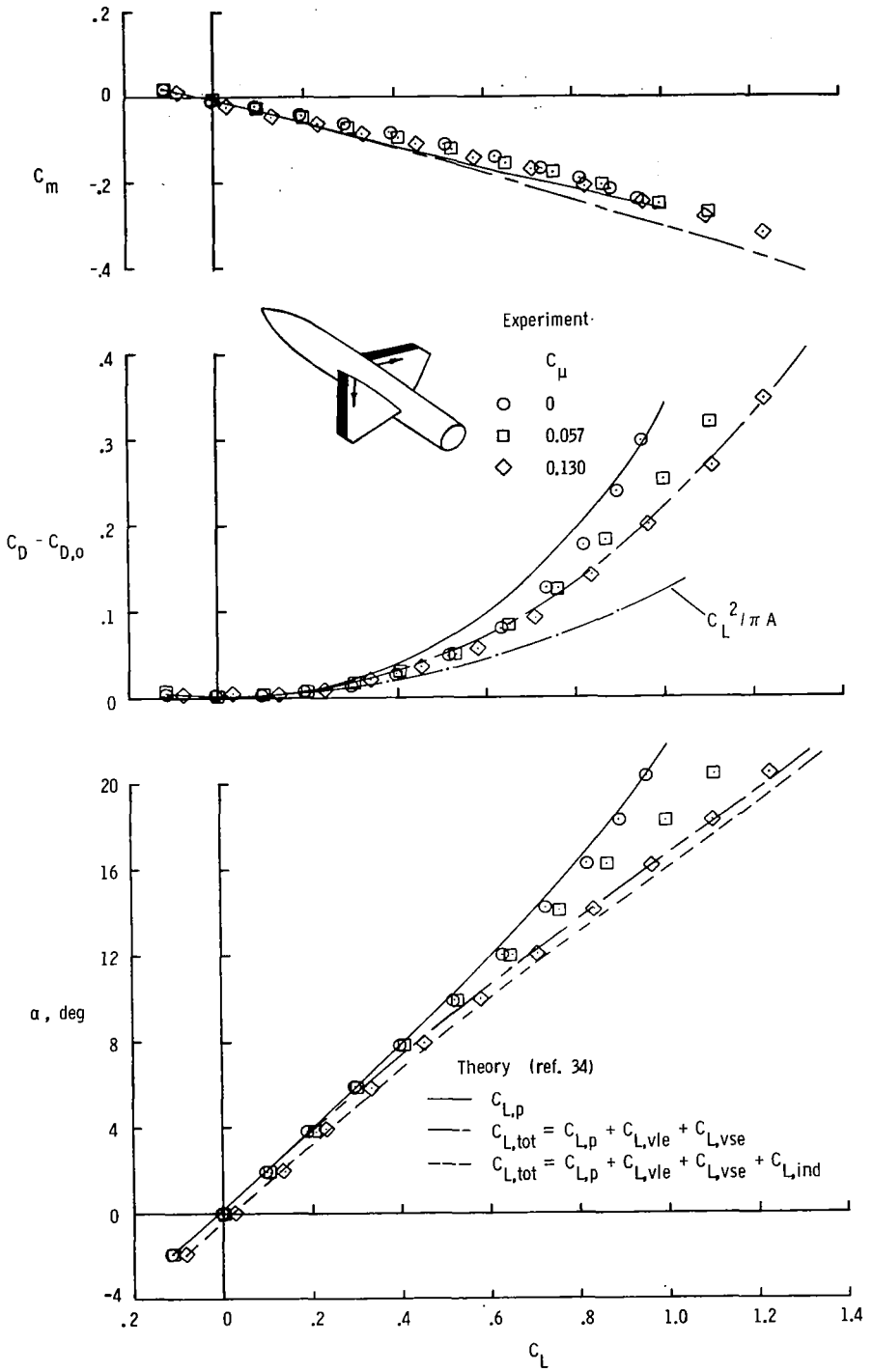

Figure 13.- Comparison of theoretical and experimental longitudinal aerodynamic characteristics of 44° swept trapezoidal wing configuration with $\delta_{le} = 8°$; $\delta_{te} = 0°$; $M_\infty = 0.30$.

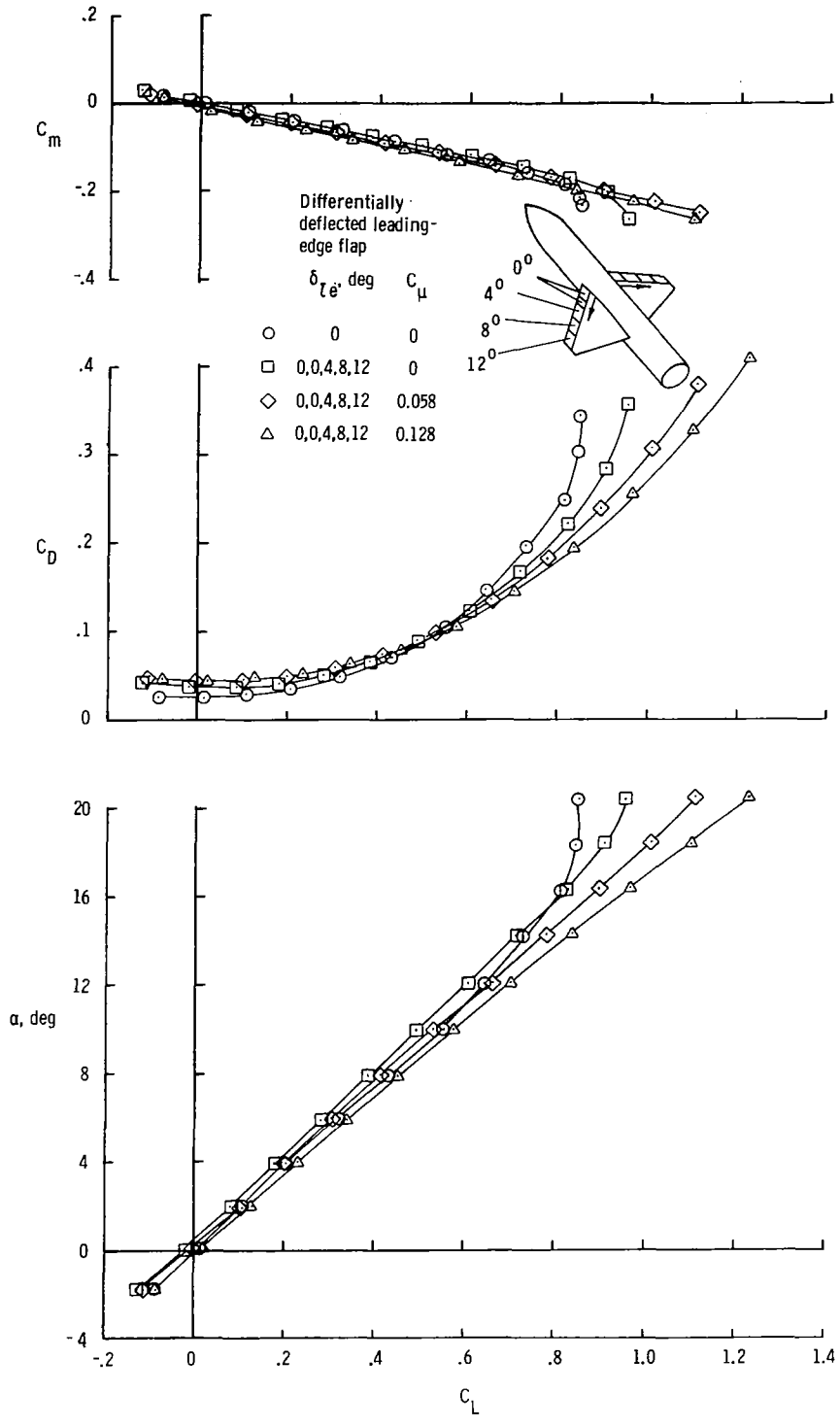

Figure 14.- Effect of spanwise blowing in conjunction with differentially deflected leading-edge flap on longitudinal aerodynamic characteristics of 44° swept trapezoidal wing configuration; $\delta_{te} = 0°$; $M_\infty = 0.30$.

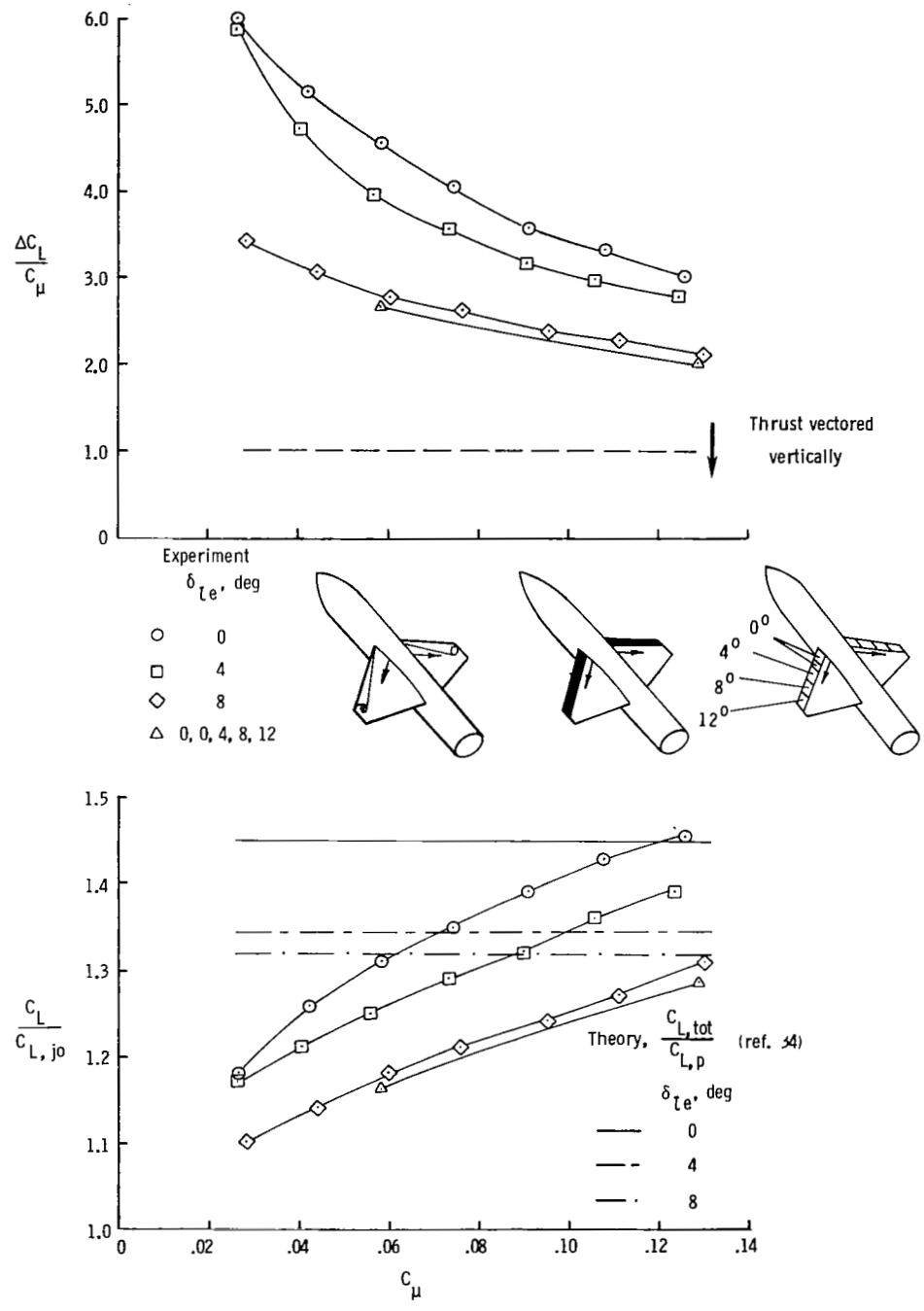

Figure 15.- Effect of C_μ and δ_{le} on lift augmentation ratio and lift effectiveness of blowing for 44° swept trapezoidal wing configuration for $\alpha \approx 20°$; $\delta_{te} = 0°$; $M_\infty = 0.30$.

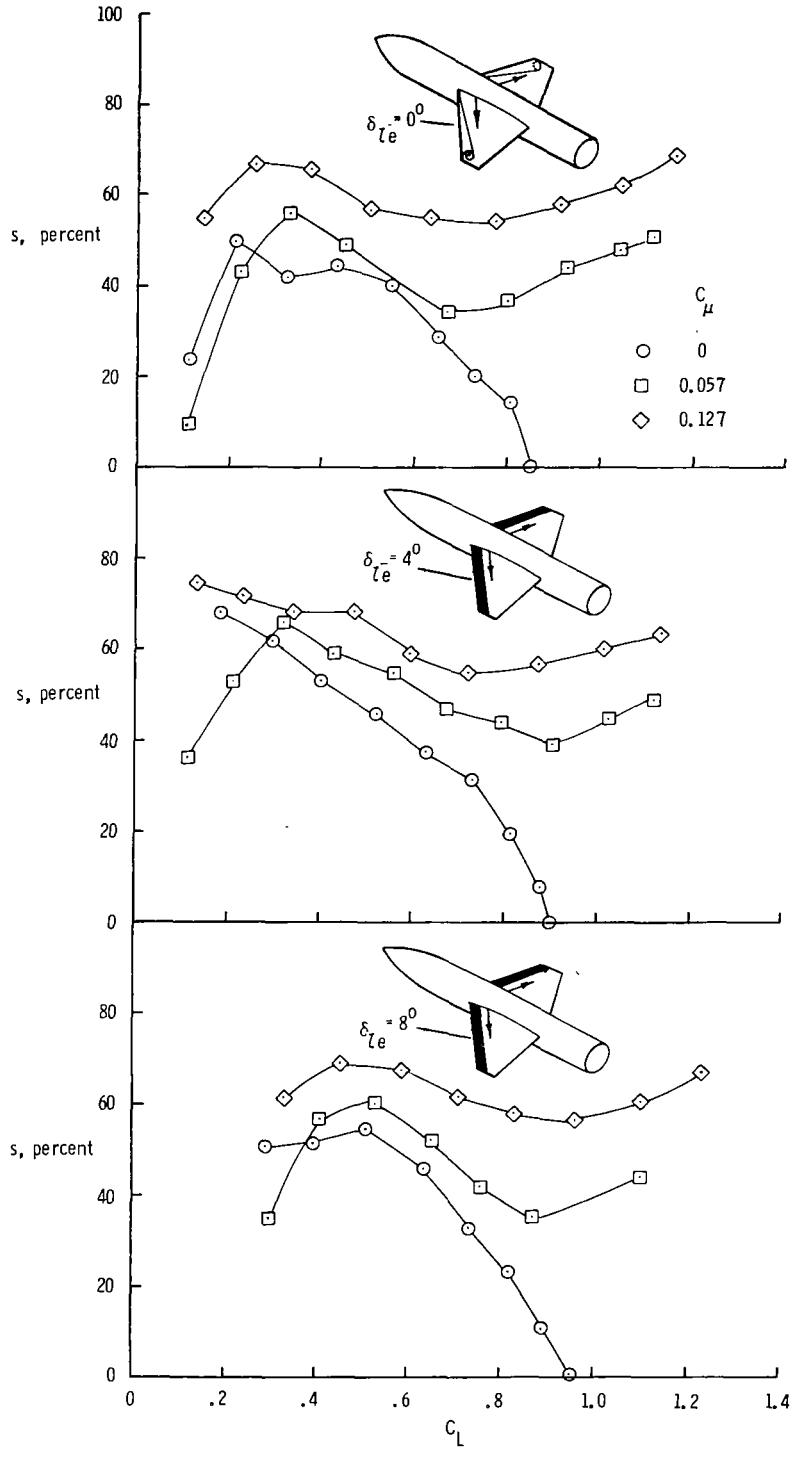

Figure 16.- Effect of C_L and C_μ on percent suction developed by 44° swept trapezoidal wing configuration for range of δ_{le}; $M_\infty = 0.30$.

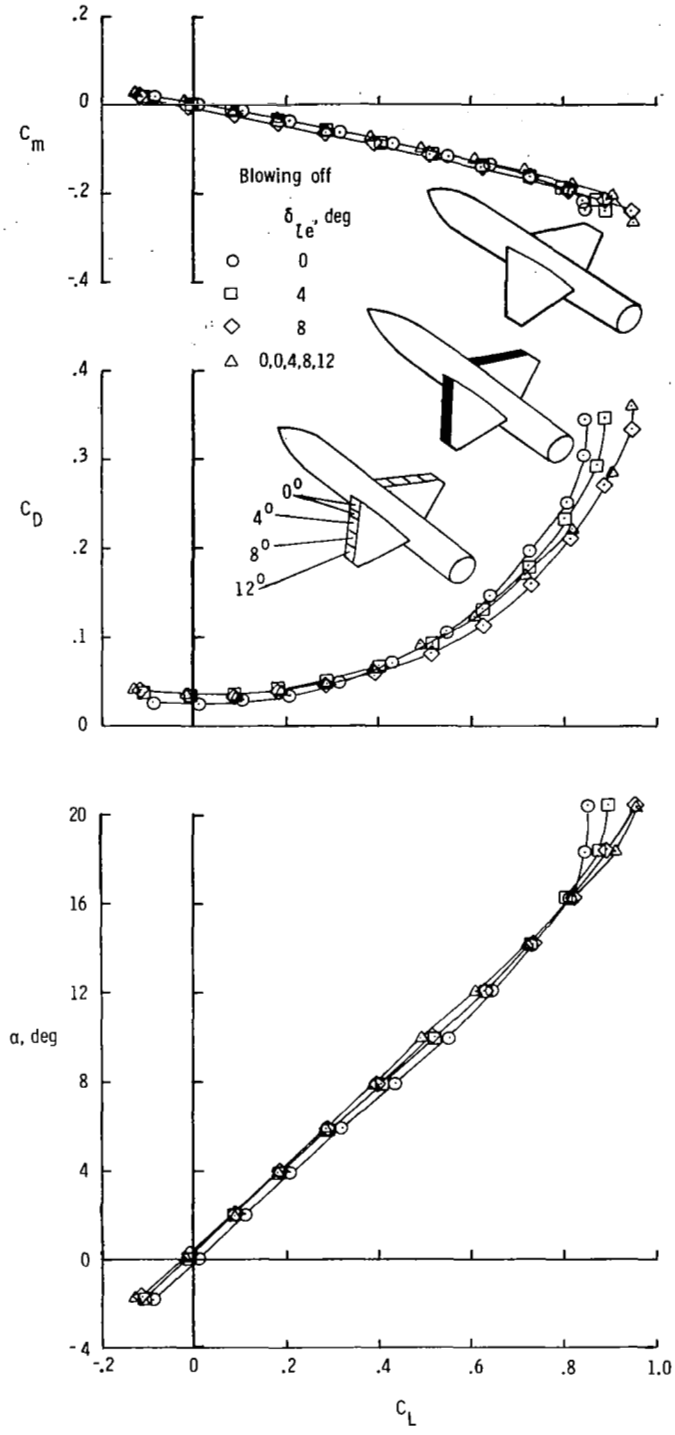

Figure 17.- Effect of leading-edge flap deflection angle on longitudinal aerodynamic characteristics of 44° swept trapezoidal wing configuration with blowing off; $\delta_{te} = 0°$; $M_\infty = 0.30$.

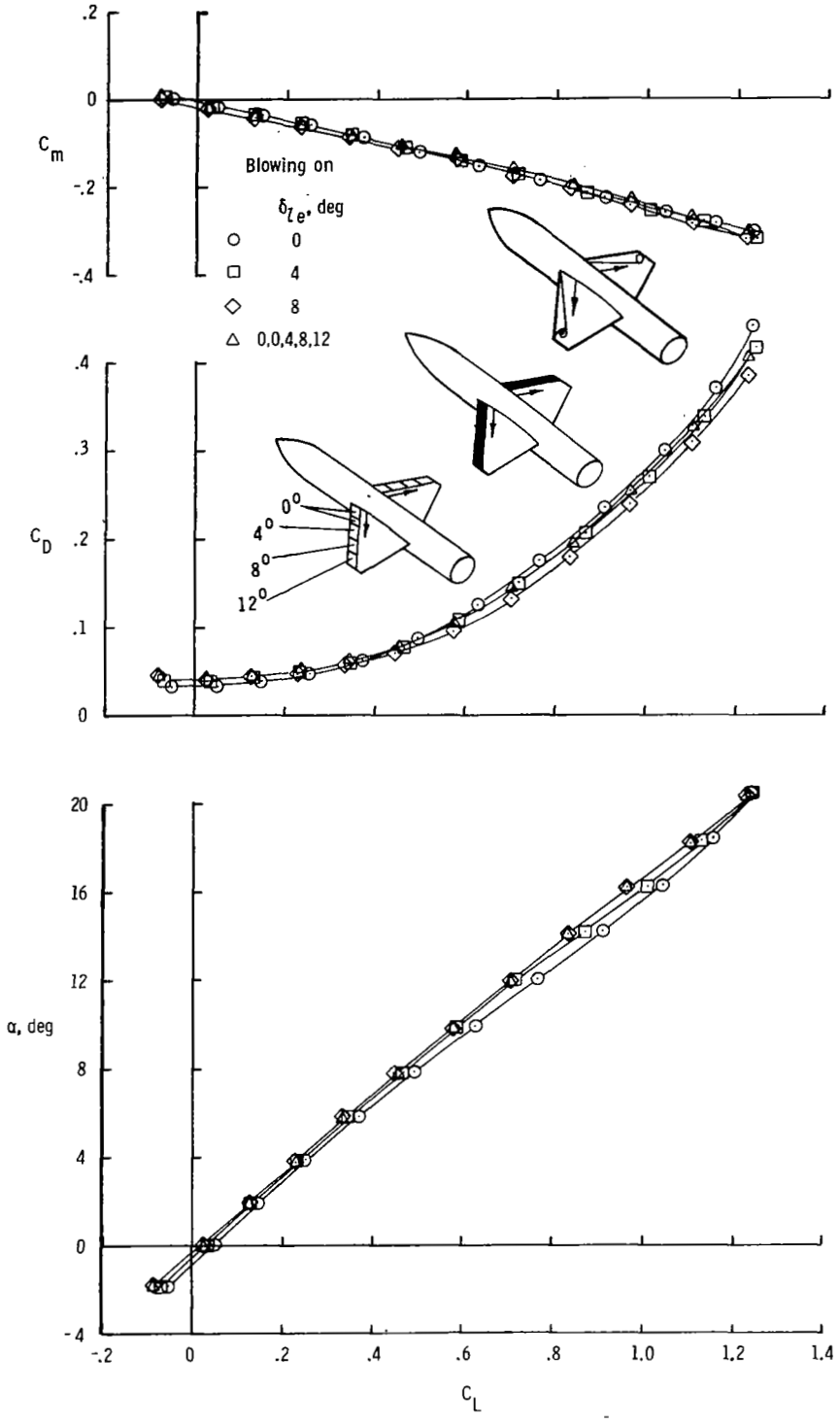

Figure 18.- Effect of leading-edge flap deflection angle on longitudinal aerodynamic characteristics of 44° swept trapezoidal wing configuration with blowing on; C_μ = 0.127; δ_{te} = 0°; M_∞ = 0.30.

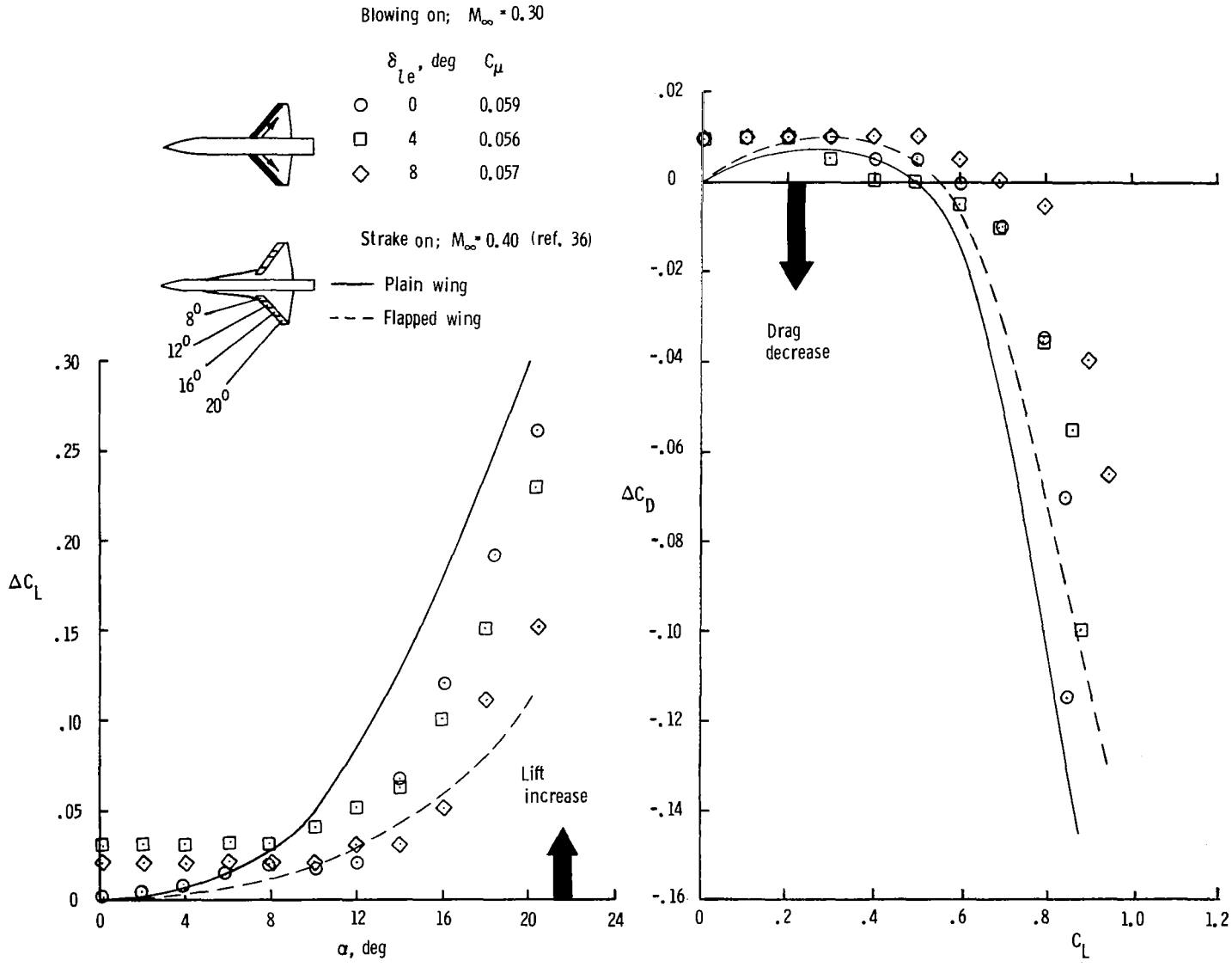

Figure 19.- Effect of leading-edge flap deflection on lift and drag increments due to wing strake or spanwise blowing.

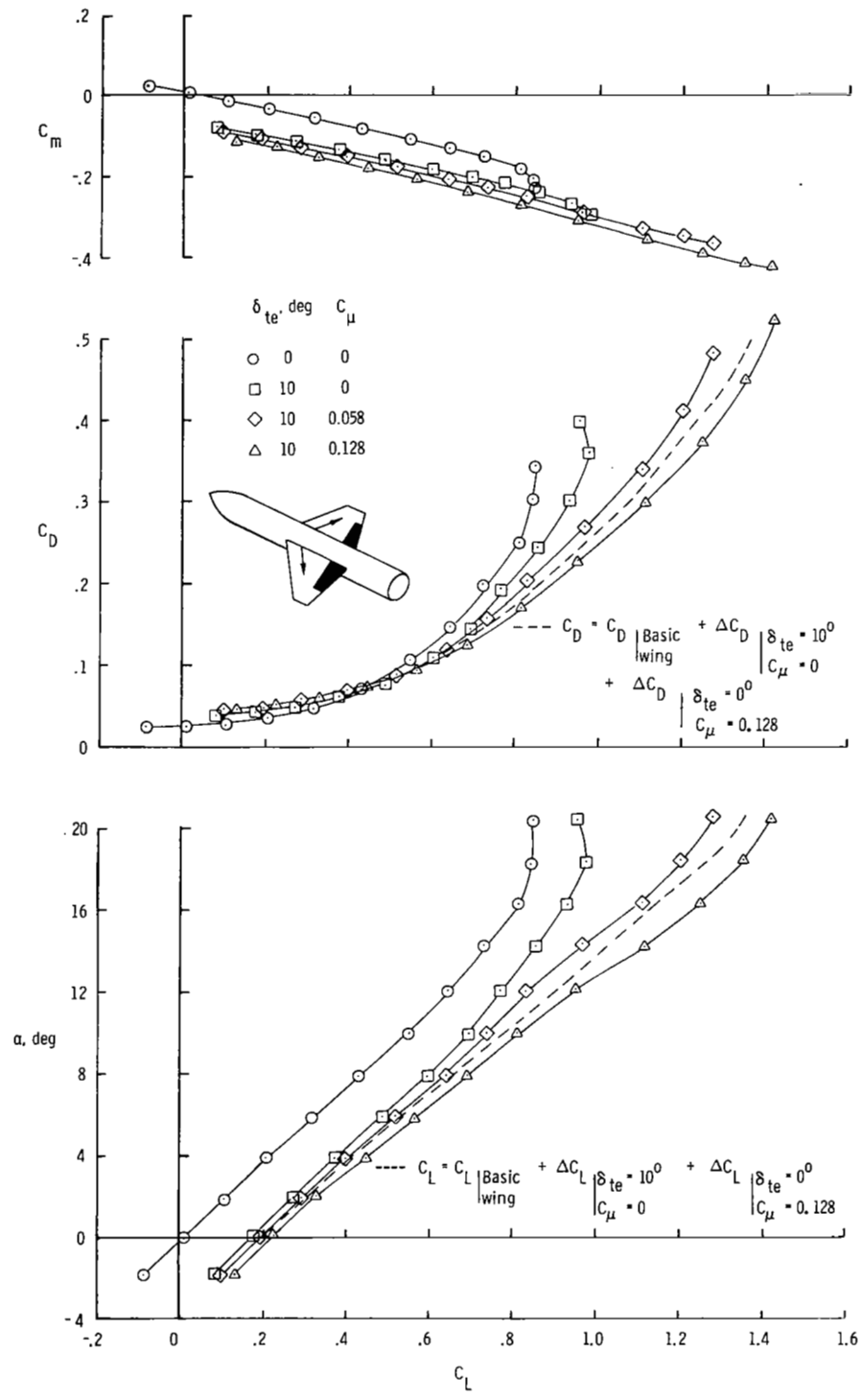

Figure 20.- Effect of spanwise blowing in conjunction with trailing-edge flap deflected to 10° on longitudinal aerodynamic characteristics of 44° swept trapezoidal wing configuration; $\delta_{le} = 0^o$; $M_\infty = 0.30$.

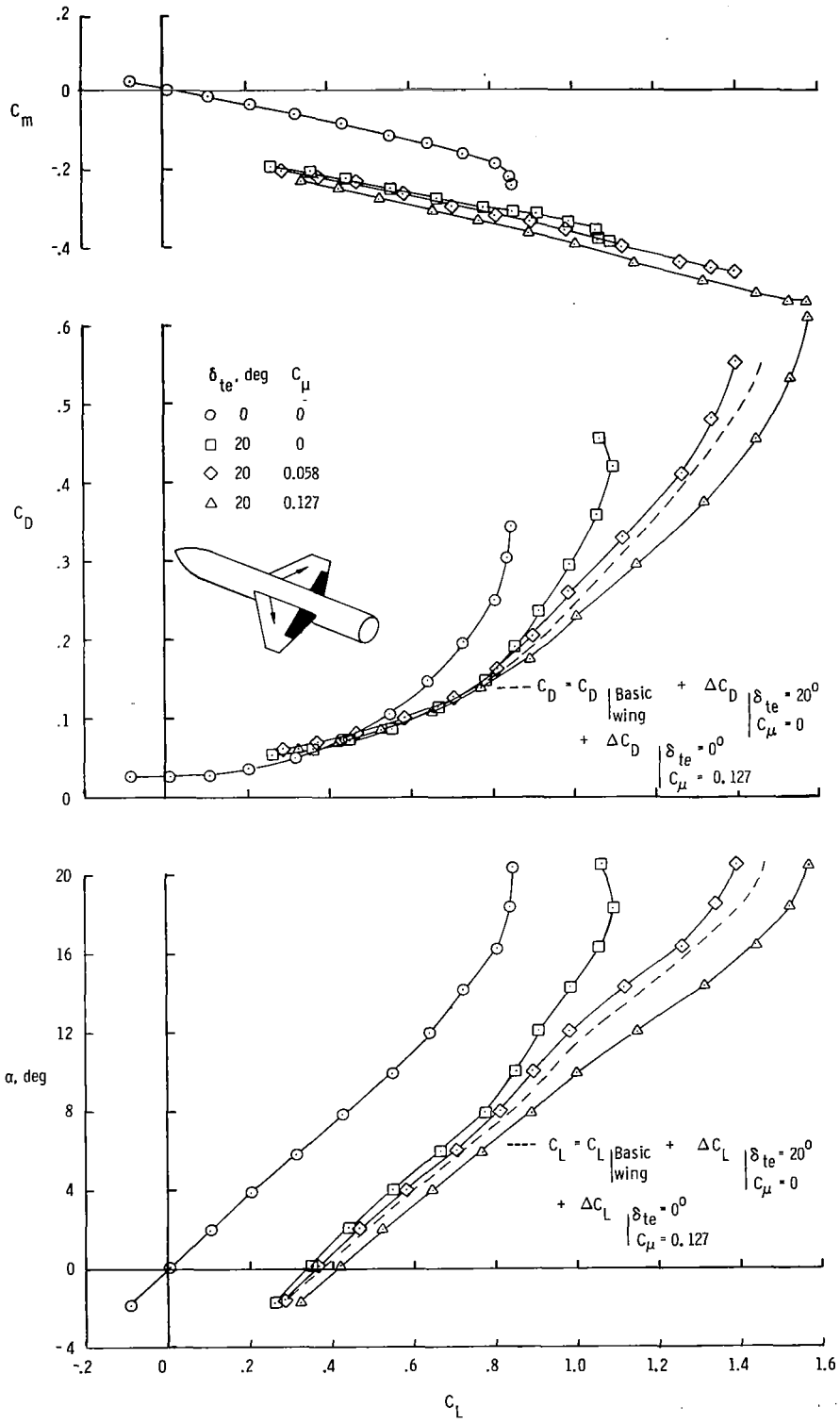

Figure 21.- Effect of spanwise blowing in conjunction with trailing-edge flap deflected to 20° on longitudinal aerodynamic characteristics of 44° swept trapezoidal wing configuration; $\delta_{le} = 0^o$; $M_\infty = 0.30$.

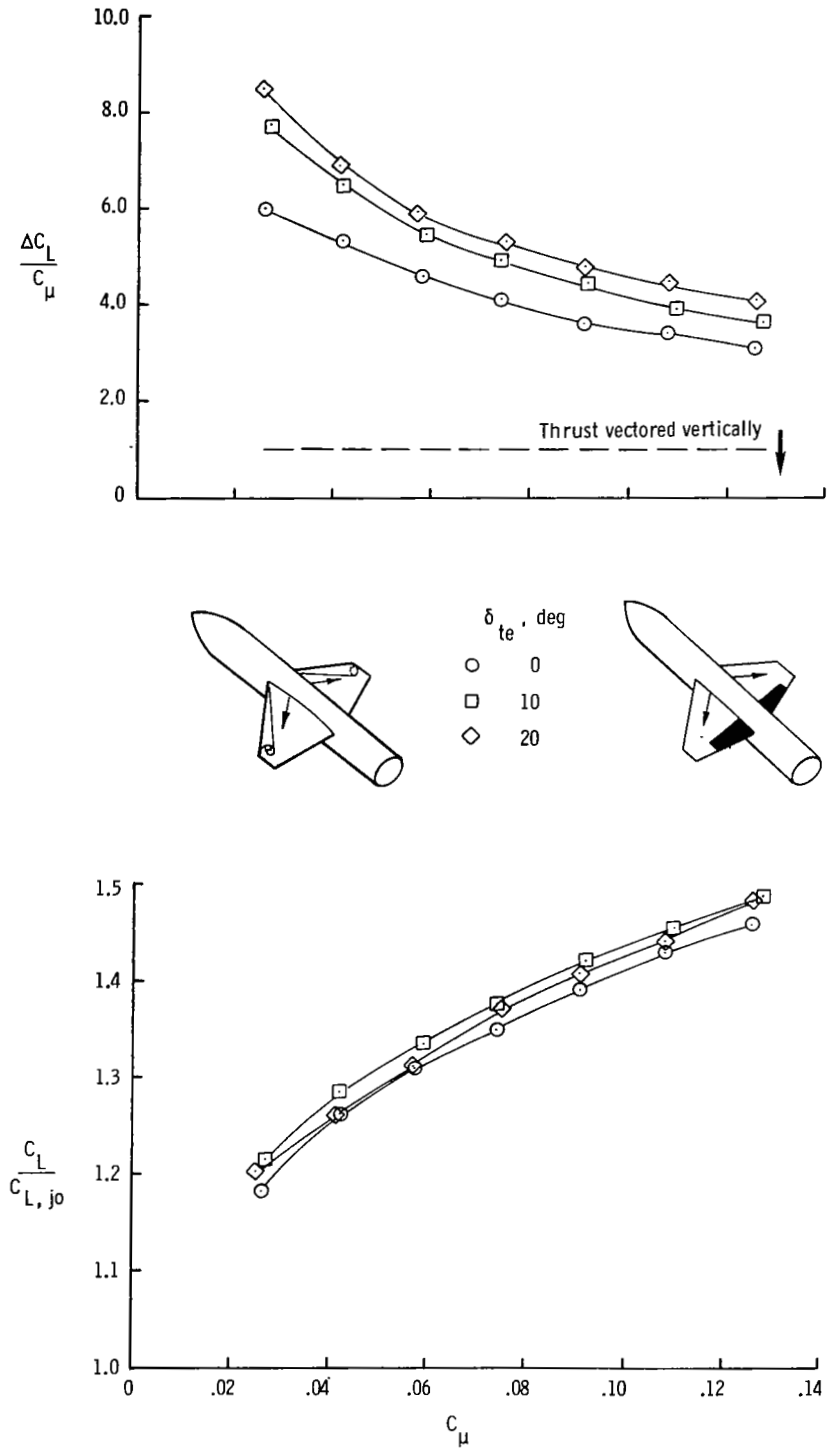

Figure 22.- Effect of C_μ and δ_{te} on lift augmentation ratio and lift effectiveness of blowing for 44° swept trapezoidal wing configuration; $\delta_{le} = 0°$; $M_\infty = 0.30$; $\alpha \approx 21°$.

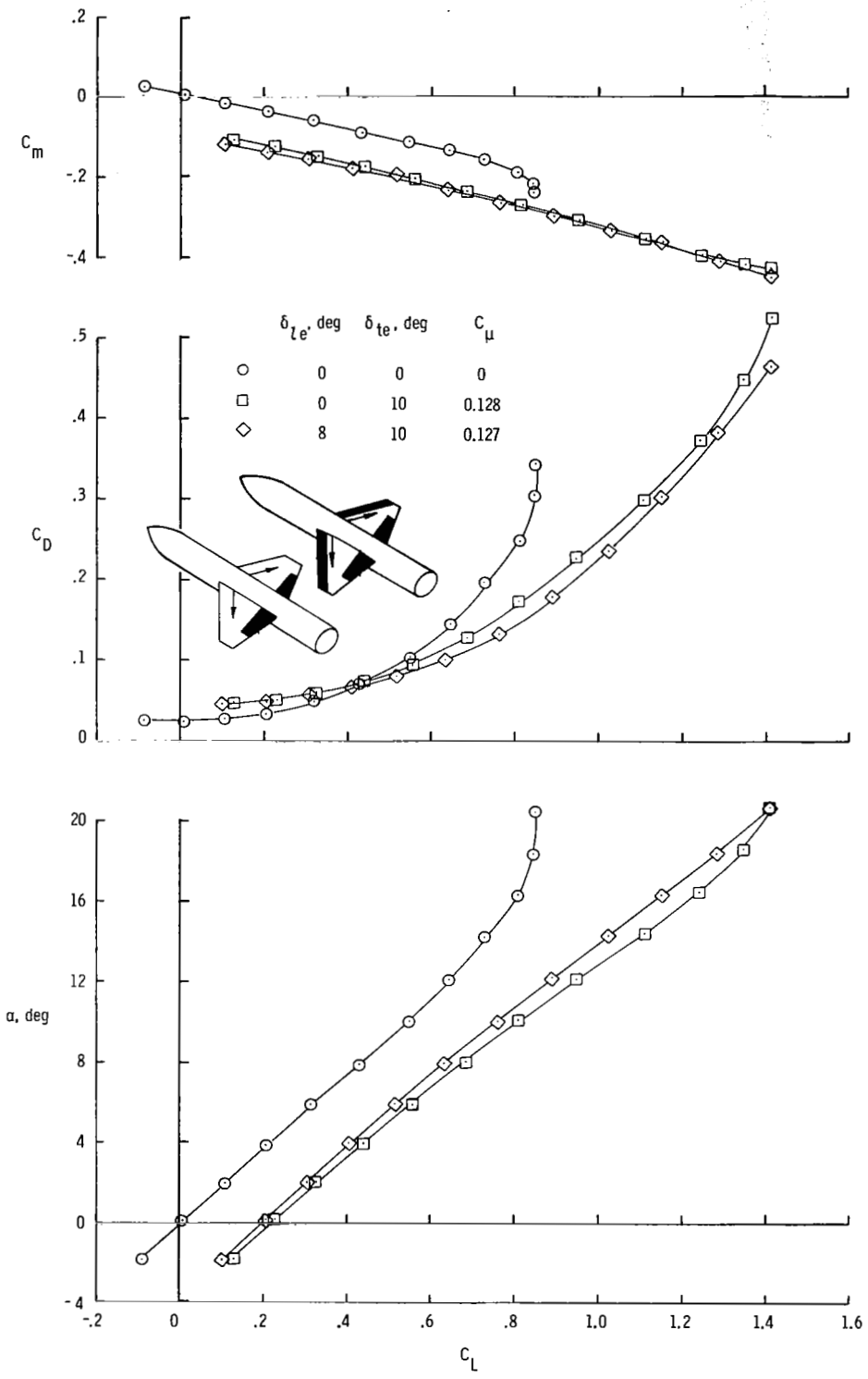

Figure 23.- Comparison of effect of spanwise blowing in conjunction with deflected trailing-edge flap and deflected leading- and trailing-edge flaps on longitudinal aerodynamic characteristics of 44° swept trapezoidal wing configuration; $M_\infty = 0.30$.

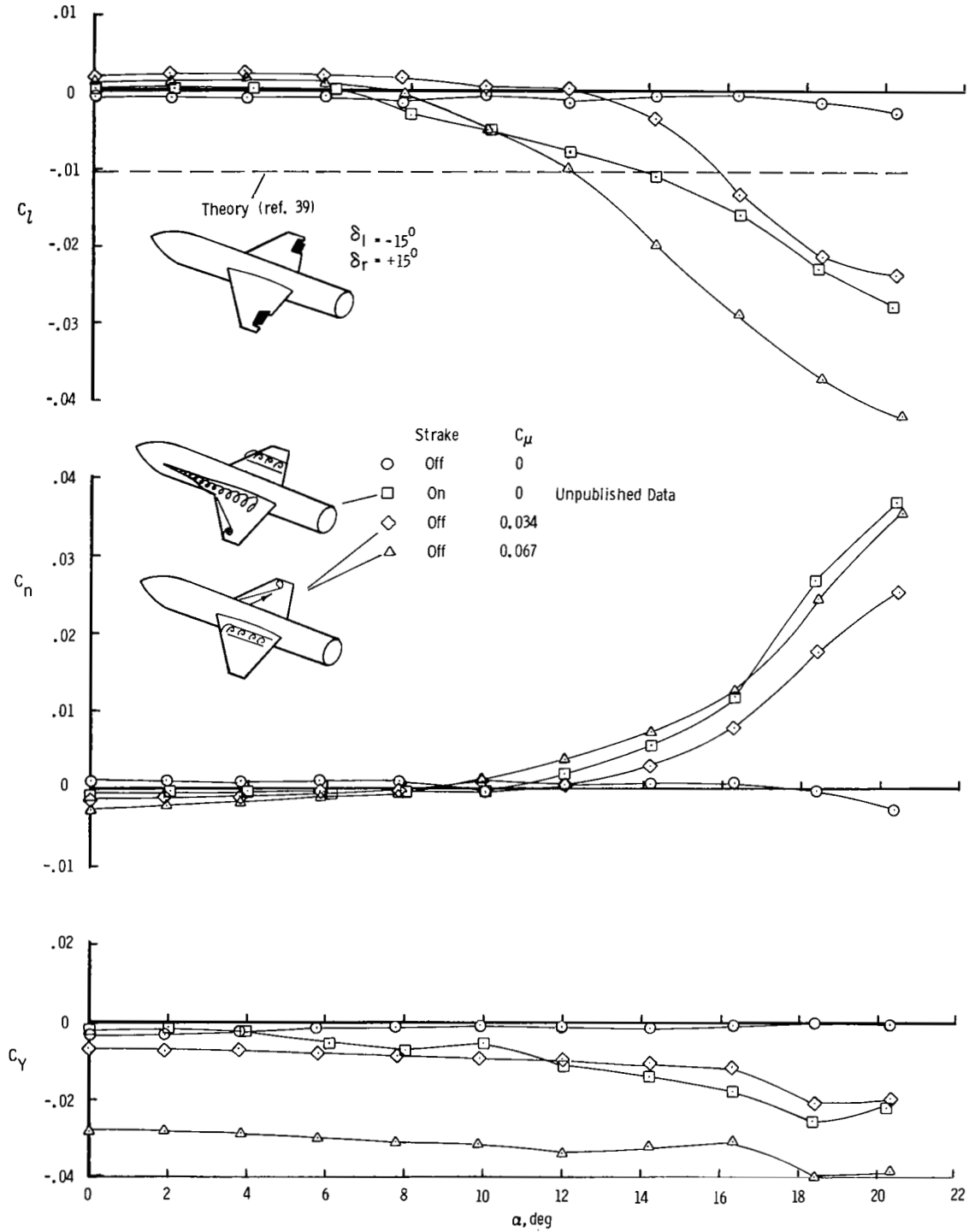

Figure 24.- Comparison of effects of differential strake and differential spanwise blowing on lateral-directional characteristics of 44° swept trapezoidal wing configuration; $M_\infty = 0.30$.

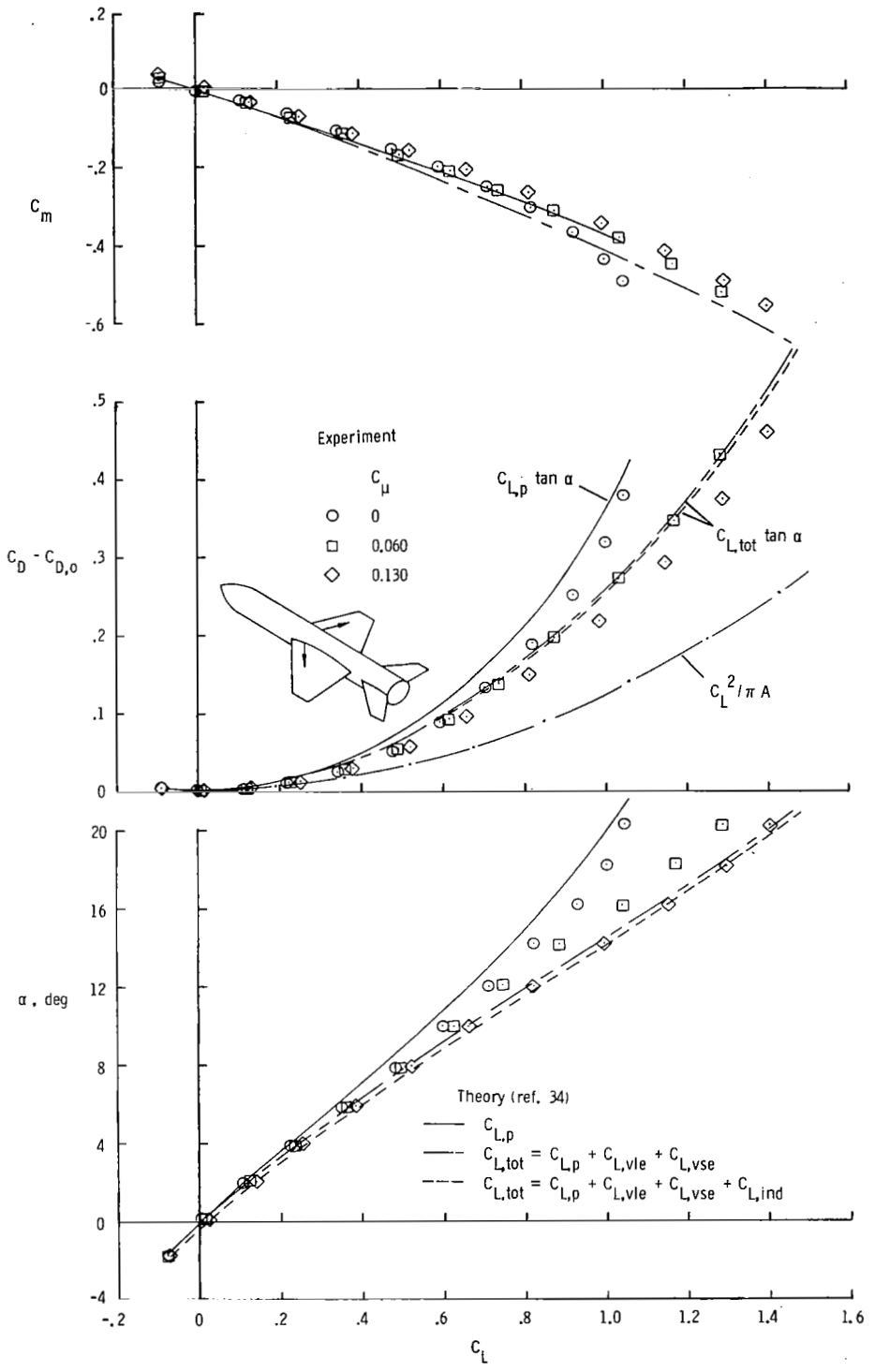

Figure 25.- Comparison of theoretical and experimental longitudinal aerodynamic characteristics of configuration with wing and horizontal tail; $M_\infty \approx 0.30$.

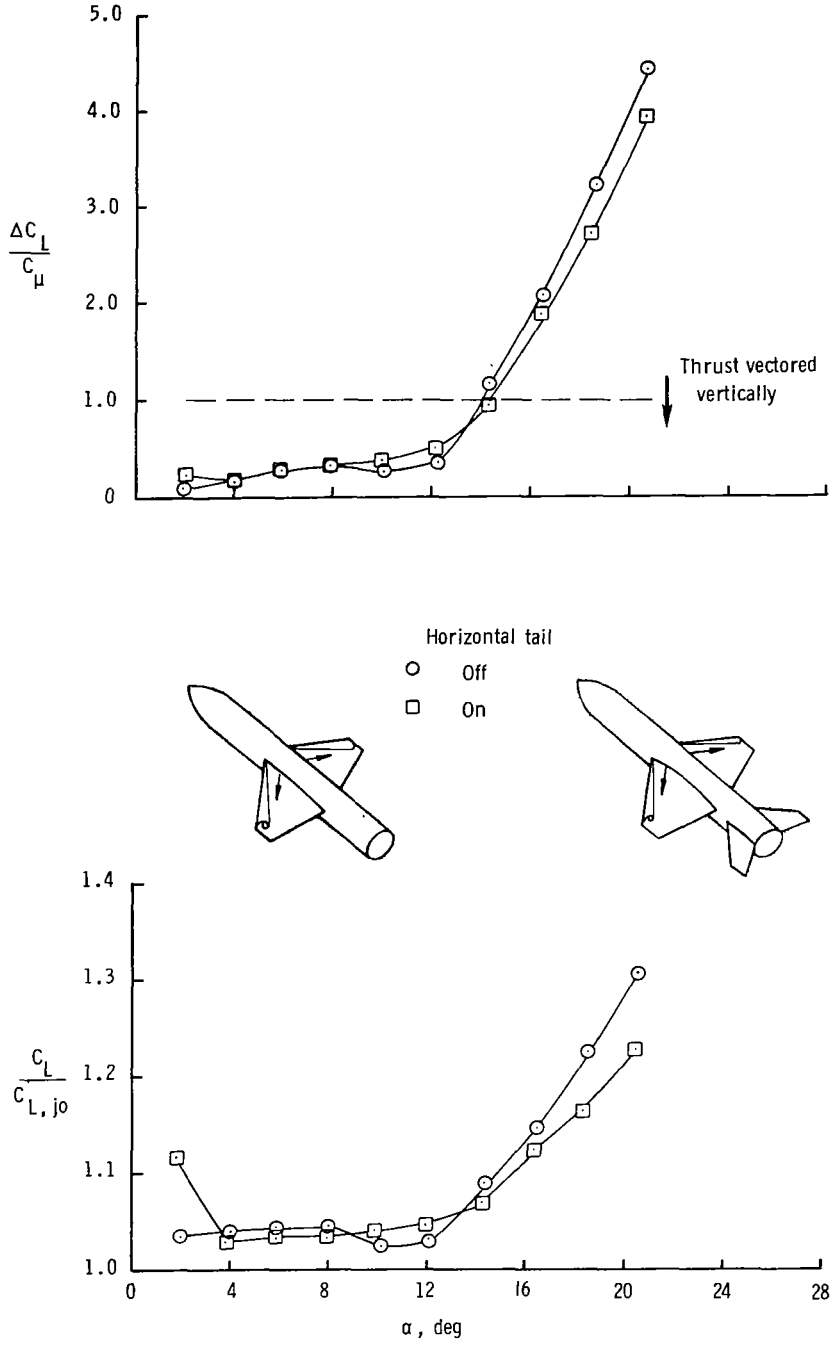

Figure 26.- Effect of angle of attack and horizontal tail on lift augmentation ratio and lift effectiveness of blowing on 44° swept trapezoidal wing for $C_\mu \approx 0.060$; $M_\infty = 0.30$.

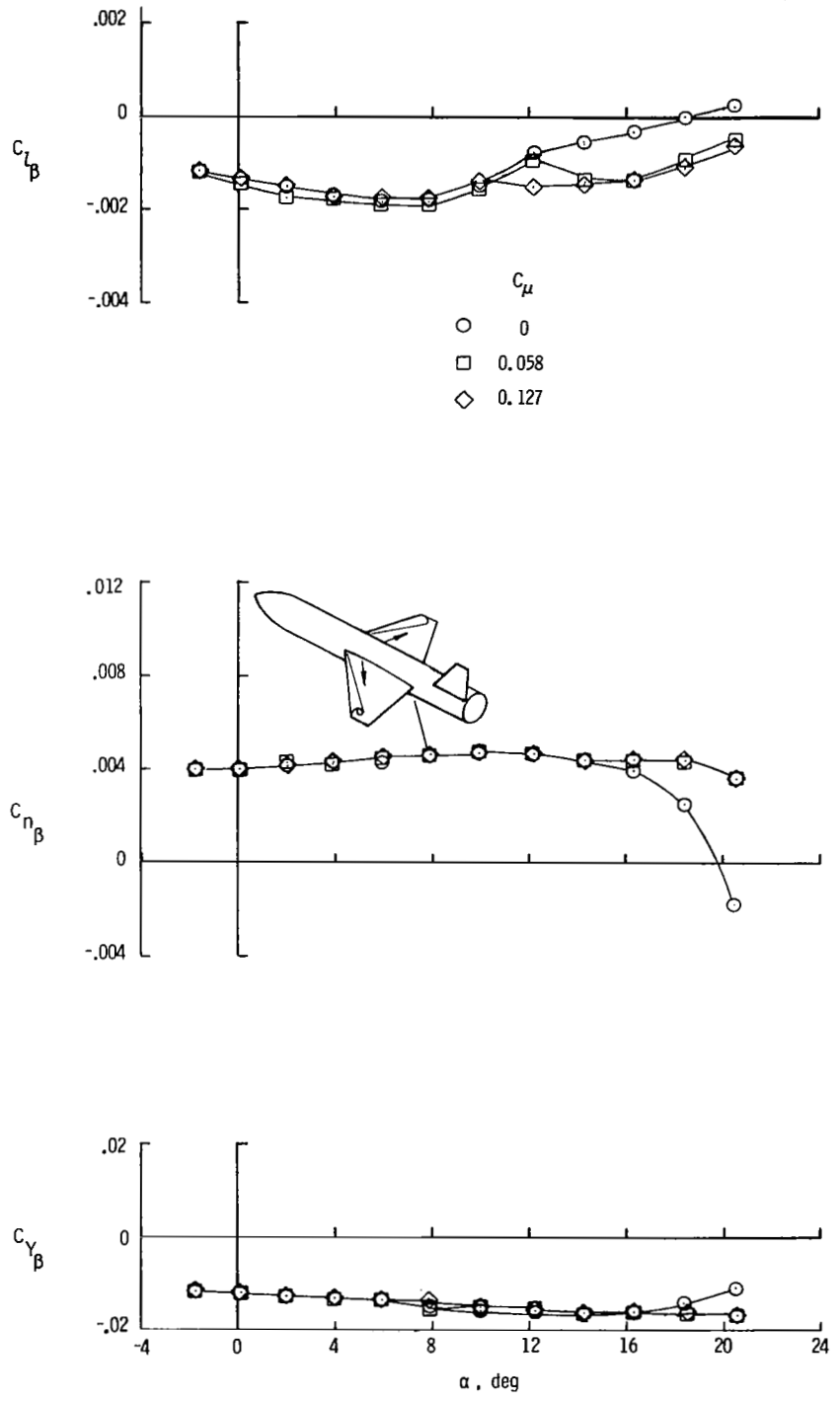

Figure 27.- Effect of spanwise blowing on lateral-directional stability derivatives of configuration with wing and vertical tail; $M_\infty = 0.30$.

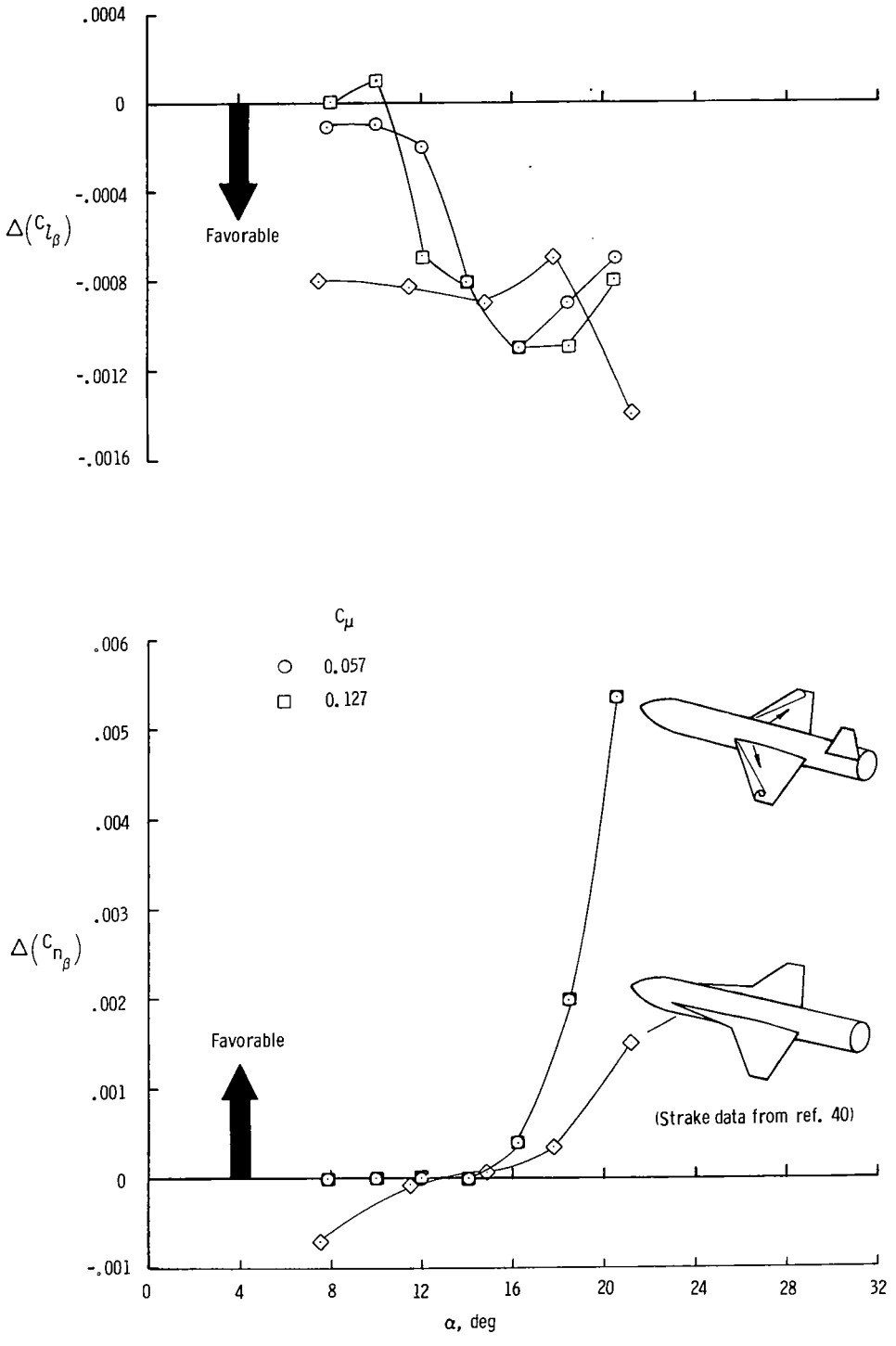

Figure 28.- Comparison of increments in $C_{n\beta}$ and $C_{l\beta}$ due to spanwise blowing or a wing strake for 44° swept trapezoidal wing configuration with vertical tail; $M_\infty = 0.30$.

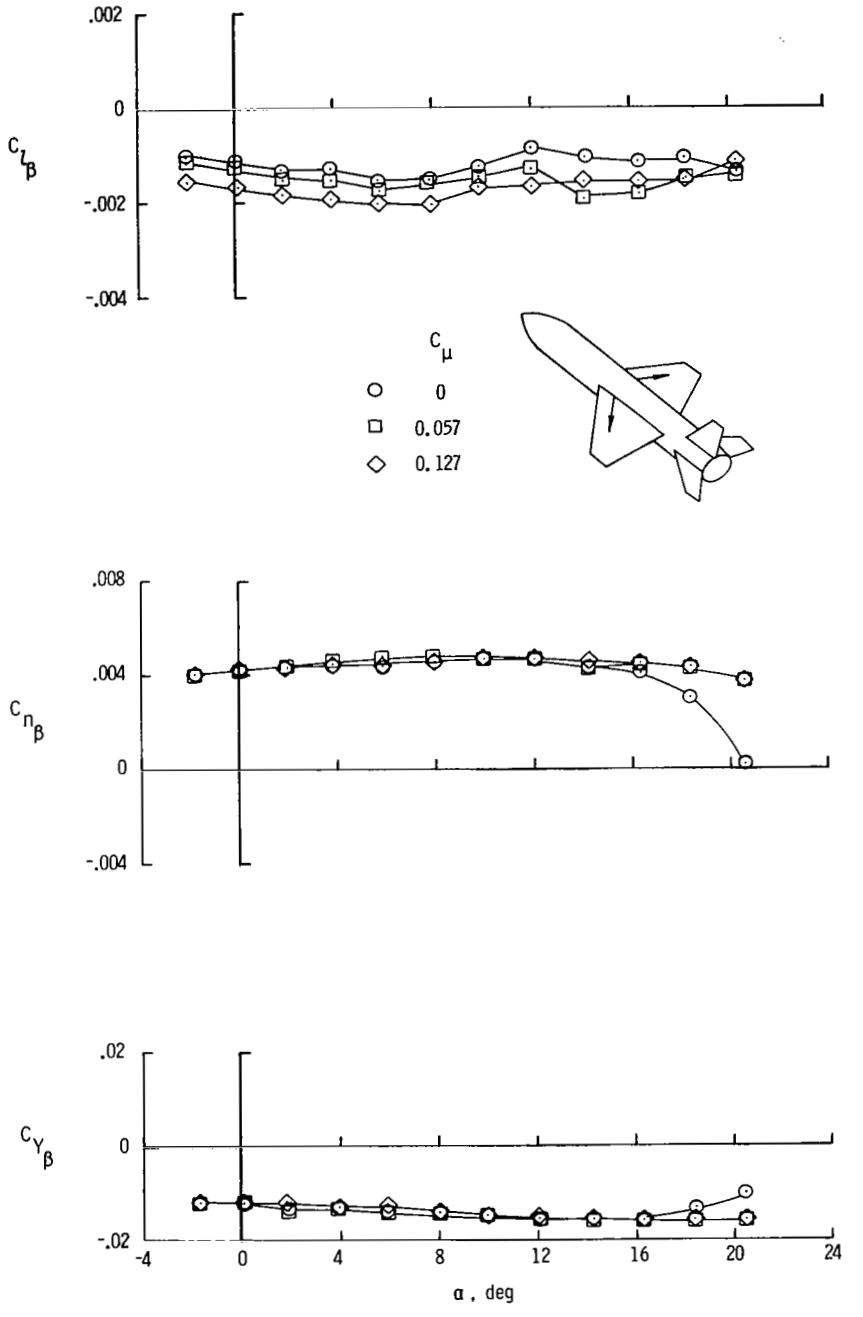

Figure 29.- Effect of spanwise blowing on lateral-directional stability derivatives of configuration with wing, vertical tail, and horizontal tail; $M_\infty = 0.30$.

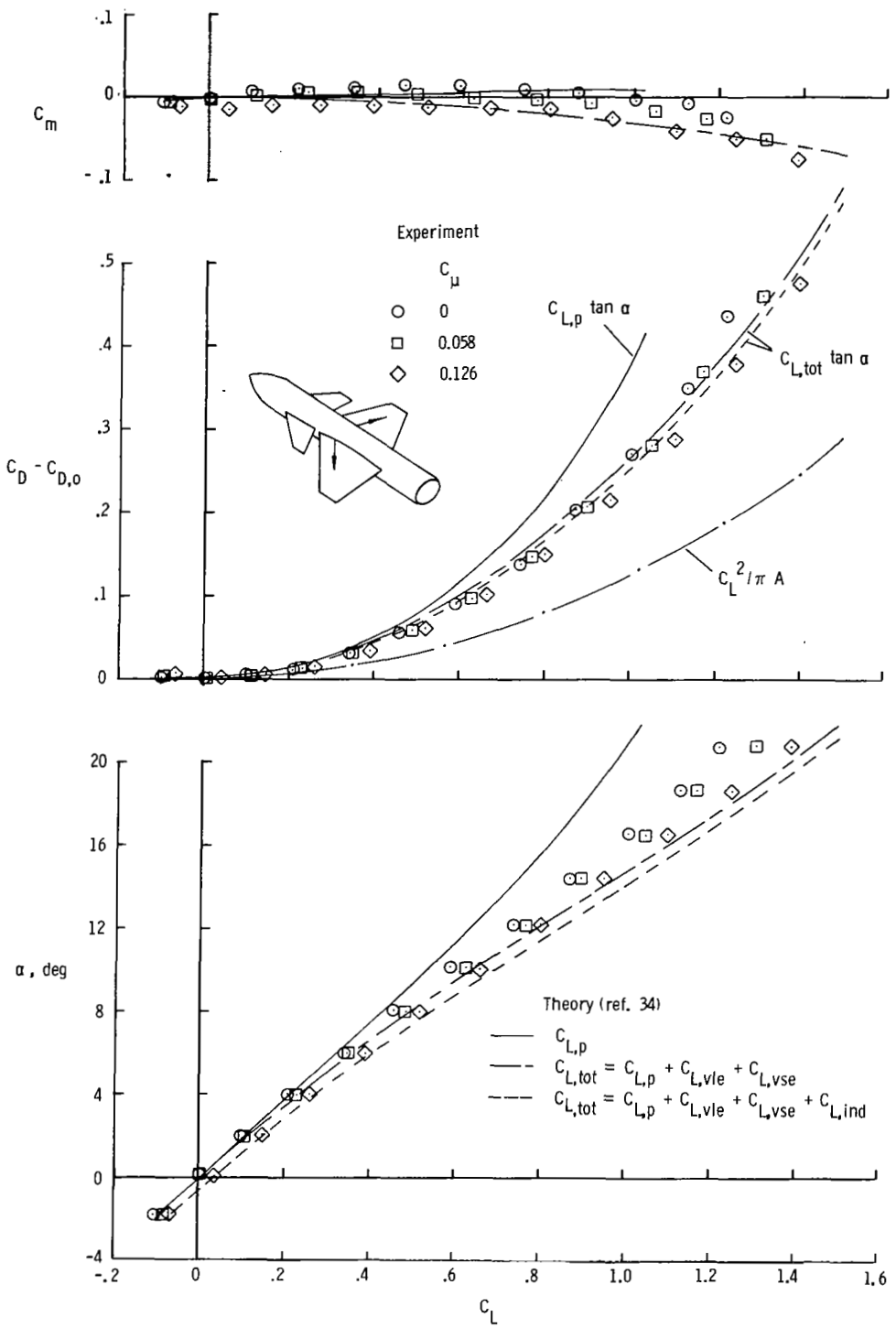

Figure 30.- Comparison of theoretical and experimental longitudinal aerodynamic characteristics of canard-wing configuration with blowing on wings; $i_C = 0^o$; $M_\infty = 0.30$.

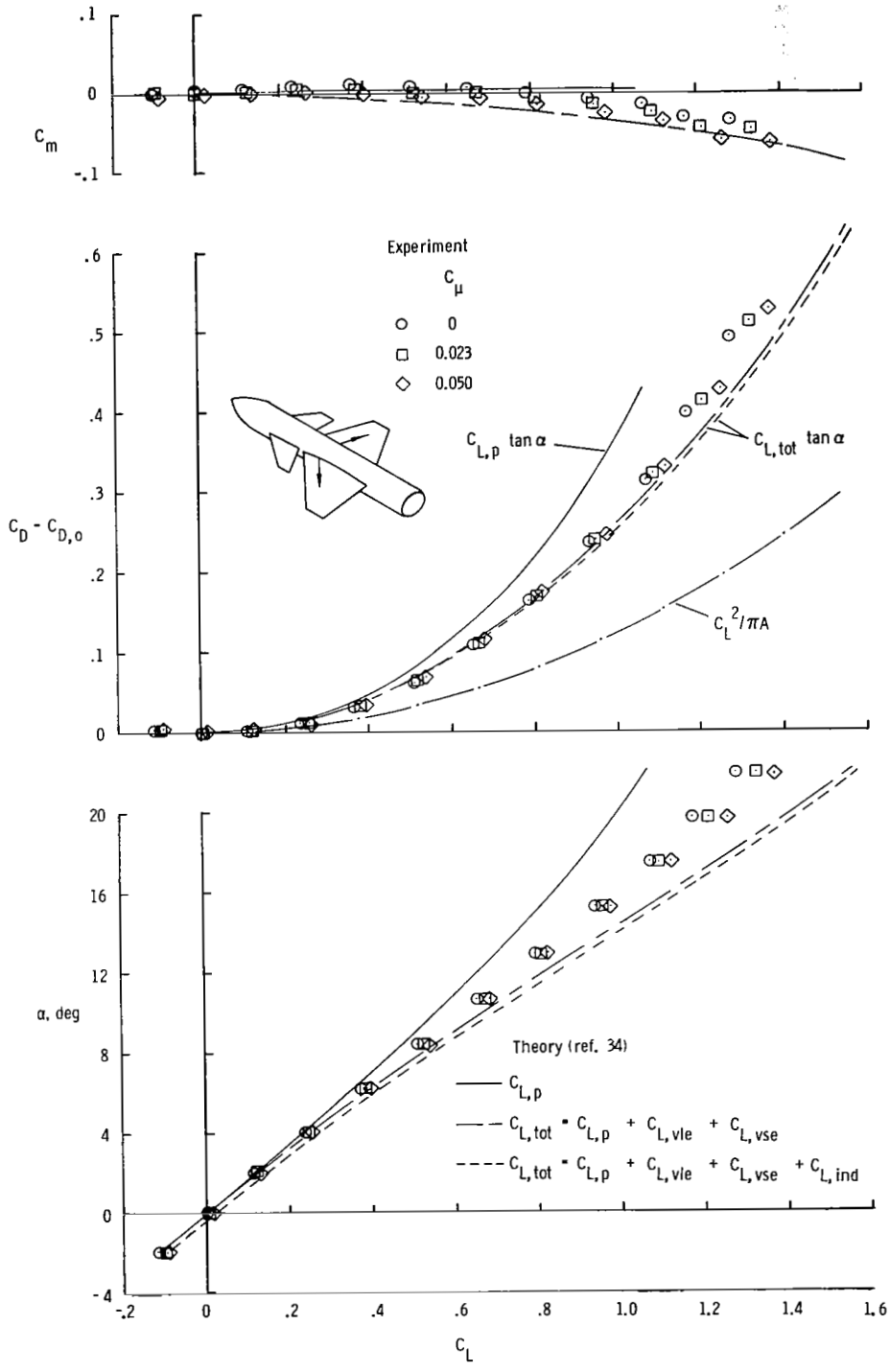

Figure 31.- Comparison of theoretical and experimental longitudinal aerodynamic characteristics of canard-wing configuration with blowing on wings; $i_C = 0^o$; $M_\infty = 0.50$.

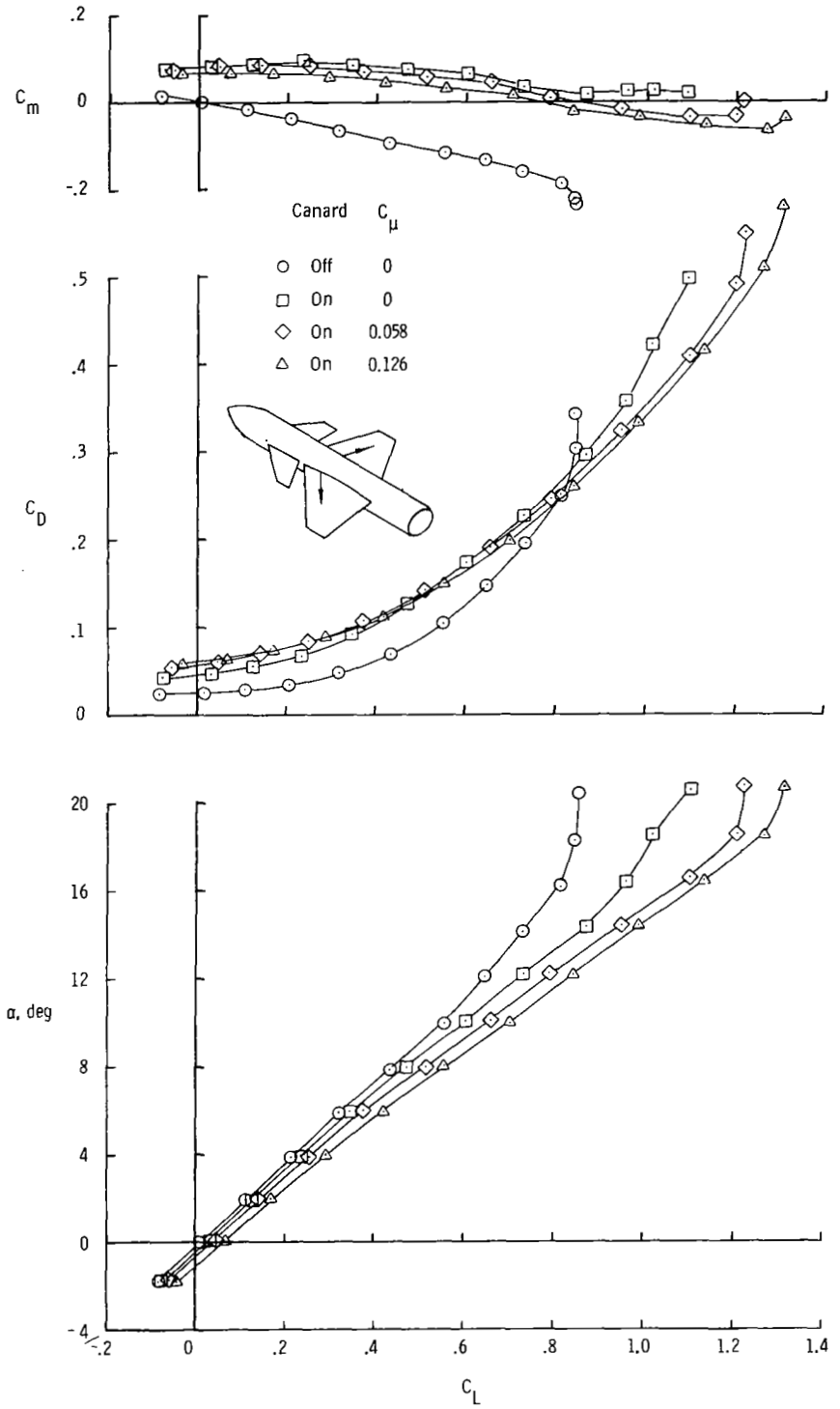

Figure 32.- Effect of spanwise blowing on 44° swept trapezoidal wing on longitudinal aerodynamic characteristics of close-coupled canard wing configuration for $i_C = 10°$; $M_\infty = 0.30$.

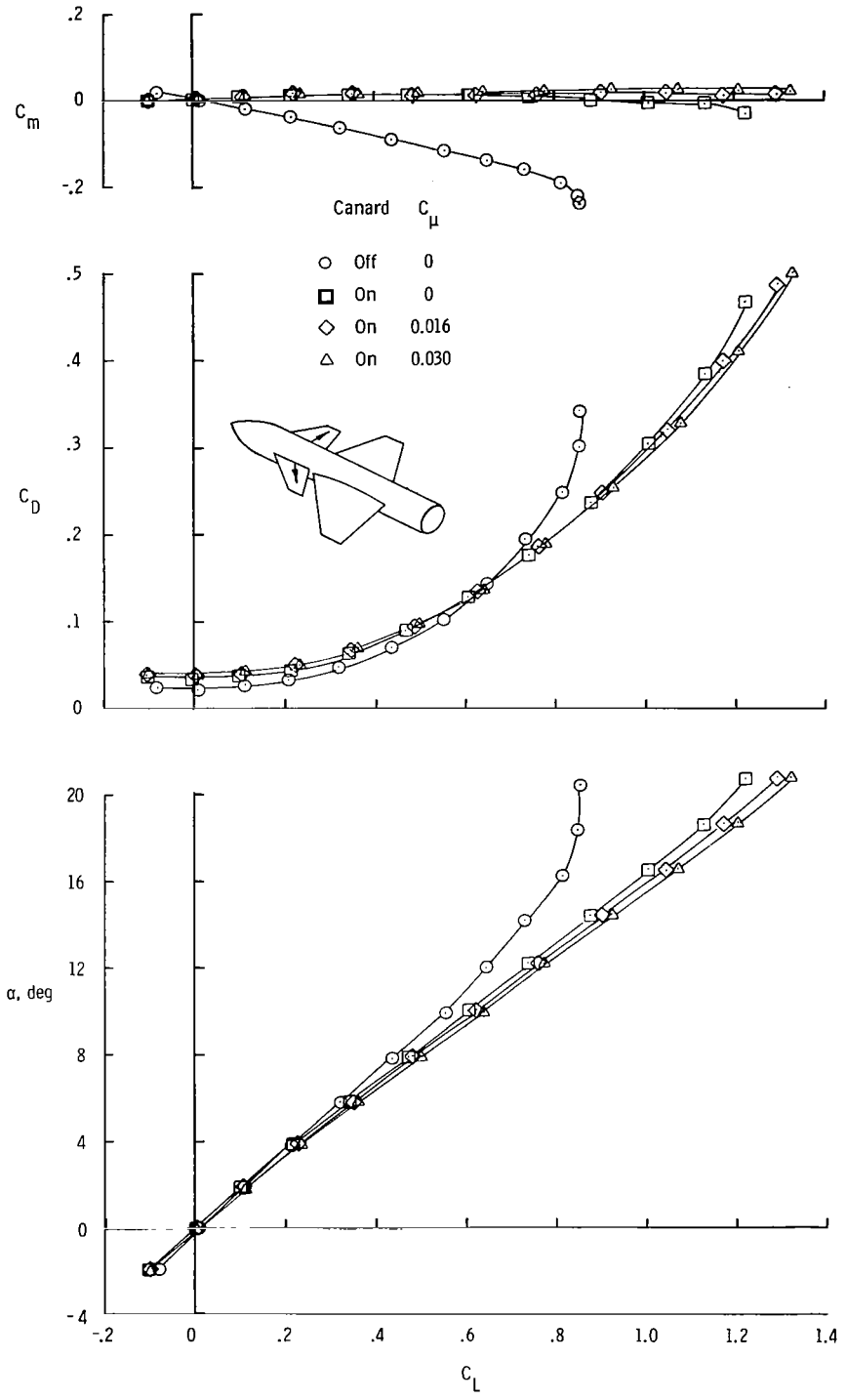

Figure 33.- Effect of canard spanwise blowing on longitudinal aerodynamic characteristics of canard-wing configuration for $i_C = 0^o$; $M_\infty = 0.30$.

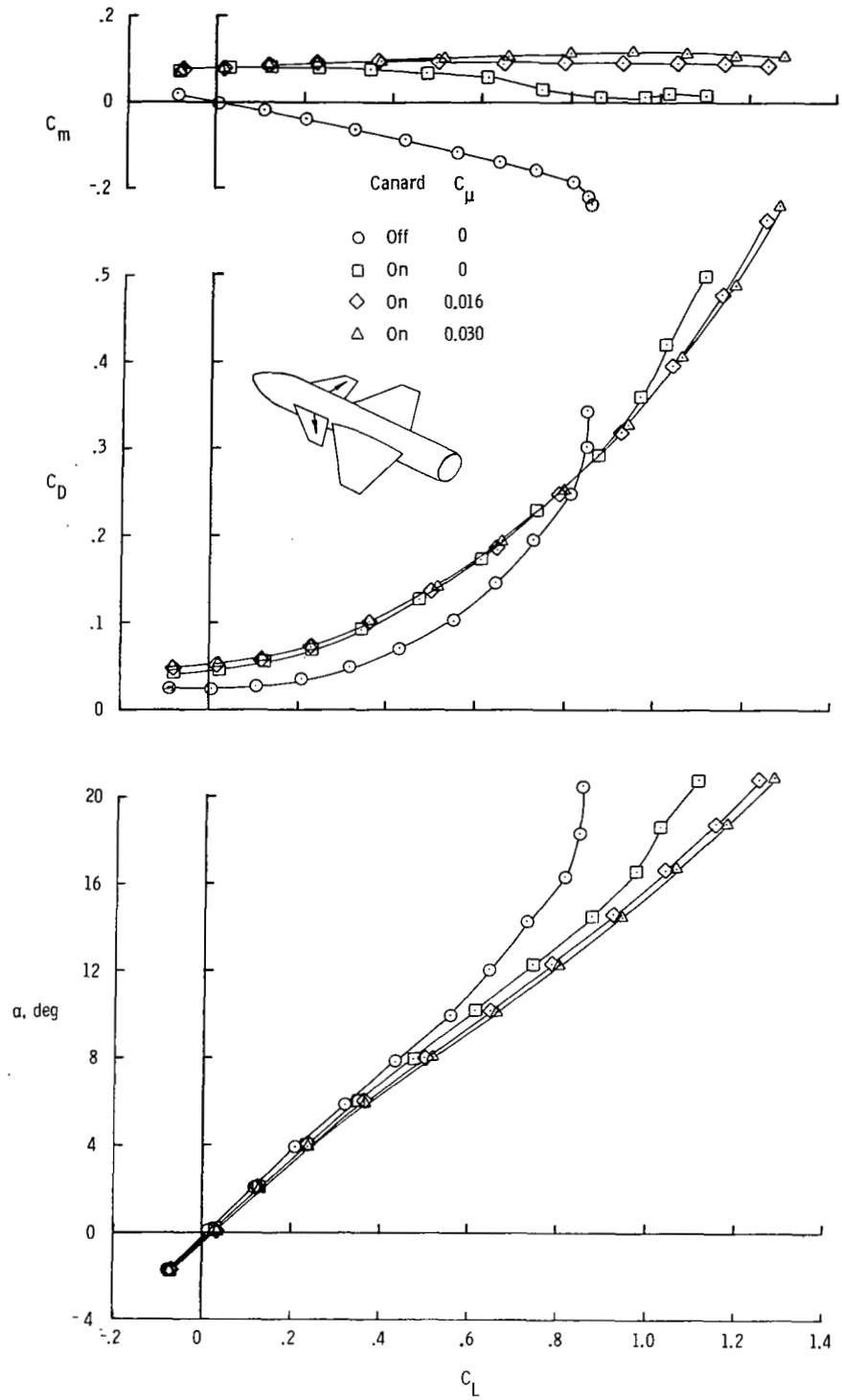

Figure 34.- Effect of canard spanwise blowing on longitudinal aerodynamic characteristics of close-coupled canard-wing configuration for $i_C = 10^o$; $M_\infty = 0.30$.

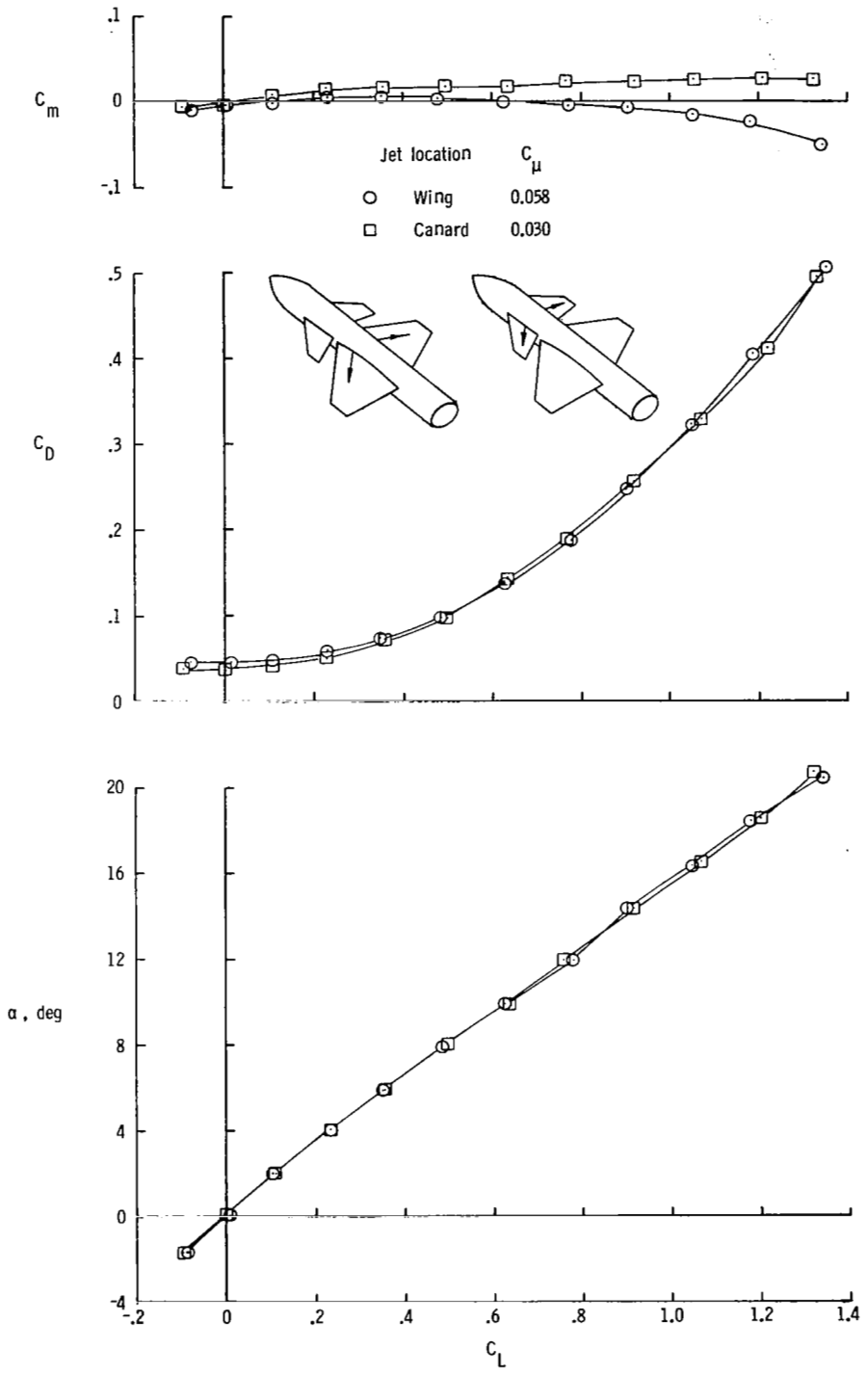

Figure 35.- Comparison of longitudinal aerodynamic characteristics of canard-wing configuration with spanwise blowing on wings and with spanwise blowing on canards for $i_C = 0^o$; $M_\infty = 0.30$.

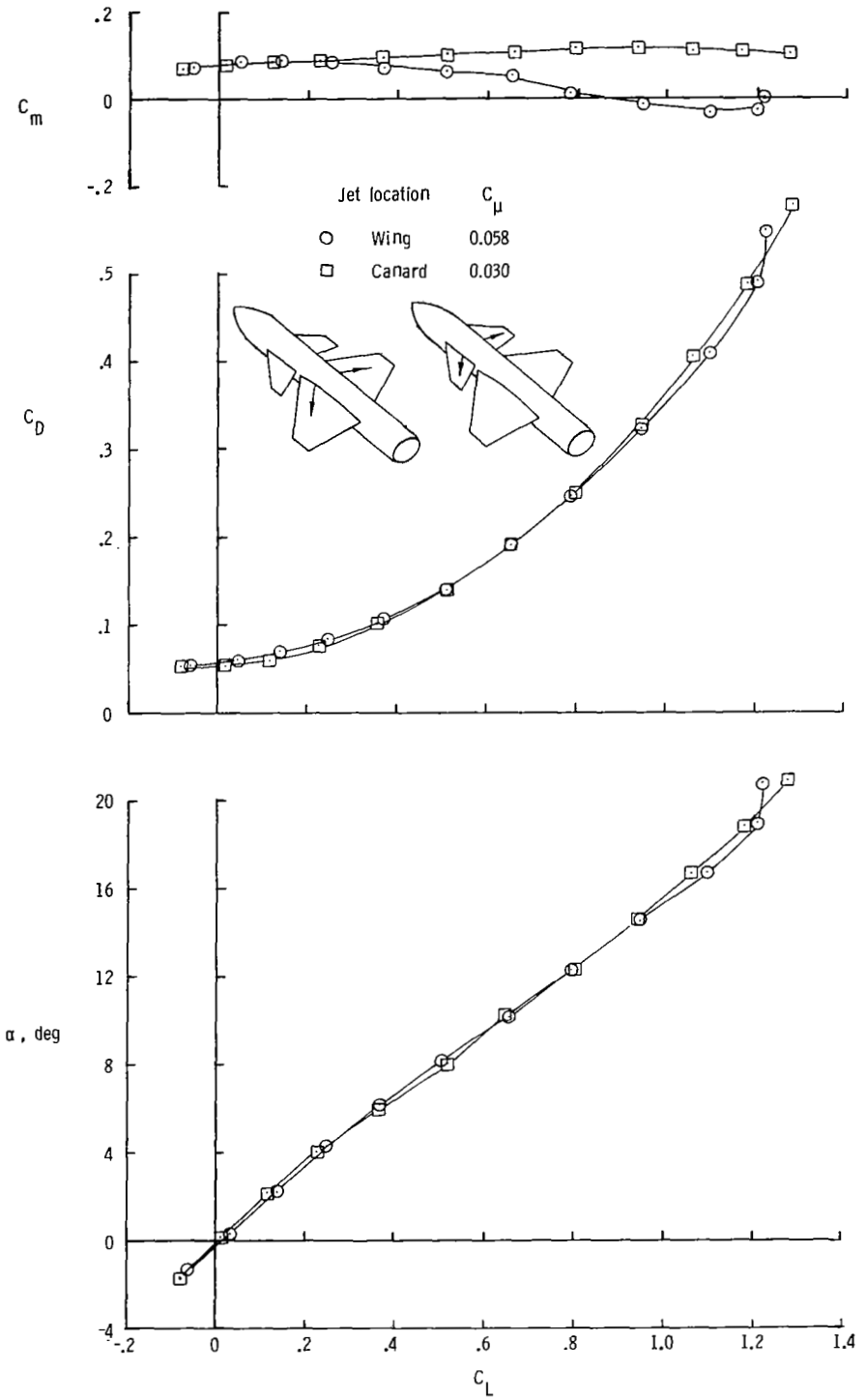

Figure 36.- Comparison of longitudinal aerodynamic characteristics of canard-wing configuration with spanwise blowing on wings and spanwise blowing on canards for $i_C = 10^o$; $M_\infty = 0.30$.

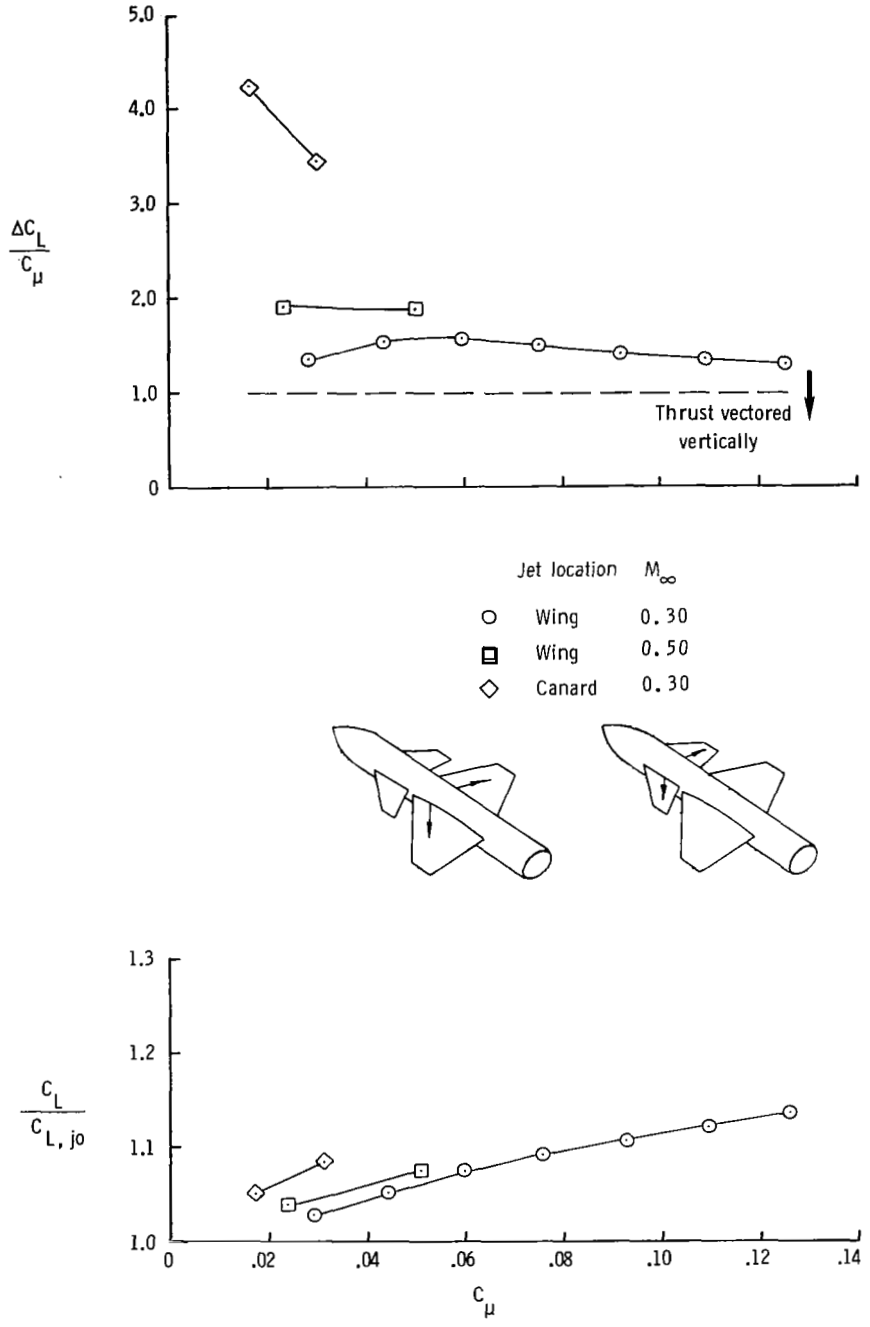

Figure 37.- Effect of C_μ, jet location, and M_∞ on lift augmentation ratio and lift effectiveness of blowing for canard-wing configuration; $i_C = 0^\circ$; $\alpha \approx 21^\circ$.

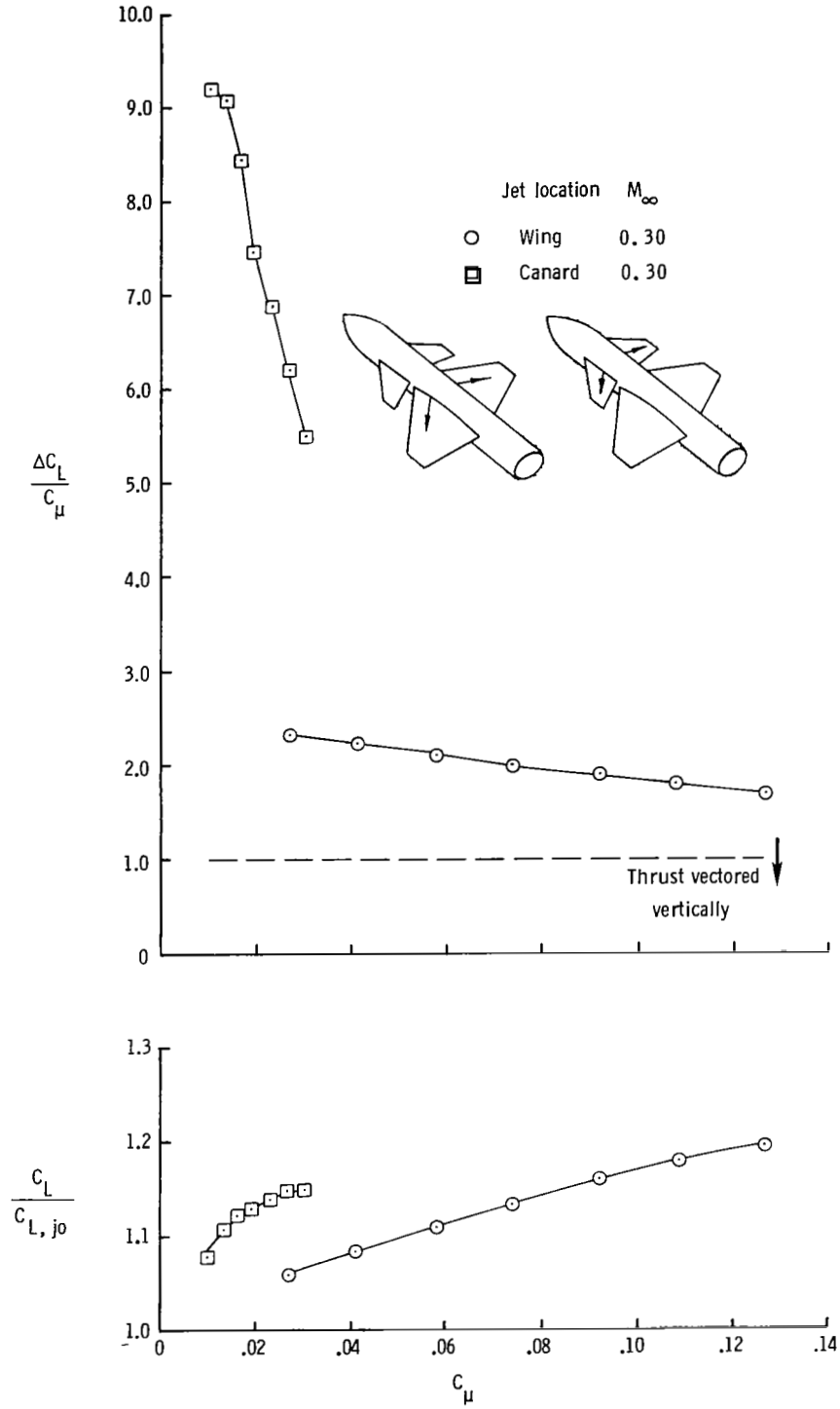

Figure 38.- Effect of C_μ and jet location on lift augmentation ratio and lift effectiveness of blowing for canard-wing configuration; $i_C = 10^o$; $\alpha \approx 21^o$.

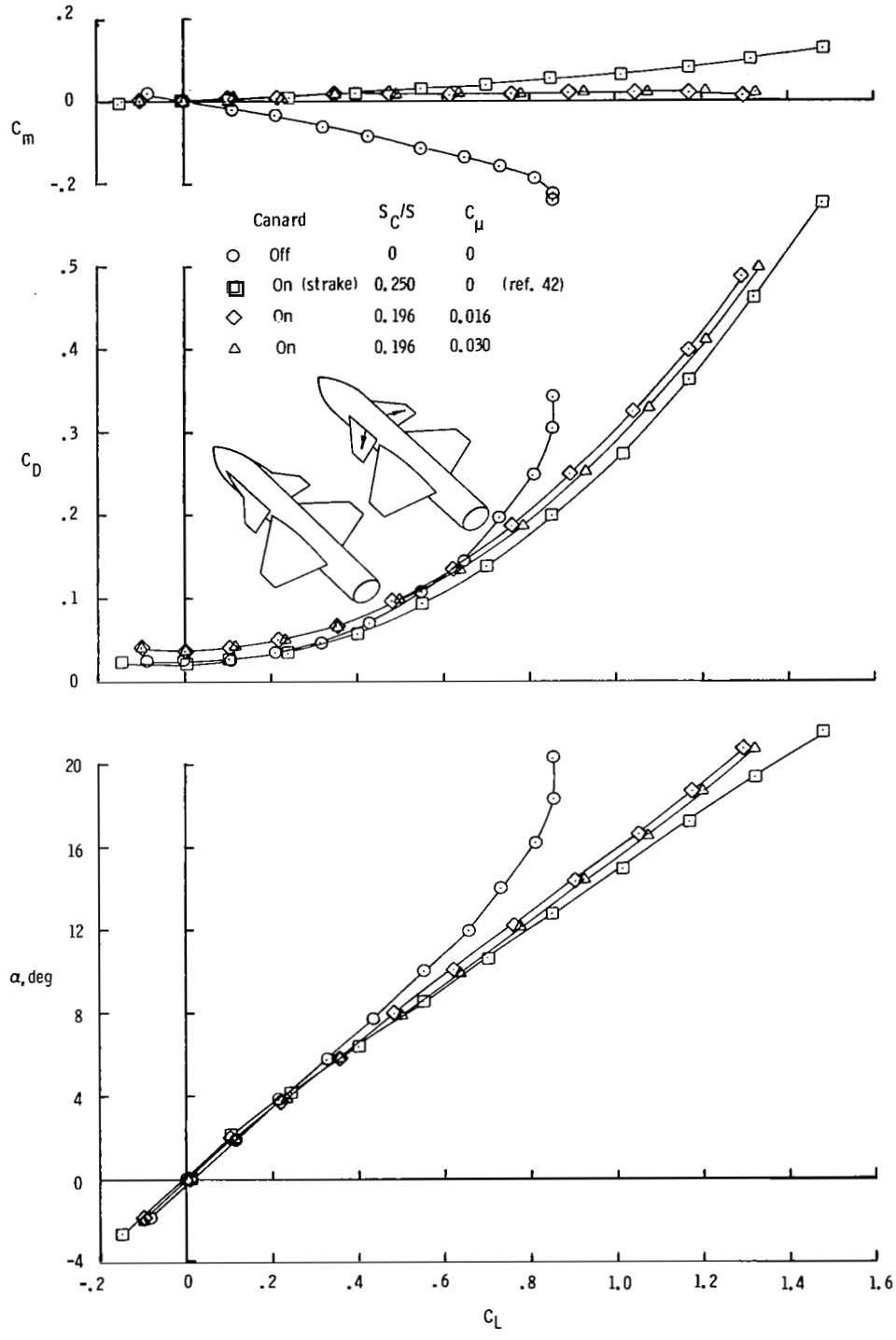

Figure 39.- Comparison of longitudinal aerodynamic characteristics of straked canard-wing configuration and canard-wing configuration featuring canard spanwise blowing; $M_\infty = 0.30$; $i_C = 0^o$.

1. Report No.	2. Government Accession No.	3. Recipient's Catalog No.
NASA TP-1065		

4. Title and Subtitle	5. Report Date
IMPROVEMENT OF MANEUVER AERODYNAMICS BY SPANWISE BLOWING	December 1977
	6. Performing Organization Code
7. Author(s)	8. Performing Organization Report No.
Gary E. Erickson and James F. Campbell	L-11642
	10. Work Unit No.
9. Performing Organization Name and Address	505-11-21-02
NASA Langley Research Center Hampton, VA 23665	11. Contract or Grant No.
	13. Type of Report and Period Covered
12. Sponsoring Agency Name and Address	Technical Paper
National Aeronautics and Space Administration Washington, DC 20546	14. Sponsoring Agency Code

15. Supplementary Notes

Gary E. Erickson: The George Washington University, Hampton, Virginia.
James F. Campbell: Langley Research Center.

16. Abstract

Spanwise blowing was used to test a generalized wind-tunnel model to investigate new component concepts in order to provide improved maneuver characteristics for advanced fighter aircraft. Primary emphasis was placed on performance, stability, and control at high angles of attack and subsonic speeds. Test data were obtained in the Langley high-speed 7- by 10-foot tunnel at free-stream Mach numbers up to 0.50 for a range of model angles of attack, jet momentum coefficients, and leading- and trailing-edge flap deflection angles.

Spanwise blowing on a 44° swept trapezoidal wing resulted in leading-edge vortex enhancement with subsequent large vortex-induced lift increments and drag polar improvements at the higher angles of attack. Small deflections of a leading-edge flap delayed these lift and drag benefits to higher angles of attack. In addition, blowing was more effective at higher Mach numbers. Spanwise blowing in conjunction with a deflected trailing-edge flap resulted in lift and drag benefits that exceeded the summation of the effects of each high-lift device acting alone. Asymmetric blowing was an effective lateral control device at the higher angles of attack. Adding the horizontal tail reduced the lift effectiveness of blowing at high angles of attack. Spanwise blowing on the wing improved the lateral-directional stability characteristics of a combination wing, horizontal-tail, and vertical-tail configuration. Spanwise blowing on the canards was more effective than spanwise blowing on the wings of a close-coupled canard-wing configuration. The leading-edge suction analogy provided reasonable estimates for the longitudinal aerodynamic characteristics resulting from spanwise blowing.

17. Key Words (Suggested by Author(s))	18. Distribution Statement
Spanwise blowing Maneuver aerodynamics Vortex lift	Unclassified - Unlimited Subject Category 02

19. Security Classif. (of this report)	20. Security Classif. (of this page)	21. No. of Pages	22. Price*
Unclassified	Unclassified	65	$5.25

* For sale by the National Technical Information Service, Springfield, Virginia 22161

NASA-Langley, 1977

5 1 1U,A, 120577 S00903DS
DEPT OF THE AIR FORCE
AF WEAPONS LABORATORY
ATTN: TECHNICAL LIBRARY (SUL)
KIRTLAND AFB NM 87117

S